

**Master's thesis**

**NTNU**  
Norwegian University of Science and Technology  
Faculty of Information Technology and Electrical Engineering  
Department of Electric Power Engineering

Yannick Cyiza Karekezi

# An In-Depth Study of Calculation Models for Hydro-Generators: Quantifying the Impact of the Energy Transition

Master's in Electric Power Engineering  
Supervisor: Jonas Kristiansen Nøland  
Co-Supervisor: Thomas Øyvang

June 2021



Norwegian University of  
Science and Technology



Yannick Cyiza karekezi

**An In-Depth Study of Calculation Models  
for Hydro-Generators:  
Quantifying the Impact of the Energy Transition**

Master's in Electric Power Engineering  
Supervisor: Jonas Kristiansen Nøland  
Co-Supervisor: Thomas Øyvang

June 2021

Norwegian University of Science and Technology  
Faculty of Information Technology and Electrical Engineering  
Department of Electric Power Engineering



Norwegian University of  
Science and Technology



# An In-Depth Study on Calculation Models for Hydro-Generators: Quantifying the Impact of the Energy Transition

Yannick Cyiza Karikezi, *Student Board Member, IEEE*

**Abstract**—This project’s background is the worldwide energy transition that takes advantage of the hydropower plant’s operational flexibility to extend the integration of renewable energy sources. This era and future operational regimes will be much more flexible. This means that today’s generators and future generators will have to operate in regimes far away from their designed condition. This report presents two calculation models and two distinct hydro generators.

The first generator is a hydro generator in a Furnas power plant in Brazil. The second generator is a hydro generator in Norway called Åbjøra. The first generator is used as an example to illustrate the different methods and procedures used for calculating the saturation level, iso-efficiency curves, total energy loss curves, total energy loss (TEL), and total energy production (TEP). This report presents two calculation models called weighted average efficiency (WAE) and accumulated average efficiency (AAE). This report also presents a simple worked example that compares the two calculation models for three different loading points. In addition to this, the calculation models are compared using more complex data sets, where the calculation models are compared using three different load distributions. The result was that the AAE superseded the calculation model WAE for all the different load distributions investigated. The difference between the calculation models is as follows. The concentrated load distribution gives a difference of 0.67%, the uniform load distribution gives a difference of 1.43%, and the synchronous condenser load distribution gives a difference of 33.18%.

This report focuses mainly on an in-depth study of the Norwegian hydro generator Åbjøra. The main issue with the calculation model WAE is that it gives a low efficiency when the generator is operated as a synchronous condenser for relatively long periods, during its yearly production. This was illustrated using an artificially made load distribution. That mimics an actual synchronous condenser distribution like the one in Bortoni’s technical report [1].

In summary, this report presents a proposal of not only calculating the efficiency at the rated point but considers all the loading points and in doing so evaluates the WAE and AAE. A histogram of discrete loading points is constructed for the two existing generators, an estimate of the duration of loading points and the percentage of time by which each loading point operates is deduced and illustrated. The reason that the generator operates at different loading points than the rated point, is due to the increasing prevalence of renewable energy sources. The integration of renewable energy sources forces conventional power plants like hydro generators to be more flexible in their operating range. This means that the entire load distribution must be taken into account instead of considering the efficiency at a single point.

## I. INTRODUCTION

This article is written as a project report in the course TET4910 "Electric power engineering, master thesis" at the

Norwegian University of Science and Technology (NTNU). The report presents a study of two different calculation models. The first calculation model is called weighted average efficiency (WAE) and the second calculation model is called accumulated average efficiency (AAE). The proposed AAE is the basis for a journal paper recently submitted to the IEEE Transactions on Energy Conversion [2]. The paper presents a comparison of the WAE and AAE of the Norwegian hydro generator Åbjøra. In this report, there are two generators under study. The first generator (G1) is a hydro generator in a Furnas hydropower plant, which is the hydro-generator under study in Bortoni’s technical report [1]. The second generator (G2) is an industry generator in Norway called Åbjøra. Generator G1 is used to illustrate the different methods and assumptions for the different calculation models. Three different methods were used to account for the saturation of the generators during different loading points. The first method is called the Anderson and Fouad method and uses saturation factors to quantify the level of saturation. The second method is the method implemented in Bortoni’s technical report [1], which uses polynomial coefficients. The third method stems from Machowski [3], which uses a fitting function to quantify the field current for different voltage levels. These three methods are compared in regards to simplicity and accuracy. This is done to calculate the total energy Losses (TEL), rather than average/expected efficiency. The significance of this approach is further explained in Section VIII Discussion. In addition to the calculation of TEL, the implementation of different zones was used to capture the discrete loading points and quantify their probability of occurrence. This was done to find the best approach for calculating the TEL. After studying the different zones a conclusion of the most appropriate zone was made. The methods and procedures were experimentally validated using measurements of the efficiency and field current extracted from the industry generator Åbjøra. MATLAB is the chosen numerical software used for calculation and results presented in this report. The University of Southeast Norway provided industry data consisting of production data for different hydro-generator in Norway. A case study of the calculation models WAE and AAE were compared using production data from the industry, an artificially made uniform load distribution, and an artificially made synchronous condenser distribution. The project report is divided into nine sections. The different sections can be seen in the list below.

### 1) Introduction

- 2) The Problem Description
- 3) An introduction to the Energy Transition
- 4) Description of the case studies
- 5) Theoretical framework for loss and efficiency calculation
- 6) The Implementation of different Methods and the Calculation Procedures
- 7) Results and discussion
- 8) Further work
- 9) Conclusion

## II. THE PROBLEM DESCRIPTION

The energy transitions' main impact is the increased prevalence of solar and wind power plants and their influence on exciting electrical grids. In addition to this, there is also a disconnection of fossil power production units. Moreover, the rising demand for fast, reliable, and sufficient power generation, in case of missing solar and wind power generation, creates a need to modernize the current grids [4]. This is necessary to assure a sufficient amount of rotational mass, such as rotational phase-shifter applications, and to build new fast-cycling power plants [5].

This master thesis aims to increase the physical understanding of the phenomena and challenges that occurs when renewable energy sources are connected to the grid. This study focuses in particular on how renewable energy sources affect hydropower plants. The increased incentives for the removal of conventional power plants like coal, gas, and nuclear power in addition to the encouragement of a faster transition to renewable energy sources create entirely new criteria regarding the operation and design of new and existing hydropower plant [6]. From the hydro generator's point of view, the increased implementation of renewable energy sources creates a bigger variation in loading points, and thus, requires reliable electrical machines with increased operational flexibility. This also creates the need for a hydro generator that can withstand higher thermo-mechanical loads, rapid load ramping, and losses related to variation in production [7]. Figure 1 shows an example of a capability diagram that indicates operation points in MVar and MW in addition to their weight. The example shows that the generator operates only 5% around its nominal rated condition (best point).

This report focuses both on the different loading points and the frequency of the loading points. This means that the generator's start and stop cycles as well as the different loading points are considered. The efficiency and losses in this study are calculated based on their loading points. The weight is calculated based on the frequency of the loading points and the total number of loading points.

This project's contribution is to investigate different methods and approaches for quantifying the impact of the energy transition. This is done by comparing two different calculation models for three different load distributions/operational regimes. This was done using hydro-generator G1, which is the hydro-generator in the Furnas power plant. An illustration of the Furnas hydropower plant can be seen in Figure 2. This project also contributes to explain and quantify the impact of the energy transition by implementing a case study of the

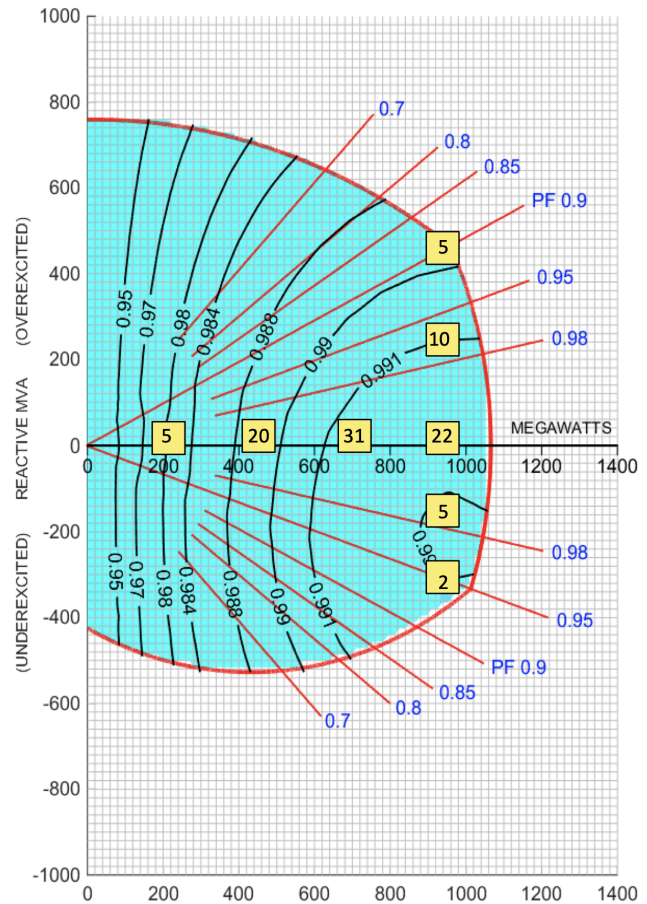


Fig. 1. Example of a capability diagram depicting efficiency contours, considering different load points and weights based on the operational regime of the generator under study [1]. The x-axis projects the active power in MW, whereas the y-axis takes the reactive power in MVar into account. The yellow squares with indication numbers show the probability for a load point to occur.

calculation models WAE and AAE. This is further explained in Section VII. Three important case studies are presented in this report using hydro generator G2. The first case study uses industry data. The second case study uses an artificially made distribution that mimics a load distribution that is evenly distributed throughout the entire capability diagram. The third load distribution is also artificially made, but this distribution mimics a synchronous condenser distribution. The characteristics of these load distributions are further explained in Section IV.

## III. AN INTRODUCTION TO THE ENERGY TRANSITION

This section goes into more detail on how renewable energy affects the grid and conventional power sources. This section primarily focuses on how it affects hydraulic units. The increasing prevalence of renewable energy sources forces turbogenerator sets and hydraulic units to be more flexible in their operational regime [9].

One example is the production phenomenon "duck curve". The California Independent System Operator (CAISO) published a graph that shows the timing imbalance caused by solar power production and energy need during a day [10]. The



Fig. 2. A Picture of a Furnas hydropower plant in Brazil [8].

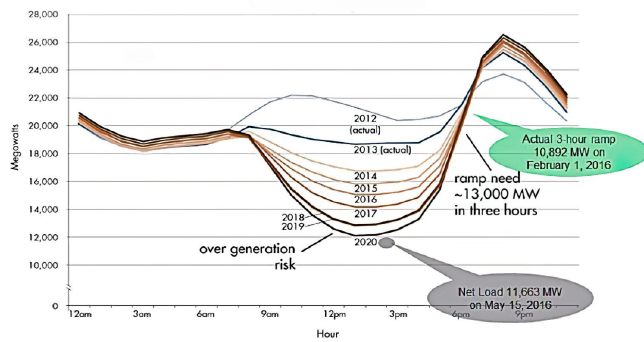


Fig. 3. Typical spring day for solar power production in California [10].

duck curve pictured in figure 3 shows that the peak demand occurs in the time when the amount of solar energy production decreases significantly [11]. This means that conventional power plants must be able to quickly ramp up production to compensate for the imbalance within a short time frame [12]. On the other hand, there is also a risk of over-generation during noontime when a lot of solar production is fed into the grid, while the consumption is low.

There has been made several incentives to increase the prevalence of renewable energy sources, and a shutdown and disconnection of conventional power source. This has led to a decrease in frequency response and an increase in non-controllability of reactive power flow in the grid [13]. The removal of large reliable power sources leads to a reduction of rational mass in the system. This is because the inertia and the reactive power provided by the conventional power sources help stabilize the frequency and assures the reliability of the grid [5]. The regulation of reactive power is very difficult without conventional power plants. This is primarily because renewable energy sources like wind and solar have limited capabilities of running in capacitive mode [14]. This means that one must often implement expensive power electronic devices in combination with renewable energy sources [6].

As previously stated several incentives have been made to get a quicker transition towards renewable energy sources. One example is California which has made several incentives to

accelerate the prevalence of the duck curve. The following key initiatives that California have set in motion are:

- 1) 50 % of retail electricity from renewable power by the year 2030
- 2) Greenhouse gas emission goal to 1990 levels;
- 3) Regulation in the next 4-9 years requires power plants that use coastal water for cooling to either re-power, retrofit or retire.
- 4) An executive order for 1.5 million zero-emission vehicles.

The same initiatives have also been set in motion by other countries. The German grid operators are also trying to increase the prevalence of renewable energy sources. The Germans have implemented something called the "Energiewende" (energy turnaround), the portion of renewable energy rose to 38.5 % in 2017, where 50 % of the renewable energy was generated by wind turbines. Wind power generation is quite difficult to predict. Wind power underlies more or less an "on/off" behavior in regards to power generation [7]. This means that there is a big risk of over-generation on windy days, and sudden energy breakdown, due to calms or storms. Figure 4 below shows the electricity generation in Germany for public power supply in 2017. This number is only increasing due to the goals of the "German Energiewende". The goals for the German Energiewende are as follows.

- 1) 55-60 % of retail electricity from renewable by 2035.
- 2) Nuclear phase-out by end of 2020.
- 3) 50 % reduction of primary energy demand by 2050
- 4) Development of energy storage devices, intelligent grids, and flexible fossil power plants.
- 5) Six million electric cars in Germany by 2030.

One can see that the increase in renewable energy in existing and future electricity production leads to the necessity of an extensive re-design of the grid topology, and the development of very reliable and flexible electrical machines [4]. It is therefore important to continuously develop the current grid. This must be done to assure a sufficient amount of rotating mass, such as the application and building of new fast-cycling power plants [15]. The variability of renewable energy sources has a significant impact on hydropower turbines [16]. The ramping capabilities of hydraulic units are highly appreciated since it is one of the best solutions to compensate for the unreliability of renewable energy sources.

There are no concrete plans from the US and European governments to reconstruct the present grid topology. This means that the increasing volatility of the current grid will be dealt with by the power plant operators. This also means that future hydro generators must be designed to handle this type of fluctuation in regards to the loading points. Most of the generators today are not designed for this kind of operational regime. Most hydro generators are designed in regards to a nominal operating point. In other words a classical mode of operation [17]. This also means that today's generators are designed for a continuous running duty cycle. Figure 5 shows the different duty cycles for generators and motor loads. As previously stated today's generators are designed for a continuous running duty cycle, but the increasing prevalence of renewable energy sources causes the operations to vary

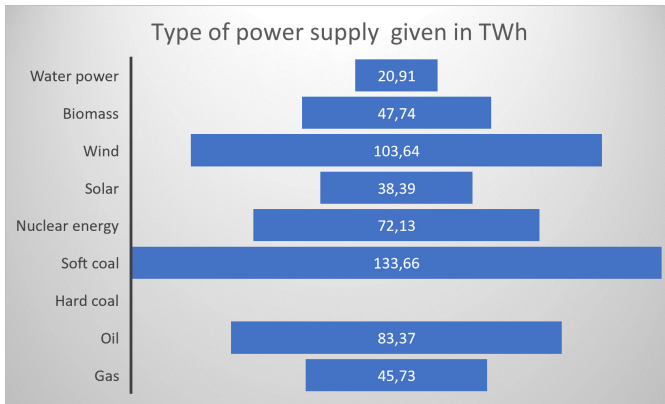
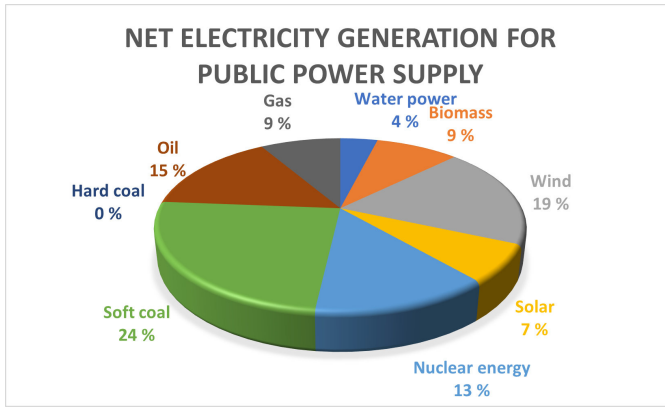


Fig. 4. The figure shows the net electricity generation for public power supply in Germany during the implementation of the Energiewende. The figure illustrates which type of electricity generation that is present and its prevalence [10].

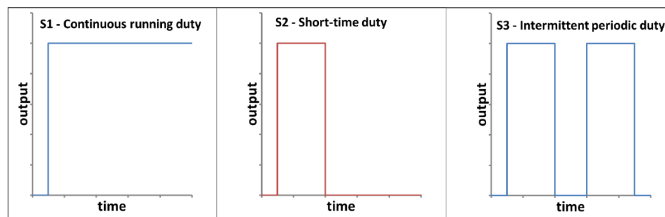


Fig. 5. Different duty cycles for generators and motor loads [10].

intermittently [18].

The introduction of renewable energy sources results in several starts and stop cycles in the day/week depending on the renewable energy generation. Due to the start and stop cycle there are frequent steps of active power and reactive power production to balance the weather dependant renewable energy sources [19]. Figure 6 shows that the introduction of renewable energy sources causes short-time duty cycles and intermittent periodic duty cycles. The increasing prevalence of this kind of operational regime gives rise to the study of calculation models to accurately quantify the impact of the energy transition.

#### A. The Energy Transitions Impact on the Short-Circuit Ratio

The short circuit capability of a power system is strongly correlated to the short circuit properties of its power genera-

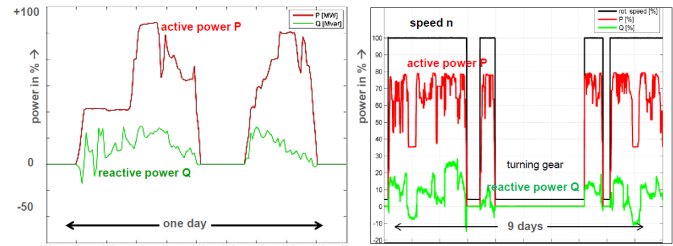


Fig. 6. Operational flexibility of Large turbine Generators-Duty Cycle. The short time duty cycle during a day (left plot) and the intermittent periodic duty cycle during nine days (right plot) [10].

tion, as well as the grid topology. The increasing mix of power generation will inevitably affect this issue. The short circuit ratio (SCR) of a generator refers to its ability to deliver a short circuit current to its terminal. The short circuit ratio can be expressed with equation 1. I.e it is the ratio of field current required to produce rated armature voltage at the open circuit, over the field current required to produce the rated armature current at short circuit [20].

$$SCR = k_c = \frac{i_{f0}}{I_{fk}} \quad (1)$$

Typical values of SCR for hydraulic units may be in the range of 1 to 1.5. The larger the SCR is, the smaller is the synchronous reactance in the d-axis. Consequently, this means that if the SCR is above 1, a power system has a good grid strength. This means that the generator will be less subjected to variations in frequency and can provide more short circuit current. The SCR can be calculated for each point on an electrical grid. I.e a point on a grid having several machines connected to it, with a SCR above a number between 1 and 1.5 has less vulnerability to voltage instability. Hence such a grid is known as a strong grid.

It is perceived that the SCR improves the grid stability, but it is observed to have a marginal performance improvement between 0.5 and 0.45 when using a fast high-gain excitation system [21]. In some grid typologies, there are long distances between the bulk production (hydro-generator) and the main consumption, this would mean a higher SCR. A high short circuit ratio for hydraulic units is important because it results in a machine that is loosely coupled to the grid and has a slow response. This increases the machines stability while operating connected to the grid, but simultaneously will increase the short circuit current delivery capability of the machine (higher short circuit current), and subsequently higher machine size and cost. The list below shows the following requirements that are usually considered in regards to the value of the SCR for hydraulic units and turbogenerators sets.

- 1) IEC 600343/IEEE C50.13 specifies a minimum SCR of 0.35
- 2) Most generators are designed to have  $SCR \geq 0.45$ .
- 3) Most grid codes require  $SCR \geq 0.5$ .

In addition to the normal SCR, a dynamic SCR might be important in cases where short-term reactive power capability (RPC) of the machine is utilized in combination with more advanced control schemes [22]. The reactive power capability



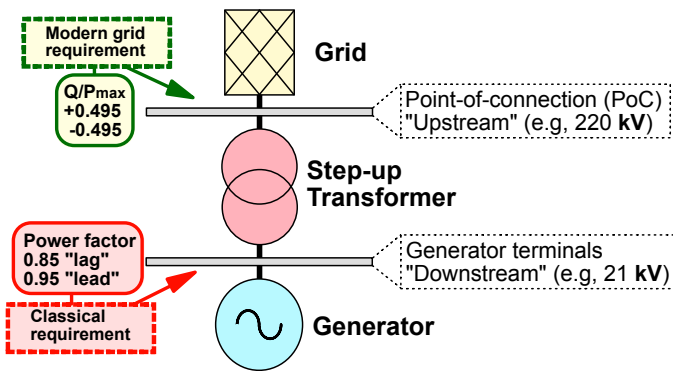


Fig. 7. Different grid code requirements for reactive power capability [25].

is closely coupled with the short circuit ratio [23]. One example could be that a high SCR enhances the RPC significantly. This is because the high SCR reduces the synchronous reactance in the d-axis  $X_d$ , which reduces the internal parasitic reactive power consumption of the generator [24]. This is important because the introduction of renewable energy causes a wider operational range in reactive power production and consumption. It is therefore important to have generators with good RPC. Figure 7 shows the grid code requirements for reactive power capability at different terminals.

### B. Energy Transitions Impact on Turbogenerator sets and Hydraulic Units

Figure 8 clearly illustrates the temperature change in generators due to future operational regimes of turbo-generator sets and hydraulic units under the influence of increased solar and wind power generation. The short and steep load ramps can result in significant thermo-mechanical stresses on the generator [26]. This is because the components in the machine are heated up during a very short period [27]. This results in a vast temperature difference from standstill to full load. The losses are proportional to the current, which means that the current-carrying parts, such as the rotor and stator windings will have significant losses [28]. This means that most of the temperature rise will occur in these parts compared to the part conducting the magnetic flux, such as the rotor body and stator body [29]. This in combination with the thermal expansion coefficient of the material will cause mechanical stresses and also contribute to accelerated aging of the insulation system [30]. Another important consideration is that the bearing and coupling are penetrated by higher mechanical stresses during this ramping time [31]. This problem is perpetuated by the fact that the number of start and stop cycles is increasing under this new operational regime.

### C. The Introduction of an Extended Capability Diagram to handle Increasing Load Variation

As previously stated the increasing start and stop cycle affects the temperatures in the generator. Adaptive cooling will be needed to avoid the high ventilation losses under low loading conditions and to reduce the repetitive thermal expansion occurring as a result of the energy transition. The

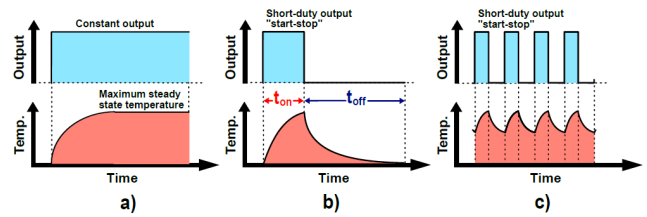


Fig. 8. The figure illustrates the temperature change in a generator for three different load cycles. Figure a) illustrates the temperature change during constant output. Figure b) illustrates the short time duty cycle during a day and figure c) illustrates the intermittent periodic duty cycles during nine days [10]

lifetime and thermal aging must be carefully considered when designing and operating the machine for future operational regimes.

Because of the increasing prevalence of renewable energy, there will be a need for utilization of an extended capability diagram [32]. Figure 8 show that "extreme points" may be realized in short periods. Figure 8 also shows that very high temperatures are reached due to the wider operational range. The operational point at the outer edges of the capability diagram is considered "extreme points". This is because the generator is not designed to operate at those points for long periods. This is mainly due to the large thermal inertia and the corresponding thermal time constants available in the machine [33]. The use of new real-time monitoring and control technology means that a dynamic envelop regime can be enforced on the generators. This would enhance the flexibility of the generator [34].

An example of these "extreme operating points" can be illustrated using a boundary profile. The European Network of Transmission System Operators for Electricity (ENTSO-E) and the Transmission System Operator (TSO), have made a boundary profile in regards to  $Q/P_{max}$  and terminal voltage. Figure 9 represents the boundary profile for a synchronous generator (eg. hydro generator) defined by ENTSO-E and the TSO requirements.

If one first considers the upper right corner (overexcited) of the envelope illustrated in figure 9 one can see that for the generator to satisfy such an operation point, the max power must be downrated to about 0.8 pu. The generator terminal has to operate at a voltage level of  $U_t = 1.10$  pu, which is outside the typical machine design specifications of  $\pm 5\%$ . Another "extreme operating point" is the lower-left corner (underexcited) of the envelope. In a condition like this, the generator needs to provide an unsatisfactory high stator current to provide the same power [35].

The new operational regime and ENTSO-requirements increase the range of the loading point points in the capability diagram. Figure 10 illustrates the distribution of loading points in the capability diagram of the 300 MVA generator. The figure also illustrates the change due to the energy transition. a) Before "German Energiewende", and b) After. In addition, the figure 10 also illustrates the probability of a loading point to occur. The figure shows an increase in range in addition to

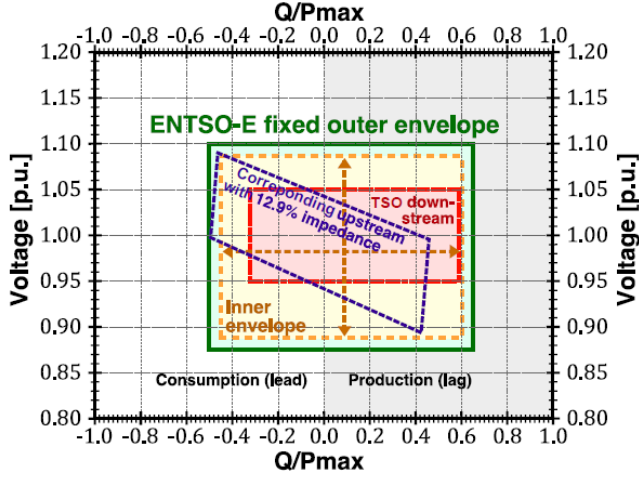


Fig. 9. Typical  $V$ - $Q/P_{max}$  requirements of a synchronous power generating module from ENTSO-E. In addition, the TSO requirements for downstream and upstream profile (referred  $Q/P_{max}$  at the generator side) are indicated. [10].

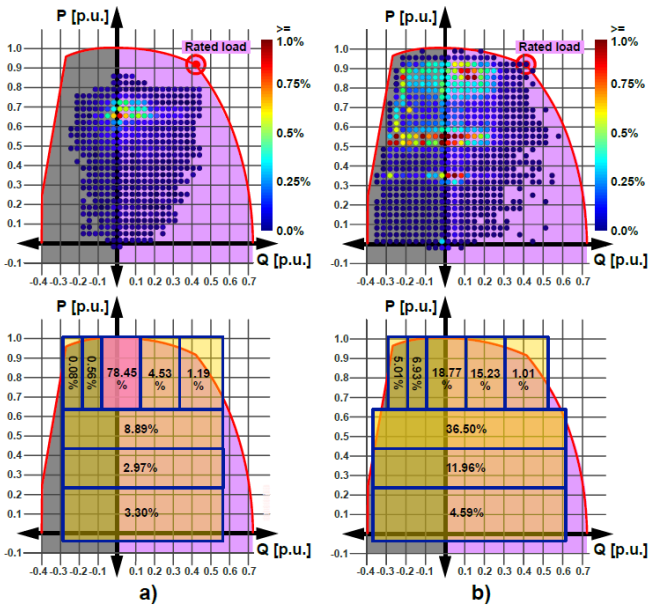


Fig. 10. The distribution of load points in the capability diagram of 300 MVA generator. The figure illustrates the relative changes due to the energy transition. a) Before the "German Energiewende" and b) After. [10]. The figure is also an example of an uniform load distribution, because the load points are much more evenly distributed.

an increase in the generator's duration time in those "extreme operating points". The probability of a loading point to occur is illustrated using zones. In other words figure b illustrates that there is a 36 % probability of occurrence for a loading point to occur when the active power is between (0.45-0.65).

#### IV. DESCRIPTION OF THE CASE STUDIES

To investigate the impact of the energy transition on the hydro-generator facilities, two distinct case studies were made. The machine under study is hydro generator G1 and G2.

TABLE I  
KEY RATED QUANTITIES OF HYDROGENERATOR G1

Symbol	Description	Value
$S_b$	Base apparent power	160 MVA
$\cos(\varphi)$	Power factor	0.95
$\eta_n$	Measured rated efficiency	98.5 %
$U_t$	Nominal armature voltage	15.0 kV
$I_t$	Nominal armature current	6158 A
$I_f$	Rated field current	1047.0 A
$f$	Nominal frequency	50 Hz
$R_a$	Armature resistance	0.00232 pu
$X_d$	Direct axis reactance	0.8 pu
$X_q$	Quadrature axis reactance	0.6 pu
$X_p$	Potier reactance	0.18 pu

TABLE II  
KEY RATED QUANTITIES OF HYDROGENERATOR G2

Symbol	Description	Value
$S_b$	Base apparent power	103 MVA
$\cos(\varphi)$	Power factor	0.90
$\eta_n$	Measured rated efficiency	98.834 %
$U_t$	Nominal armature voltage	11 kV
$I_t$	Nominal armature current	5406 A
$I_f$	Rated field current	1065 A
$f$	Nominal frequency	50 Hz
$n$	Nominal speed	500 rpm
$R_a$	Armature resistance	0.002 pu
$X_d$	Direct axis reactance	1.059 pu
$X_q$	Quadrature axis reactance	0.676 pu
$X_p$	Potier reactance	0.141 pu

The generator under focus in Section VI. Methods is hydro-generator G1 which is the generator used in the Furnas hydropower plant in Brazil. The data for this generator is extracted from the technical report written by Bortoni [11].

The Norwegian hydro generator Åbjøra (hydro-generator G2) is used in the Section VII. Results to illustrate that this study can be applicable for hydro-generator of different sizes and characteristics. The studies that were done in Section VI and VII show that one can develop an algorithmic procedure for calculating the WAE and AAE using the generators rated data and losses at the rated operation as input for the algorithm. The rated quantities for generator G1 and G2 is illustrated in table I and II. The rated losses for the generators can be seen in Table III.

TABLE III  
LOSS DATA OF THE MACHINES EXTRACTED AT RATED CONDITION.

Loss component	hydro generator G1		hydro generator G2	
	SI value	PU value	SI value	PU value
$P_a$	327.05 kW	0.0020 pu	187.46 kW	0.00182 pu
$P_s$	237.07 kW	0.0015 pu	89.16 kW	0.0009 pu
$P_{wf}$	710.47 kW	0.0044 pu	172.92 kW	0.0017 pu
$P_c$	539.87 kW	0.0034 pu	211.92 kW	0.0021 pu
$P_b$	156.17 kW	0.0009 pu	240.9 kW	0.0023 pu
$P_f$	477.81 kW	0.0030 pu	173.65 kW	0.0017 pu
$P_{ex}$	33.96 kW	0.0002 pu	15.88 kW	0.0002 pu
$P_{br}$	5.93 kW	0.0000 pu	2.13 kW	0.0000 pu
$P_{loss}$	2488.33 kW	0.0154 pu	1094.02 kW	0.01062 pu

## V. THEORETICAL FRAMEWORK FOR LOSS AND EFFICIENCY CALCULATION AND IMPORTANT DEFINITIONS

This section consists of the theoretical basis for the main objective of this report, which is comparing the calculation models WAE and AAE. The important nomenclature used in this project can be seen below.

### NOMENCLATURE

$\Delta t_i$	Discrete time interval for a load point, [h] or [s]
$\delta$	Rotor loading angle, [rad] or [°]
$\eta$	Generator's operation point efficiency, [pu] or [%]
$\eta_a$	Accumulated average efficiency (AAE), [pu] or [%]
$\eta_n$	Generator's nominal efficiency, [pu] or [%]
$\eta_w$	Weighted average efficiency (WAE), [pu] or [%]
$\mathcal{E}_g$	Induced generator voltage, [pu] or [V]
$\mathcal{E}_p$	Induced voltage behind potier reactance, [pu] or [V]
$\overline{P}$	Average power, [pu] or [kW]
$\overline{P}_{loss}$	Average power loss, [pu] or [kW]
$\theta$	Angle behind the potier reactance, [rad] or [°]
$\varphi$	Power factor angle, [rad] or [°]
$A_i$	Weighting factor for an operation point, [pu] or [%]
$b_v$	Slope constant of the generator's air gap line curve
$C_m$	Saturation constant for the generator's saturation curve
$E$	Total energy production, [GWh]
$E_{loss}$	Total energy losses, [GWh]
$I_a$	Stator armature current, [pu] or [A]
$I_f$	Rotor field current, [pu] or [A]
$k$	Slope constant for approximating the generator' saturation curve in the air gap line region
$m$	Saturation curve's exponential constant
$P$	Generator's active power, [pu] or [MW]
$P_a$	Stator armature winding resistive loss, [pu] or [kW]
$P_{be}$	Bearing loss, [pu] or [kW]
$P_{br}$	Rotor brush loss, [pu] or [kW]
$P_c$	Stator armature iron core loss, [pu] or [kW]
$P_{ex}$	Excitation system loss, [pu] or [kW]
$P_f$	Rotor field winding resistive loss, [pu] or [kW]
$P_{loss}$	Generator's total losses, [pu] or [kW]
$P_s$	Stator stray load loss, [pu] or [kW]
$P_{wf}$	Windage and friction loss, [pu] or [kW]
$Q$	Generator's reactive power, [pu] or [MVar]
$R_a$	Armature resistance, [pu] or [ $\Omega$ ]
$S$	Generator's apparent power, [pu] or [MVA]
$U_a$	Terminal voltage, [pu] or [V]
$X_d$	Direct axis synchronous reactance, [pu] or [ $\Omega$ ]
$X_p$	Potier reactance, [pu] or [ $\Omega$ ]
$X_q$	Quadrature axis synchronous reactance, [pu] or [ $\Omega$ ]
N	The number of elements
T	The number of discrete loading points

The equations used for calculating the losses in the different loading points and the efficiency of the generator during different loading points can be seen in equations (2)-(9). The active power losses marked with "\*\*", represent the different losses during rated operations. The current and voltage marked with "\*" represent the rated armature current ( $I_A$ ), field current

( $I_F$ ), and terminal voltage ( $U_a$ ) respectively.

$$P_a = P_a^* \left( \frac{I_A}{I_A^*} \right)^2 \quad (2)$$

$$P_f = P_f^* \left( \frac{I_F}{I_F^*} \right)^2 \quad (3)$$

$$P_s = P_s^* \left( \frac{I_A}{I_A^*} \right)^2 \quad (4)$$

$$P_{br} = P_{br}^* \left( \frac{I_F}{I_F^*} \right)^2 \quad (5)$$

$$P_{ex} = P_{ex}^* \left( \frac{I_F}{I_F^*} \right) \quad (6)$$

$$P_c = P_c^* \left( \frac{U_A}{U_A^*} \right)^2 \quad (7)$$

$$P_{Loss} = P_a + P_f + P_s + P_{br} + P_{ex} + P_b + P_{wf} + P_c \quad (8)$$

$$\eta = \frac{P}{P + P_{Loss}} \quad (9)$$

To better grasp the concepts and the challenges facing the energy transition some definitions have been made and articulated.

1) *Exact/specific loading point*: A specific loading point is defined as a loading point with two decimals or less that occurs frequently in a production dataset, meaning more than once. This could for example be the nominal operating point of hydro generator G2 which is (0.33, 0.95), or an arbitrary operating point (0.1,0.4).

2) *Discrete loading point*: A discrete loading point is defined as an operating point that is not exact, in other words, a loading point that is unique in a dataset. This means that the loading point only occurs once in a production dataset and often consists of several decimals.

3) *Density/resolution*: In this study, the density is referred to as the space between the loading points. This means that high density represents several discrete loading points in close proximity.

4) *Iso-efficiency curves*: Non-concentric curves that depict the efficiency at different loading points.

5) *Weight*: The probability of occurrence for an exact/specific loading point. This means that the frequency of an exact loading point is counted. In other words the duration of a particular loading point.  $\Delta t$  represents the duration (hour) of a particular loading point i.e the frequency of occurrence. The constant T represents the generators running time during a year. Bortoni's definition of weight is therefore the time interval of a loading point over the total duration time of a generator during a given year. The equation for the weight is illustrated below.

$$A_i = \frac{\Delta t}{T} \quad (10)$$

6) *Equal weight distribution*: The calculation model Accumulated Average Efficiency assumes an "equal weight distribution". This means that the discrete loading point is not rounded up to two decimals. Instead of counting the frequency of an exact loading point, every discrete loading point in a dataset is unchanged. This also means that every discrete loading point has the same weight therefore the name "equal weight distribution". It also means that the weight for discrete loading points is constant and not dependant on the time intervals because they only occur once. In other words, the weight is constant and equal to  $1/T$ . The weight when an equal distribution is assumed can be seen in equation [11]

$$A_i = \frac{\Delta t}{T} = \frac{1}{T} \quad (11)$$

7) *Concentrated load distribution*: Most of today's generators operate with concentrated load distribution, meaning most of the loading points are concentrated within a relatively small area. The production data from Åbjøra is a prime example. From this data, one can see three distinct characteristics. The first characteristics are that most of the loading points are around  $P_{max}$ , and not as much evenly distributed throughout the capability diagram. The second characteristics are that the range in reactive power production and consumption does not vary that much. In Åbjøra's case, it varies from -0.08 to 0.175 pu. The third characteristics are that almost all of the loading points are above 0.6 pu, in most cases the loading point below this value is usually because the generator is turned off.

8) *Uniform load distribution*: Future hydro generators will operate with uniform load distribution, meaning the load distribution will be uniformly distributed throughout the capability diagram. Figure [10] is a prime example of the difference between concentrated load distribution and uniform load distribution. Figure a) shows the load distribution before Germany's "Energiewende", while figure b) shows the load distribution when the "German Energiewende" is set in motion. This figure illustrates what happens when there is a disconnection of conventional power plants and a lot of renewable energy sources are connected to the grid. Uniform load distribution has primarily three characteristics. The first characteristics are that the loading point is more or less evenly distributed throughout the capability diagram. The second characteristics are that the range in reactive power consumption and production varies drastically. The third characteristics are that more loading points are below 0.6 pu compared to concentrated load distribution, this is primarily because the generator operates more often as a synchronous condenser. The reason for this is further explained in Section [IV]

9) *Synchronous condenser distribution*: The synchronous condenser distribution is "The worst-case scenario". This kind of distribution is illustrated in figure [24]. In this distribution, a lot of the loading points are concentrated around 0 pu active power. Forcing the generator to operate as a synchronous condenser. For the case in figure [24], the generator is operating below 0.02 pu active power 50 % of the time. This figure also illustrates what happens when a lot of renewable energy sources are connected to the grid. Renewable energy sources like wind and solar do not produce reactive power only active

power. This forces hydro generators to produce little or no active power. This is because the active power demand is satisfied by renewable energy sources. This means that a lot of the time, the hydro generators either provide or consumes reactive power from the grid. The hydro generators work as a synchronous condenser by producing little or no active power and mostly providing or consuming reactive power. This gives rise to the name synchronous condenser distribution.

#### A. Important Presuppositions Regarding Calculations done in this Report

1) *Steady state*: All the loading points are assumed to be steady-state. This means that there are no transient or sub-transient events for the different loading points.

2) *Infinite grid*: The generator is connected to an infinite grid. This means that the voltage is stiff and equal to 1 pu for all loading points. The generator terminal is chosen as the reference point and is therefore given the value 1 pu and 0 degrees. This also means that the armature current is directly proportional to the apparent power. This can be seen in equation [12]

$$I_A = \frac{S}{U_A} = \frac{\sqrt{(P^2 + Q^2)}}{1} \quad (12)$$

3) *Synchronous reactance*: The synchronous reactance used in this report is the reactance from the generator to the generator terminal. This implies eg. that the synchronous reactance in the d-axis is the summation of the armature reaction reactance and the leakage reactance.

4) *The armature resistance*: The armature resistance is included in all the calculations except for the calculation of the practical stability limit (PLS). It is assumed to be 0 for the PLS calculation.

## VI. METHOD

### A. Magnetic Saturation

In this subsection, three methods for calculating the magnetic saturation are presented. Determining saturation is a difficult task. In the book power system stability [36] Kundur states that "Any practical method of accounting for saturation effects must be based on semi-heuristic reasoning and judiciously chosen approximations, with due consideration to the simplicity of model structure, data availability, and accuracy of results.". The first method presented is the Anderson and Fouad method. The Anderson and Fouad method was used in the specialization project [37] to quantify the level of saturation and replicate the iso-efficiency curves in Bortoni's technical report. This subsection also explains Bortoni's method of quantifying saturation. The third method uses a fitting function to quantify the field current during saturation. These three methods are presented to illustrate that one can use several methods to determine magnetic saturation. These methods are compared in regards to their simplicity and accuracy.

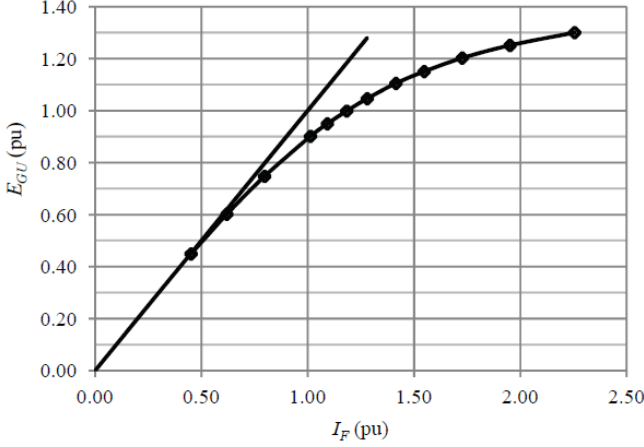


Fig. 11. The airgap line and the open circuit characteristics of the hydrogen-generator G2 [1].

1) *Anderson and Fouad method*: Operating a generator with a very flexible operational range causes high stresses on the excitation system [38] and significant excitation losses [39]. This means that more robust excitation systems must be built in the future [32]. This must be done so that future excitation systems can withstand the thermo-mechanical stresses [40]. Another alternative is to implement expensive power electronics to reduce the variation in reactive power [33].

As previously stated the new operational regimes causes an increase in thermal-mechanical loading and load variation, which again causes significant stresses on the excitation system. Consequently, the losses related to the field current and magnetic saturation play a much more significant role in determining the losses and the efficiency of the hydro-generator during different loading points. In other words, this means that one can not assume that the generator's field current  $I_f$  is directly proportional to the induced voltage  $E_g$ .

Several assumptions must be made before one determines the saturation. The main assumption is presented below in chronological order:

- 1) The Leakage inductance and Potier inductance are independent of saturation.
- 2) The only inductance affected by saturation is the mutual inductance  $L_{ad}$ .
- 3) Since the generator's understudy is salient pole generators it is assumed that the saturation occurs only in the d-axis.
- 4) Because load tests is not available. Saturation is determined using the open-circuit characteristics.
- 5) The induced voltage  $E_g$  is equivalent to the terminal voltage  $U$ , This is because the saturation is determined during no-load.

The open-circuit characteristics (OCC) can be seen in figure [1]. The figure shows the induced voltage in the air gap as a function of the field current. This means that one must select an appropriate method and procedure to determine the saturation for all operations. This is because saturation must be determined based on the available data and the most applicable

method. One of the most applicable methods is the method developed by Anderson and Fouad. The procedure for the method is further explained in the journal "Computer-aided analysis of saturation in synchronous machines" [41]. Equation [13] is used to fit the saturation curve.  $V$  is the terminal voltage,  $n$  is either number 7 or 9,  $c$  and  $k$  are arbitrary constants. The induced voltage  $E_g$  can be used instead of  $V$  in the fitting function. The slope of the air gap is equal to 1 pu. This means that the assumption made for the air gap line is that field current is directly proportional to the induced voltage. The airgap line is replicated using equation [14]. When generators have a linear characteristic, i.e. the field current is directly proportional to the induced voltage, saturation is neglected. The equation for the armature reaction reactance, when saturation is neglected, can be seen in equation [15]. Notice that the Potier reactance is used instead of the leakage reactance  $X_l$ . Another noticeable remark is that saturation only occurs in the d-axis. This is because the flux takes the path of least reluctance. The reluctance is much smaller in the d-axis because the air gap is much smaller in the d-axis compared to the q-axis. In other words, the airgap is non-uniform in a salient pole generator forcing the flux to travel mostly through the d-axis.

$$I_{fd} = (V + C * V^n) * k \quad (13)$$

$$I_f = E_g \quad (14)$$

$$X_{adu} = X_d - X_p \quad (15)$$

As previously stated, the equation determining the armature reaction reactance when saturation is neglected is given by equation [15]. By rearranging the equation one can determine the synchronous reactance in the d-axis  $X_d$ . The synchronous reactance is illustrated in equation [16]. The equation illustrates that the armature reaction reactance and the synchronous reactance are both affected by saturation.

$$X_d = X_{adu} + X_p \quad (16)$$

To get the correct slope of the saturation curve the saturation curve was optimized around the three points marked in figure [12]. The light blue line and the orange lines intersection point are used to optimize the saturation curve around the intersection point (2.25,1.3). The light blue line and the orange line are used to optimize the saturation curve around the point (1.5,1.1). The pink and yellow lines intersection point is used to optimize the saturation curve around the point (1.0,0.9). The green line was used as a proxy to see if the slope of the saturation curve between the intersection point were also correct. These points were chosen based on the fact they were relatively easy to read/estimate from the given OCC.

The Anderson and Fouad method state that once the air gap line and the saturation curve are plotted the following step of the procedure is to then determine the saturation factor  $S$ , which is scaled in regards to the open circuit characteristics

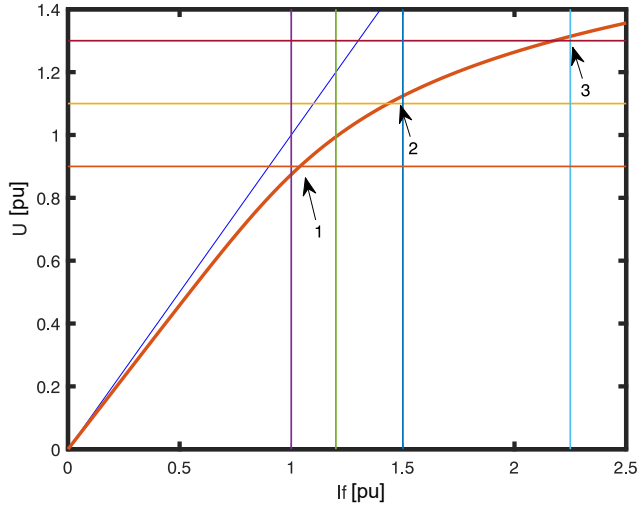


Fig. 12. The figure illustrates the three points that the saturation curve was optimized around [37].

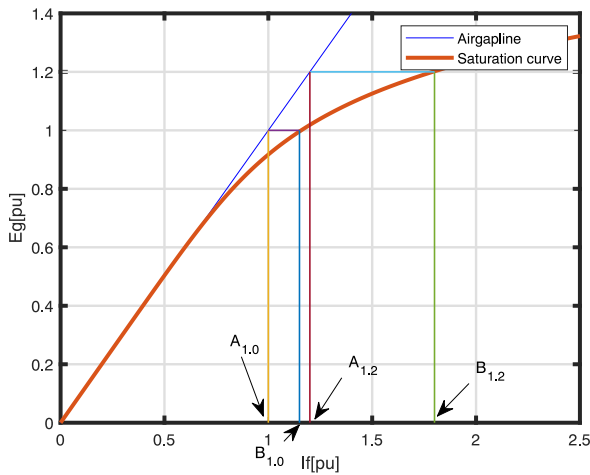


Fig. 13. The figure illustrates the procedure for calculating the saturation factors  $S_{1.0}$  and  $S_{1.2}$  [37]. By using the constants  $A_{1.0}$ ,  $A_{1.2}$ ,  $B_{1.0}$  and  $B_{1.2}$ .

of the generator. The first step is to calculate the saturation factor  $S$  when the induced voltage/terminal voltage is at its rated value and 20 % overvoltage. The saturation factor is determined from the computed air gap line and saturation curve. This procedure can be seen in figure [13]. The figure illustrates the field current giving the air gap line and the saturation curve a terminal voltage of 1 pu. and 1.2 pu. These field currents are used to determine the saturation factor  $S_{1.0}$   $S_{1.2}$

As one can see from figure [13], the saturation factor at rated terminal voltage  $S_{1.0}$  and the saturation factor at 20 % overvoltage  $S_{1.2}$  is found from the saturation curve. The saturation factors are calculated using equation [17] and [18]. The constants  $A_{1.0}$ ,  $A_{1.2}$ ,  $B_{1.0}$  and  $B_{1.2}$  are equivalent to the field currents giving rated terminal voltage, and 20% overvoltage for the airgap line and the saturation curve.  $A_{1.0}$  and  $A_{1.2}$

represent the field currents resulting in a terminal voltage equal to 1 pu and 1.2 pu on the air gap line. The constant  $B_{1.0}$  and  $B_{1.2}$  represent the field currents resulting in a terminal voltage equal to 1 pu and 1.2 pu on the saturation curve. The saturation factors  $S_{1.0}$  and  $S_{1.2}$  are then used to calculate two saturation constants  $A_{sat}$  and  $B_{sat}$ . The equation used for calculating  $A_{sat}$  and  $B_{sat}$  can be seen in equation [19] and [20].

$$S_{1.0} = \frac{B_{1.0} - A_{1.0}}{A_{1.0}} \quad (17)$$

$$S_{1.2} = \frac{B_{1.2} - A_{1.2}}{A_{1.2}} \quad (18)$$

$$A_{sat} = \frac{S_{1.0}^2}{1.2 * S_{1.2}} \quad (19)$$

$$B_{sat} = 5 \ln(1.2 \frac{S_{1.2}}{S_{1.0}}) \quad (20)$$

The saturation factor for all operations is expressed as an exponential function. The saturation factor  $S$  is given in equation [21]. The saturation factor is an exponential function consisting of the saturation constants  $A_{sat}$ ,  $B_{sat}$  and the threshold voltage  $U_T$ , which is 0.43 in this case. The saturation factor is a function of the induced voltage and therefore scaled in regards to the induced voltage  $E_g$ .

$$S = A_{sat} * e^{B_{sat} * (E_g - 0.43)} \quad (21)$$

The saturation factor is then converted to the saturation factor  $K_{sd}$ . This is done because the saturation factor  $K_{sd}$  can be multiplied with the armature reaction reactance  $X_{adu}$  to give a lower value of  $X_{adu}$  depending on the level of saturation. This is done to quantitatively express the decrease in armature reaction reactance when there is an increase in saturation. By using equation [21], [22] and [23]. One can model the level of saturation for different induced voltages and quantify its influence on the armature reaction reactance and field current.

$$K_{sd} = 1/1 + S \quad (22)$$

$$X_{adsat} = X_{adu} * K_{sd} \quad (23)$$

$$X_{dsat} = X_{adsat} + X_p \quad (24)$$

If one assumes that all load conditions are steady-state, the use of  $X_p$  instead of  $X_l$  is believed to make an empirical allowance for the difference between the saturation during the loaded condition and no-load condition.

This is primarily because the leakage flux under loaded conditions and the no-load condition are different. The field leakage under loaded conditions is higher. The Potier reactance accounts for the difference and is higher than the leakage inductance. This means that the field current can be expressed using equation [25] and [26] below.

$$E_{gsat} = U_A * \cos(\delta) + R_A * I_A * \cos(\delta) + X_{dsat} I_A \sin(\phi + \delta) \quad (25)$$

TABLE IV  
THE POLYNOMIAL COEFFICIENTS OF HYDRO GENERATOR G1.

Symbols	$b_0$	$b_1$	$b_2$	$b_3$	$b_4$
Values	2.0737	-10.959	24.85	-22.228	7.4417

$$I_{fd} = \frac{E_{gsat}}{X_{ad,sat}} \quad (26)$$

An important assumption in regards to the OCC is that the saturation is divided into segments these segments are called linear characteristics, nonlinear saturation characteristics, and linear saturation characteristics. The linear saturation characteristics are neglected. This is because this generator does not operate with an induced voltage giving a linear saturation characteristic. It is also because linear characteristics and non-linear saturation characteristics are usually the only segments of interest. This is further explained in kundur's power system and stability [36].

2) *Bortoni's method*: During linear characteristics, the field current is directly proportional to the induced voltage with the assumption that the slope  $b_v$  in pu is 1. This can be seen in equation [27], but as soon as the generator reaches its threshold voltage one must include the saturation increment.

$$I_{fu} = \frac{E_g}{b_v} \quad (27)$$

Bortoni's method does not use saturation factors, Bortoni's method takes a fourth-order polynomial regression of the non-linear saturation characteristic to get five polynomial coefficients. He then uses the polynomial coefficient to calculate the field current during non-linear saturation characteristics, which he refers to as the saturation increment. This can be seen in equation [28].

$$I_{fs} = \left( \sum_{i=1}^n b_i E_p^i \right) - \frac{E_p}{b_v} \quad (28)$$

This means that the field current of the generator when it's past the threshold voltage is  $E_g$  plus the saturation increment. This can be seen in equation [29]. Bortoni states that "The saturation increment is the difference between the excitation current value required to induce  $E_p$  on the air-gap line and value of field current corresponding to  $E_p$  on the no-load saturation curve." [1]. In other words for Bortoni's case, the threshold voltage is reached when  $E_p > 0.43$  and not  $E_g$  like in the Anderson and Fouad method. The polynomial coefficient of the generator can be seen in Table [IV].

$$I_f = \frac{E_g}{b_v} + \left( \sum_{i=1}^n b_i E_p^i \right) - \frac{E_p}{b_v} = I_{fu} + I_{fs} \quad (29)$$

3) *fitting function as saturation increment*: This report introduced a new approach to accurately quantifying the saturation. As previously mentioned, the new operational regimes cause significant changes in the load cycling of the generator's excitation system. Consequently, the losses related to the field current and the machine's magnetic saturation play a much more significant role in determining the losses and the

efficiency. This means that it is very important to accurately quantify the saturation. If this is not accurately done it will manifest itself in the iso-efficiency curves. The results section in this report uses the fitting function illustrated in equation [13] which stems from Machowski's power system dynamics and control [3]. This report's contribution is that the constant  $k$  is added to the original equation. This is done to align the saturation curve with the air gap line. Making it possible to use the equation to model the linear characteristics and non-linear saturation characteristics. The equation and assumption used to model the field current can be seen below. This method is chosen because it is more user-friendly and highly accurate. This is because one can visually adjust the constants  $C_m$  and  $k$  to fit the air gap line and non-linear saturation characteristics exactly and then directly implement the function to calculate the field current.

$$I_{fs} = k(\mathcal{E}_g + C_m \mathcal{E}_g^m) \quad (30)$$

$$I_f = I_{fu} + I_{fs} = \frac{\mathcal{E}_g - \mathcal{E}_p}{b_v} + k(\mathcal{E}_p + C_m \mathcal{E}_p^n) \quad (31)$$

4) *comparing the methods*: Using the fitting function as saturation increment is the most user-friendly and least time-consuming. The method is also very accurate and is, therefore the chosen method in Section [VII]. The Anderson and Faoud method is accurate because the saturation factor can be tuned to approximate the non-linear saturation characteristics. The drawback is that it is time-consuming to calculate the saturation factors. Bortoni's method is less time-consuming, but the method is not as accurate as the Anderson and Faoud method and fitting function method. This is because the polynomial coefficients are difficult to tune, once the fourth-order regression is done.

## B. V-Curve Family

As previously stated the armature current is directly proportional to the complex power output. The field current must be calculated for each operating point considering saturation as previously described. For the generator under study the  $X_d$  is 0.8 pu,  $X_q$  is 0.6 pu and  $X_p$  is 0.18 pu and  $R_a$  is 0.00232 pu. If one applies the equation for the armature current and the equation for the field current one can obtain the Mordey diagram also known as the V-curve family. This can be done by relating the armature current to the field current, for several constant active powers. Figure [14] presents the Mordey diagram, for powers varying from 0 to 1 in steps of 0.2. This means that the active power is held constant and the reactive power is gradually changed, which changes the field current. Once the reactive power is gradually increased from minimum to maximum, the active power is increased with a step of 0.2. The purpose of the V-curve is to show the variation in magnitude of the armature current as the field current is varied. The power factor of the synchronous generator can be controlled by varying the field current  $I_f$ . If one assumes that the generator is running in no-load the armature current is reduced to its minimum value. The generator operates with a lagging value until it reaches this point. If the field current

is increased further, the armature current increase and the generator starts operating with a leading power factor. The lowest point of all the V-curves for various power levels is called the unity power factor compounding curve. The curves on each side of the unity PF compounding curve are called compounding curves. This is illustrated in figure 15. Some V-curve family plots also include the armature core end heating limit. Two primary points are considered when including the armature core end heating limit. The first point is defined as 75 % of the rated armature current and 25 % of the rated excitation current. The second point is defined as 100 % of the rated armature current and the rated power factor. The field current is then determined as depicted in figure 15.

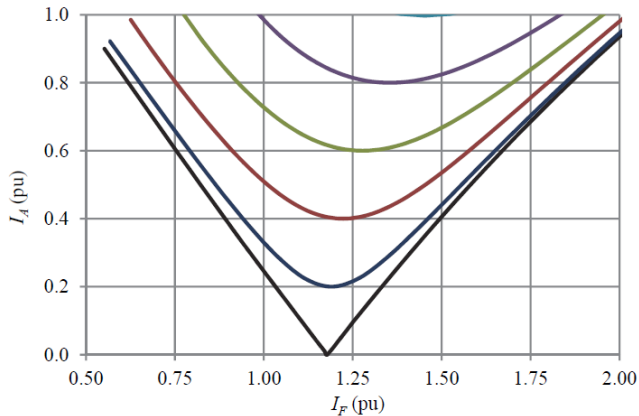


Fig. 14. The figure illustrates the V-curve of hydro generator G1 [11].

The V-curve family does not show the power factor of the generator for all the different loading points. The capability diagram and power factor lines are often used to illustrate the different power factors of the generator for different loading points. This can be seen in figure 16.

### C. Iso-Efficiency Curves

Once the saturation model and V-curve family are established one can determine the iso-efficiency curves. Figure 17 is the iso-efficiency curves calculated using Bortoni's method. The data points of these iso-efficiency curves were extrapolated so that they could be experimentally compared with the iso-efficiency curves calculated using the Anderson and Fouad method, and the given OCC of the generator illustrated in figure 11. As one can see from figure 18, the iso-efficiency curves are almost perfectly aligned with the extrapolated data points. If one compares figure 17 and 18 one can see that they are almost identical. This illustrates that one can use several methods to quantify the level of saturation.

From the iso-efficiency curves, one can see that the iso efficiency curve close to the nominal operating point is 98.4, which is the rated efficiency for the generator given in Table 1. This also indicates that the iso-efficiency curves are correct.

The saturation modeling is the most sensitive loss component, this means that if the field currents saturation characteristic is not accurately model. The discrepancy between the

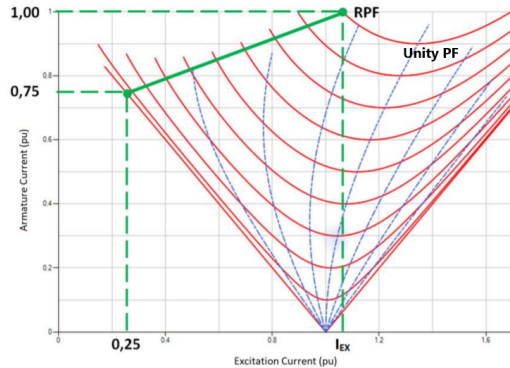


Fig. 15. The figure illustrates the V-curve of hydro generator G1 [11] with armature end heating limit.

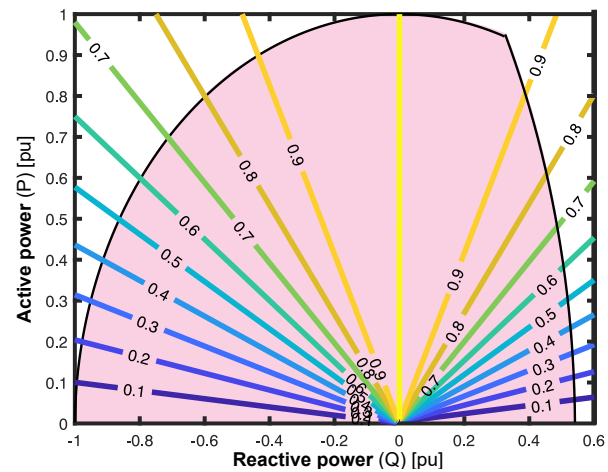


Fig. 16. The different power factors of generator G1 for different loading points [37].

iso-efficiency curve labeled 98.4 and the nominal operation will be vast and prevalent in the iso-efficiency map.

The iso-efficiency curves are non-concentric curves because of the saturation. When the generator reaches its threshold voltage, the relationship between the field current and the induced voltage is no longer linear. The reason for this is because the iron cores in the generator saturate and reach a magnetic saturation [31]. This means that the excitation system in the generator must provide a higher field current to produce the same induced voltage as the generator during linear characteristic [42]. This is illustrated as a decrease in efficiency and a small downward tilt of the iso-efficiency curves. I.e the generator becomes more saturated as it increases its reactive power production.

### D. Determining the Boundaries of the Capability Diagram

This subsection focus on how the outer limits of the capability diagram can be determined. This subsection also determines the underlying mechanism and theoretical basis for the limits. The MATLAB code used to illustrate the capability diagram is placed in the appendix.



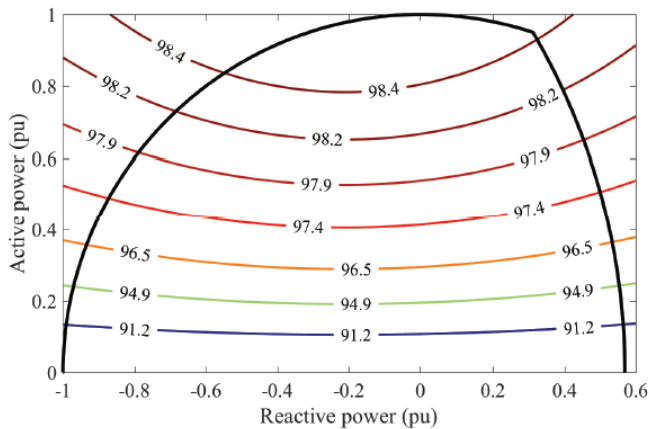


Fig. 17. The machine under study from the technical report [1] (hydro generator G1).

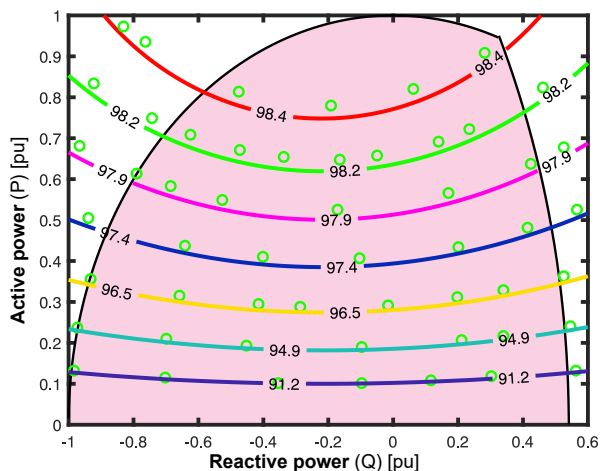


Fig. 18. The iso-efficiency curves of generator G1 experimentally compared with the extrapolated datapoints of the iso-efficiency curves calculated using Bortoni's method. [37].

To explain the capability diagram one must first determine the underlying mechanism and theoretical basis. This must be done to explain the important characteristic and assumptions limiting the capability diagram. Bortoni's technical report [1] illustrates a capability diagram bounded by its armature current and maximum field current. The rated data of generator G1 is given in actual values and converted to a per-unit value system before the capability diagram is plotted. The rated data for this generator can be seen in Table I. The main literature used to replicate the capability diagram in Bortoni's technical report is the paper "MATLAB Model for Visualization of PQ diagram of a Synchronous Generator" [43].

The capability diagram has maximum and minimum active and reactive power. The reactive power limitation is a function of the real power output of the generator. This means that when the real power increases, the reactive power limitation moves closer to zero. The reactive powers maximum and minimum limitation is limited by the generator's maximum and minimum induced voltage.

I.e. the reactive power is limited by the generator's excitation system. This is because the excitation system has a field current limitation. This means that the DC-exciter has a maximum current that it can provide through the field windings. The same principle applies to the under-excitation of the generator. I.e. the generator has a maximum limit of how much reactive power it can consume. As previously stated the field current is proportional to the induced voltage. This means that the generator's maximum and minimum induced voltage is limited by the generator's maximum and minimum field current. The minimum induced voltage is smaller in magnitude compared to the maximum induced voltage. It is usually between 0.2-0.3 of  $E_{max}$ .

The turbine speed is regulated by the governor. This means that the maximum and minimum active power is regulated by the governor. This is because speed and active power are closely related. The generator has a maximum power limit because operating the generator above its maximum active power causes mechanical and thermal stresses on the machine which reduces its lifetime. The same applies to the minimum active power. Operating the generator below minimum active power causes huge electromechanical stresses on the machine, which reduces the lifetime of the generator. The minimum active power limit is not included in the capability diagrams illustrated in this report.

The quantities limiting the generator's capability diagram are plotted to illustrate the underlying mechanisms limiting the capability diagram. The capability diagram can be seen in figure 19. The boundaries are plotted in MATLAB to illustrate the important parameters limiting generator G1, capability diagram. The blue circle illustrates the stator current limitations, i.e. the apparent power limitation. The red arc is the maximum induced voltage ( $E_{max}$ ) in the generator. The yellow arc is the minimum allowed induced voltage ( $E_{min}$ ) in the generator. Figure 19 shows all the important characteristics of generator G1. Table I shows the rated data which are important parameters limiting the capability diagram. One example is  $\cos(\phi)$  which is the nominal power of the machine in a pu system.

In summary the figure shows the nominal operation point (N), rated load angle ( $\phi_n$ ), rated power angle ( $\delta_n$ ), the minimum induced voltage ( $E_{min}$ ) and the maximum induced voltage ( $E_{max}$ ). The figure also shows the different values of the induced voltage ranging from 0.1-0.3 with its center between  $A_x$  and  $B_x$ . The constants  $A_x$  and  $B_x$  are calculated using equations 32 and 33 respectively.

$$A_x = \frac{-V_n^2}{X_q} \quad (32)$$

$$B_x = \frac{-V_n^2}{X_d} \quad (33)$$

#### E. The Practical Stability Limit and the Minimum Field Current of the Generator

This subsection presents the underlying theory and assumptions for the practical stability (PLS) and minimum field

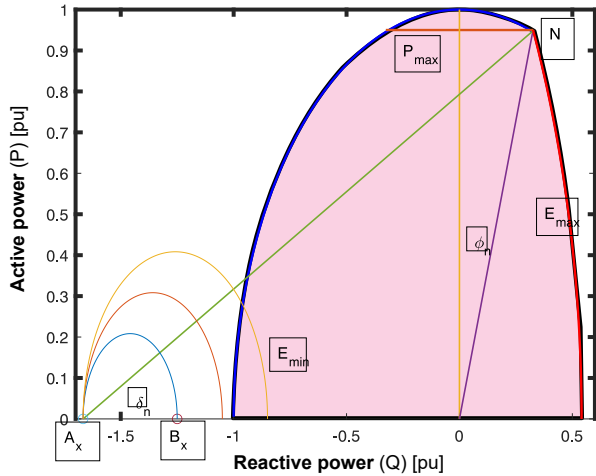


Fig. 19. The figure illustrates the capability diagram of hydro generator G1 and the different parameters limiting the capability diagram.

current. Bortoni [1] did not include the practical stability limit and the minimum field current of the generator in his technical report. This report, therefore, extends his analysis by including the PLS and minimum field current.

The practical stability limit represents the maximum power angle the generator can operate with, without stepping out of synchronism with the grid. When the power angle is increased beyond the breakover angle the electromagnetic torque is no longer in balance with the mechanical torque. The breakover angle can be determined for which  $P_{max}$  is reached. The theoretical stability limit is not used as the boundary for the capability diagram. This is because it does not provide a safe operating condition. A slight increase in the load could easily cause the generator to slip out of synchronism, thus a practical stability limit is determined. The theoretical stability limit must then be multiplied with a stability margin. The stability margin is often 10 %. This is to ensure a good stability margin.

Figure 20 (a) illustrates that the theoretical stability limit is far away from the capability diagram. To get the stability limit inside the capability diagram one must have a stability margin of 20 %. This seemed very high and unusual. Usually, the stability margin is 10 %. To validate the methods two different were used. The PLS using the first method was calculated using the following assumptions:

$$P = \frac{VE_q}{X_d} \sin(\delta) + \frac{V^2}{2} \left( \frac{X_d - X_q}{X_d X_q} \right) \sin(2\delta) \quad (34)$$

$$Q = \frac{VE_q}{X_d} \cos(\delta) - \frac{V^2}{X_d} - V^2 \left( \frac{X_d - X_q}{X_d X_q} \right) (\sin(\delta))^2 \quad (35)$$

First, the maximum permissible steady-state rotor angle can be deduced from the active power equation. The rotor angle is then a parametric curve of  $E_q$  which can be placed in P and Q to calculate the theoretical stability limit. This means that the theoretical stability limit is a parametric curve of  $E_q$ .  $E_q$  is ranged from 0-1 with a step of 0.1. The theoretical stability limit is then converted to the PLS by multiplying 0.8 with P

and Q to account for a stability margin of 20 %. The practical stability limit can be seen in figure 20 (b).

$$\frac{\partial P}{\partial \delta} = 0 \quad (36)$$

$$\cos(\delta) = \frac{1}{4} \left( -\frac{E_q X_d}{V(X_d - X_q)} + \sqrt{\left( \frac{E_q X_d}{V(X_d - X_q)} \right)^2 + 8} \right) \quad (37)$$

As previously stated to verify the findings a second method was used. The second method was calculated using the equations for active power and reactive power for salient pole generators, as previously illustrated in equation 34 and 35. The power angle was then plotted as a contour plot. The figure illustrates that this particular generator has a large stability margin. This is because the power angle within the capability diagram is very low. This means that the breakover angle must be low for the generator to run stably. One would expect that the breakover angle would be between 65-75 degrees, but this is not the case. The reason for this is due to the low values of the synchronous reactance's. The low value of the synchronous reactance of the d-axis and q-axis forces this generator to have a low breakover angle. If one increases the synchronous reactance one can observe that the generator needs a smaller stability margin.

Once the practical stability limit was determined, the minimum field current was calculated. The minimum field current is the induced voltage with its center between  $A_x$  and  $B_x$ . The induced voltage is gradually increased from 0-1, with a step increase of 0.1 pu. The minimum field current is usually where the first induced voltage arc crosses the armature current limitation. For this case the induced voltage is equal to 0.3 pu. Figure 21 illustrates the complete capability diagram, where the capability diagram is limited by the armature current, practical stability limit, minimum induced voltage, and maximum induced voltage.

#### F. What is Weighted Average Efficiency?

This subsection presents the calculation model developed in Bortoni's technical report. The calculation model offers a viable solution /alternative to quantify the impact renewable energy sources have on hydro generators. The particular computation scheme is suitable for the calculation of the efficiency at the rated point and efficiency estimation for different loading conditions. This calculation model can model different load distribution/ operational regimes and therefore able to quantify the impact of the energy transition.

In the technical report, Bortoni focuses on WAE where he calculated the unique efficiency at different loading points and multiplies it with its corresponding weight to calculate the expected/average efficiency. To illustrate this principle a figure of several different loading points and their corresponding weight and efficiency is illustrated in figure 22. Notice that Bortoni calculates the frequency of occurrence for an exact loading point and then calculates the efficiency of this exact/specific loading point. A dataset usually consists of a generator's yearly production where measurements are made

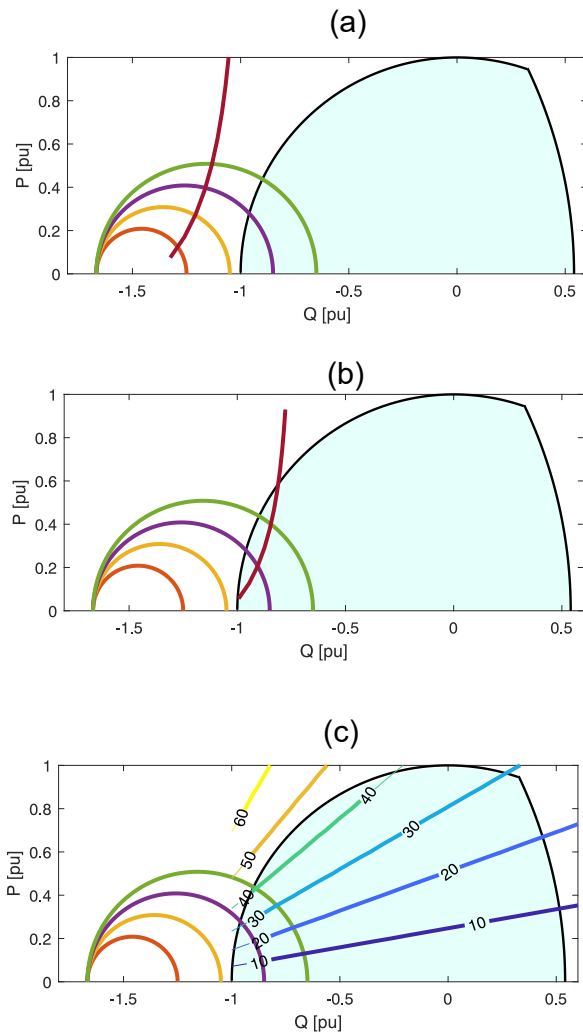


Fig. 20. Figure (a) illustrates the theoretical stability limit for hydro generator G1. Figure (b) illustrates the practical stability limit for hydro-generator G1. Figure (c) illustrates the breakover angle for different practical stability limits.

every hour for an entire year. A dataset could for example consist of 8610 different discrete loading points, i.e. where the loading point only occurs once. Bortoni has rounded up the loading points to two decimals, therefore giving the illusion that a particular loading point occurs with a certain frequency, but in most cases, very few operations are the same. These exact loading points give a unique efficiency that corresponds to that particular loading point. This can also be seen in figure 22.

The Weighted Average Efficiency (WAE) is obtained as the summation for diverse loading points, of the observed efficiency multiplied by a weight. For brand new generators, the weights are established from experience or based on the importance of given loading points. For existing generators, the weight is calculated as the probability of occurrence for a given loading point. The studies done in this report are based on existing generators therefore this particular definition of

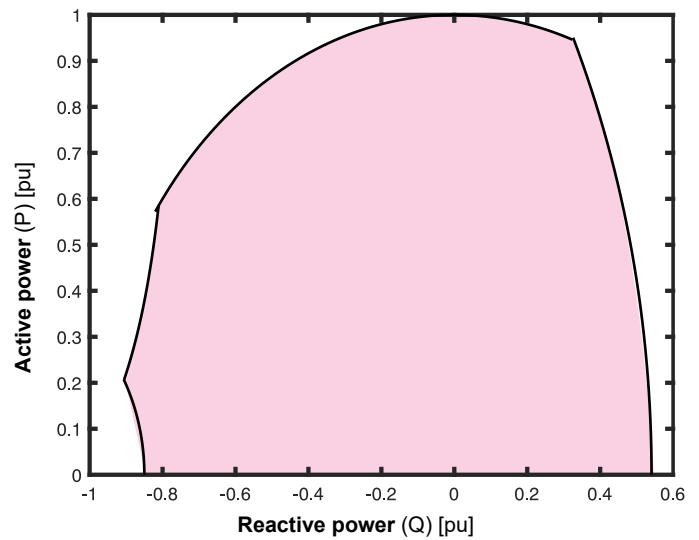


Fig. 21. The figure illustrates the capability diagram of hydro generator G1, where the practical stability limit and the minimum induced voltage is included.

P (pu)	0.2	0.4	0.6	0.8	0.8	0.8	0.8	0.8
Q (pu)	0	0	0	0	-0.4	-0.2	0.2	0.4
$A_i$	0.05	0.20	0.30	0.20	0.05	0.10	0.05	0.05
$\eta_{\#1}$ (%)	96.70	98.10	98.47	98.59	98.55	98.61	98.49	98.53
$\eta_{\#2}$ (%)	96.37	98.03	98.54	98.76	98.75	98.78	98.70	98.59

Fig. 22. The figure illustrates several exact loading point and its corresponding weight and efficiency for two different generators [1].

weight is used when calculating the WAE.

The weighed is denoted as  $A_i$  and represents the probability of occurrence for a particular loading point. the weight is illustrated in equation 38. Where  $\Delta t$  represent the duration (hour) of a particular loading point. The constant T represents the generators running time during a year. Figure 23 is a general illustration that shows the duration of several specific efficiencies throughout an entire year.

$$A_i = \frac{\Delta t}{T} \quad (38)$$

The WAE is illustrated with the following formula. Where  $\eta_w$  is the WAE.  $A_i$  and  $\eta_i$  are respectively the weight factor and efficiency at a particular loading point, and n is the number of considered loading points.

$$\eta_w = \sum_i^n A_i * \eta_i \quad (39)$$

The working principle is best illustrated using equation 40. The equation illustrates that the calculation model considers one loading point at a time and calculates the efficiency and weight for that loading point. This gives several elements of average efficiencies. These average efficiencies are summed, resulting in a WAE.

$$\eta_w = \sum_{i=1}^n \eta_i \frac{\Delta t_i}{T} = \sum_{i=1}^n \eta_i A_i = \eta_1 A_1 + \eta_2 A_2 + \dots + \eta_n A_n \quad (40)$$

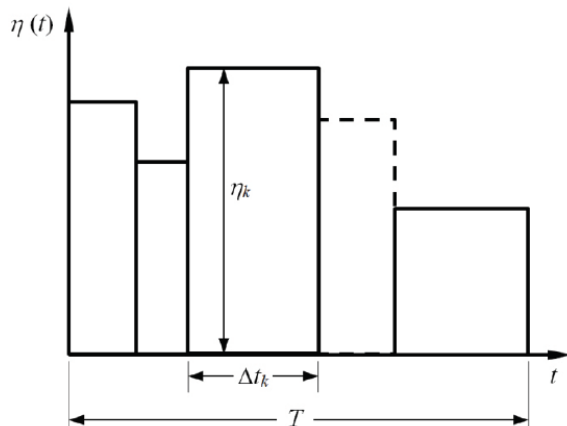


Fig. 23. The time dependant efficiency trend for exact efficiency's, in order to compute the WAE. [1].

Figure 22 also illustrates quantitatively what happens with the efficiency, when one operates the generator at different loading points. The report "An In-Depth Study of Hydro-Generator Losses and Efficiencies for Different loading points" [37] studies qualitatively and quantitatively how the increasing prevalence of renewable energy sources forces the generator to operate at different efficiencies for different loading points. Figure 27 illustrates the iso-efficiency curves of hydro-generator G1 at different loading points. i.e Figure 27 illustrates qualitatively how the efficiency of the generator differs for different loading points.

1) *Advantages and disadvantages with weighted average efficiency*: The advantage of weighted average efficiency is that it offers a viable solution /alternative to quantify the impact renewable energy sources have on hydro generators. The particular computation scheme is suitable for the calculation of the efficiency at the rated point and efficiency estimation for different loading conditions, resulting in a WAE. Consequently, it is shown that this particular procedure is necessary because regular synchronous generators can no longer be designed for a nominal operating point. Under these new operational regimes losses of diverse nature must be accurately modeled.

This calculation model has one primary weakness, which is that it considers the efficiency for one loading point at a time and not the accumulation of the loading points. This means that if the generator is operated purely as a synchronous condenser for a long time, one gets a lot of the elements that are zero in the summation of efficiencies. This is because the generator is producing zero active power which gives zero efficiencies. This can be seen quantitatively in equation 41.

$$\eta = \frac{0}{0 + P_{loss}} = 0 \quad (41)$$

In the technical report, Bortoni states that the hydro-generator understudy has a WAE of 64.84 %. The synchronous condenser-dominated load distribution of this generator can be seen in figure 24. If one compares the WAE of this hydro generator with the rated efficiency of 98.4 %, one can see that there is a 33.56 % difference in the efficiency. This means

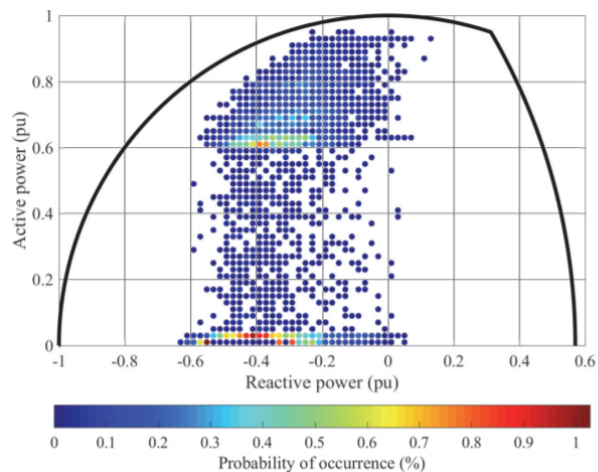


Fig. 24. The figure illustrates A 2D histogram of how many times a discrete loading points occur around an exact loading point "zone". I.e the figure illustrates the frequency and probability of occurrence for specific loading points. [1]. The figure is also an example of a synchronous condenser load distribution, where the generator operates 50 % of the time below 0.02 pu active power.

that there is a loss of 33.56 % in efficiency because the generator varies in its operational point. The low value of WAE found for this particular generator is due to the subsequent periods this machine operates at low active power generation and low energy conversion efficiency. Figure 25 illustrates the cumulative probability and the conversion efficiency as a function of active power. From the figure, one can observe that 40 % of the time the active power is higher than 0,6 pu, with an efficiency greater than 97 %, on other hand 50 % of the time the active power is below 0.02 pu with efficiency lower than 55 %.

Bortoni's suggests a lower limit of active power generation of 0.6 pu, which then results in WAE of 98.01 %. Which is closer to the rated efficiency of 98.41 %. This suggestion considerably reduces the operational flexibility of the generator. This would mean that one would have to implement very expensive power electronics to compensate reactive power. This is because operating a generator above 0.6 pu active power limits the generator's reactive power consumption and production capability. This is explained in much greater detail in section VIII. Discussion. These disadvantages give rise to the study of a new calculation model.

### G. Accumulated Average Efficiency

This subsection presents a new calculation model called accumulated average efficiency (AAE). This report presents the concept of accumulated average efficiency (AAE) as a new and useful method to compute the overall efficiency of synchronous generators when they frequently vary their operating conditions. An illustration of the concept is depicted in figure 23. The method is compatible with both exact load points or load-grid distributions clustered in discrete points.

1) *Discrete loading points and the accumulation of loading points*: The calculation model accumulated average efficiency (AAE) does not use the same weight definition and assumption

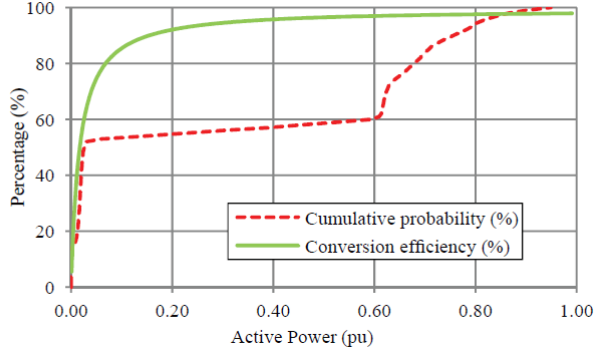


Fig. 25. The cumulative probability and conversion efficiency as a function of active power for hydro generator G1 [1].

regarding the loading points as Bortoni. Bortoni converts the discrete loading point from a given dataset to exact loading points by rounding up the discrete loading point to a loading point consisting of two decimals or less. He then counts the number of times these "exact loading points" occur and then divides the frequency of these loading points with the total number of loading points. The calculation model AAE calculates the accumulation of all the discrete loading points and the accumulation of all the discrete losses, to calculate an AAE. This means if a dataset consists only of discrete loading points the time intervals in figure 23 are not considered.

AAE assumes an "equal weight distribution". This means that every discrete loading point has an equal probability of occurrence. I.e this means that every discrete loading point has the same weight therefore the name "equal weight distribution". It also means that the weight is constant and can be quantitatively illustrated as  $A_i = \frac{\Delta t}{T} = \frac{1}{T}$ , which is 1 over the total number of discrete loading points. The weight during equal distribution can be seen in equation 42. Figure 26 illustrates the discrete-time intervals for the pu values of  $P_{loss}$  and  $P$ .

$$A_i = \frac{1}{T} \quad (42)$$

The discrete-time intervals are equal, and the summation of all the discrete-time intervals are equal to the total number of discrete loading points.

$$T = \sum_i^n \Delta t_i = \Delta t_1 + \Delta t_2 + \dots \Delta t_n \quad (43)$$

The equation below illustrates that the weight is distributed among the discrete loading points, if one sum all the weights one gets a value equal to 1.

$$1 = \sum_i^n \frac{\Delta t_i}{T} = \sum_i^n A_i = A_1 + A_2 + \dots A_n \quad (44)$$

2) *Calculation procedure:* The calculation model AAE follows an entirely different calculation procedure. The sum of all the pu power loss elements is multiplied by the weights to get the average value. From the equation, one can also see that the average pu power loss is equivalent to the total energy losses divided by the number of discrete loading points.

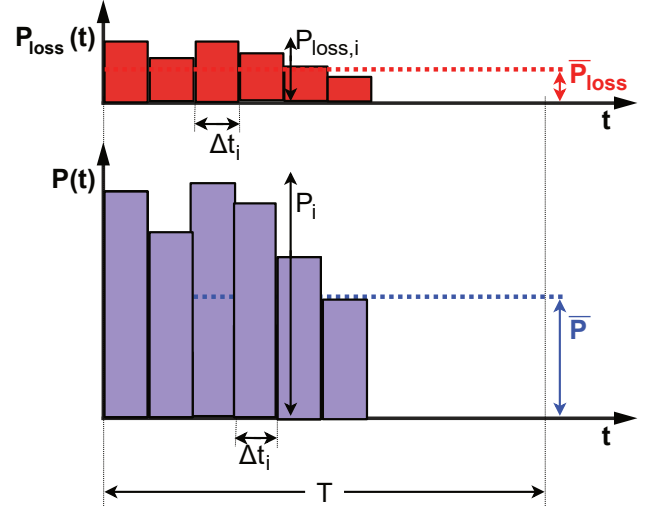


Fig. 26. Generic load cycling sequence for accumulation of the generator's energy loss ( $E_{loss}$ ) and energy generation ( $E$ ) over time formulated by discrete time intervals.  $E_{loss}$  is equal to the sum of all red areas, while  $E$  is the sum of all blue areas. The average power loss in pu ( $\bar{P}_{loss} = E_{loss}/T$ ) and the average power generation in pu ( $\bar{P} = E/T$ ) are also indicated.

$$\begin{aligned} \bar{P}_{loss} &= \frac{E_{loss}}{T} = \sum_i^n P_{loss,i} A_i \quad (45) \\ &= P_{loss,1} A_1 + P_{loss,2} A_2 + \dots P_{loss,n} A_n \end{aligned}$$

$$E_{loss} = \sum_i^T P_{Loss(i)} A_i \quad (46)$$

The same principle applies to the pu average active power production and total energy production. This means that one must first start by calculating the sum of the pu active power production for all the discrete loading points. The average pu power production, and total energy production ( $E$ ) can be seen in equation 47 and 48

$$\bar{P} = \frac{E}{T} = \sum_i^n P_i A_i = P_1 A_1 + P_2 A_2 + \dots P_n A_n \quad (47)$$

$$E = \sum_i^T P_i A_i \quad (48)$$

The values can also be converted to actual values, rather than pu. Equation 49 shows that the vector consisting of active power losses in pu is multiplied with the generator's nominal apparent power, which is the base apparent power of the generator. The vector elements are also multiplied by the weight and the number of hours in a year. This means that the average power is converted to energy, and the energy calculations are scaled according to if the generator were to run for an entire year. The sum is then divided by  $10^9$ . This is done to get the value in GWh/year. The total energy losses ( $E_{loss}$ ) and production ( $E$ ) can be seen in equation 49 and 50.

$$E_{loss} = \sum_i^T P_{Loss(i)} A_i \frac{S_n * 8760}{10^9} \quad (49)$$

$$E = \sum_i^T P_i A_i \frac{S_n * 8760}{10^9} \quad (50)$$

Once the total energy Losses ( $E_{loss}$ ) for the entire year and the total energy production ( $E$ ) for an entire year are established. One can determine the AAE. The AAE is found by dividing the total energy production out, with the total energy production in. The AAE can also be calculated using the average power losses and average power productions. The AAE can be seen in equation 51 and 52 respectively.

$$\eta_a = \frac{E}{E + E_{loss}} \quad (51)$$

$$\eta_a = \frac{\bar{P}}{\bar{P} + \bar{P}_{loss}} = \frac{\sum_i^n P_i A_i}{\sum_i^n (P_i + P_{loss,i}) A_i} \quad (52)$$

3) *A worked example comparing WAE against AAE:* To illustrate the implementation of the calculation procedure a worked example has been made. In this worked example, the generator is assumed to operate in three loading points throughout the entire year. The three loading points and their duration time can be seen in Table V. This simple example is used to give a simple illustration of the core principle and the significance of the principles. This is because one can get confused with larger datasets. The larger datasets add complexity. It is harder to grasp and articulate the challenges and benefits of the calculation models with a larger dataset if the fundamentals are not properly articulated.

It is assumed that the generators run 8760 h in a year. The generators running time is divided into three, representing that the generator operates in three loading points for the entire year. Table V also illustrates key quantities used to calculate the WAE and AAE. The example is so simple that one can analytically deduce the results presented in Table VI using the equations 40 and 52

$$\eta_w = \left(\frac{1}{3} * 0\right) + \left(\frac{1}{3} * 98.56\right) + \left(\frac{1}{3} * 97.77\right) = 65.44\% \quad (53)$$

$$\eta_a = \frac{\bar{P}}{\bar{P} + \bar{P}_{loss}} = \frac{0.5}{0.5 + 0.0128} = 97.5\% \quad (54)$$

This worked example illustrates the benefits of the calculation model AAE. This worked example also illustrates the significance of the weight, especially for the WAE. From the example above one can see that weight lowers the WAE. The calculation model AAE shows that the weight is multiplied with the pu active power production and pu active power loss, giving an average value for the pu active power production and pu active power loss. In the equation for the AAE, the weight is in the numerator, and the denominator for both the addend parts. This means that the weight is negligible for the calculation of the AAE. I.e., the weight is insignificant in the equation for AAE. The weight is only significant for the calculation of the average pu active power production and pu active power loss. This is illustrate in equation 52. The equation illustrates that one can remove the weight without it affecting the AAE.

The primary reason for the disparity between the calculation models is the zero in efficiency in the first addend part for the WAE calculation. This is because the generator produces no active power. Consequently, the WAE is reduced  $\frac{1}{3}$ . An important and distinct difference between the calculation models is that the calculation model AAE assumes an accumulation of all active power production. This means that one mitigates the low efficiencies caused by loading points with low active power production. Instead of having a case of low efficiency, like in the WAE model, the low active power production is mitigated by adding all the active power production. The WAE considers only one loading point at a time and then calculates the summation of all the average efficiencies, causing a significant reduction in the WAE. This worked example has illustrated the influence of weight and low energy conversion efficiency. The example has shown that if one eliminates the weight in the AAE equation, then the remaining quantities are the sum of all the active power production and the sum of all the active power loss. This is the core principle of the calculation model. Equation 55 illustrates that it is the summation of the active power production that prevents a low value for the AAE. The equation illustrates that the summation of the active powers prevents a low efficiency. The significance of this benefit is further explained in Section VIII.

$$\eta_a = \frac{\sum_i^n P_{(i)}}{\sum_i^n P_{(i)} + \sum_i^n P_{Loss(i)}} \quad (55)$$

#### H. Illustration Models (zones) for Calculation of AAE

The calculation model WAE considers efficiency for different loading points. The iso-efficiency curves in figure 27 partly illustrate what the calculation model does, by depicting the efficiency for different loading points. The 2D histogram depicted in figure 24 illustrates the weight or the probability of occurrence for specific loading points. These two illustration models show illustratively what the calculation model does. This subsection presents possible illustration models that can be used for the calculation model AAE.

The calculation model AAE considers all the discrete loading points, rather than the frequency of occurrence for specific loading points. I.e the 2D histogram in figure 24 shows the frequency of occurrence for specific loading points, while the AAE histogram shows the discrete loading points and their density. This subsection presents some illustration models/zones that may be considered for calculating the total energy losses, using discrete loading points. The total energy loss is used as the only example in Section VI-H2 and VI-H3 because the same principles apply to total energy production. This subsection presents some new illustration models and arguments for why some models are better than others. To simplify the calculations, the density is evenly distributed throughout the capability diagram. In reality, the density is uneven. One example could be a generator that is operating mostly around its rated active power. This would cause the generator to have a high density of discrete loading points around its rated active power output.

There are primarily two considerations that must be taken into account in regards to the sub-sub section VI-H3. To sim-

TABLE V  
WORKED EXAMPLE OF GENERATOR OPERATING IN THREE DISTINCT LOAD POINTS OVER A YEAR

Output	#1	#2	#3	Sum
$P_i$	0.0 pu	1.0 pu	0.5 pu	
$Q_i$	0.5 pu	0.0 pu	0.5 pu	
$\Delta t_i$	2920 h	2920 h	2920 h	8760 h
$A_i$	1/3	1/3	1/3	1
$P_{loss,i}$	0.0124 pu	0.0146 pu	0.0114 pu	
$\eta_i$	0%	98.56%	97.77%	
$E_i$	0.00 GWh	451.46 GWh	225.73 GWh	677.19 GWh
$E_{loss,i}$	5.60 GWh	6.59 GWh	5.14 GWh	17.36 GWh

TABLE VI  
FINAL OUTPUTS FROM WORKED EXAMPLE WITH THREE DISTINCT LOAD POINTS OVER A YEAR

	$E$	$E_{loss}$	$\bar{P}$	$\bar{P}_{loss}$	$\eta_w$	$\eta_a$	$\eta_a - \eta_w$
Value	677.19 GWh	17.36 GWh	0.5 pu	0.0128 pu	65.44%	97.5%	+32.06%

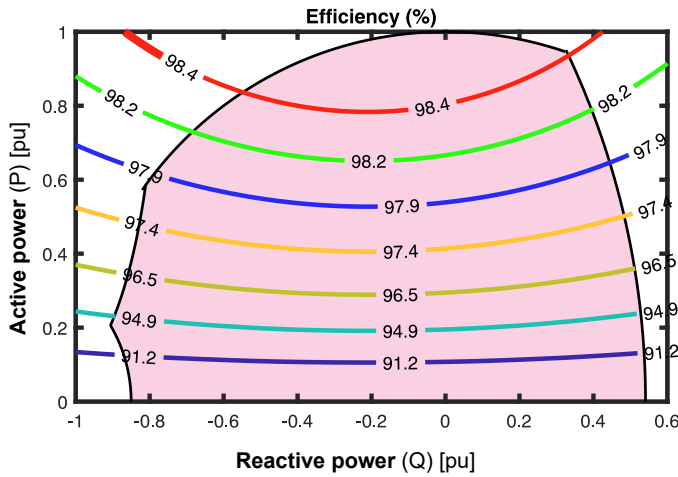


Fig. 27. The figure illustrates the iso-efficiency curves of hydro generator G1.

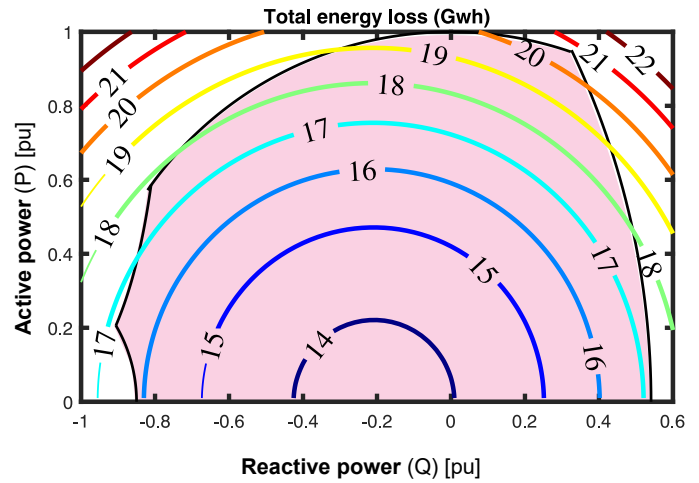


Fig. 28. The total yearly energy loss (GWh/year) as curves, with the capability diagram in the background.

ply the calculations, the discrete loading points are assumed to have the same density, meaning the space between the loading point is evenly distributed. They are also assumed to have the same probability of occurrence in their respective zones. In other words, a discrete loading point within a zone has the same probability of occurrence as all the other discrete loading points within that zone.

1) *Iso-efficiency curves vs total energy curves*: As previously stated the calculation model WAE considers efficiency for different loading points. The iso-efficiency curves partly illustrate what the calculation model does, by depicting the efficiency for different loading points. This can be seen in figure 27. The calculation model AAE considers total energy production and loss for different loading points. This means that one can partly illustrate what the calculation model does, by depicting the total yearly energy production and losses for different loading points as total energy production lines and total energy loss curves. These values can be illustrated in pu as power loss and power production or in GWh as total yearly energy loss and production. In this case, the values are illustrated in GWh and can be seen in figure 28 and 29 respectively.

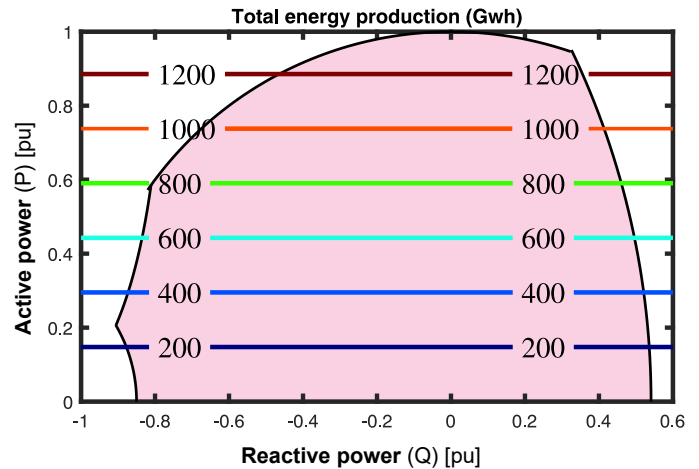


Fig. 29. The total yearly energy production (GWh/year) as lines, with the capability diagram in the background.

2) *Important considerations in regards to the total energy losses*: To make sure that the total energy losses (TEL) was correct, the density was increased until the TEL converged. In other words, increasing the density would make little to

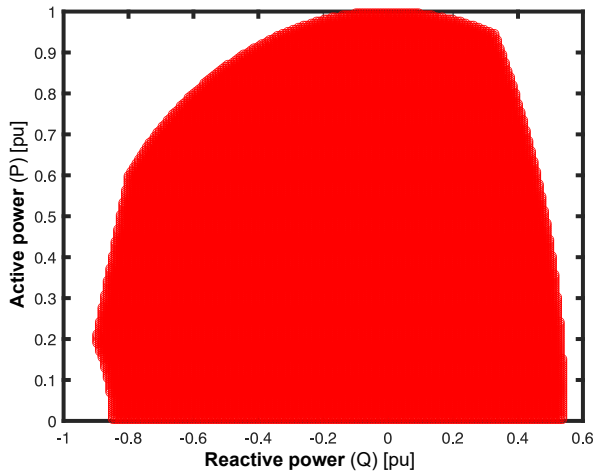


Fig. 30. The figure illustrates all the loading points inside the capability diagram with equal probability of occurrence, were the number of discrete loading points are 250 000, i.e a dataset equal to a matrix size of 500X500.

no difference in the total energy losses. Figure 31 illustrates the converging value of the discrete loading points inside and outside the capability diagram. The converging value of the discrete loading points within the capability diagram is equal to 16.5 GW.

The TEL ( $E_{loss}$ ) for all the discrete loading points (blue and red circles) converges to 17.39 GW when the matrix size is 500X500. In other words when the total number of discrete loading points is 250 000. This particular matrix size is chosen because of convenience. Increasing the matrix size/number of discrete loading points would mean more computational time. Another reason for the specific matrix size is because there is little to no difference in the TEL by increasing the matrix size to for example an 800X800 matrix. Figure 30 illustrates the discrete loading points inside the capability diagram when the total number of discrete loading points is 250 000. This is the chosen matrix size/number of discrete loading point for all the calculations throughout sub subsection VI-H2 and VI-H3. This is done to make the calculations consistent and eliminate the difference in results due to uneven density.

The losses of interest are inside the capability diagram. Therefore the total energy losses in focus for this study are within the capability diagram of generator G1. Three distinct resolution/densities have been chosen to better illustrate what is happening when one increases the density and assumes that the loading points are evenly distributed. Figure 32 illustrates that there is still space between the discrete loading points when the number of discrete loading points is 121, i.e the total number of discrete loading points does not give a converging value of the TEL. Figure 33 shows that if one increases the number of discrete loading points to 12 100 the density becomes much more compact, but there is still some space between the discrete loading points, i.e the number of discrete loading points is so high that TEL has started to reach a converging value. Figure 34 illustrates 121 000 discrete loading points and shows that there is no space between the discrete loading points. This means that increasing the number

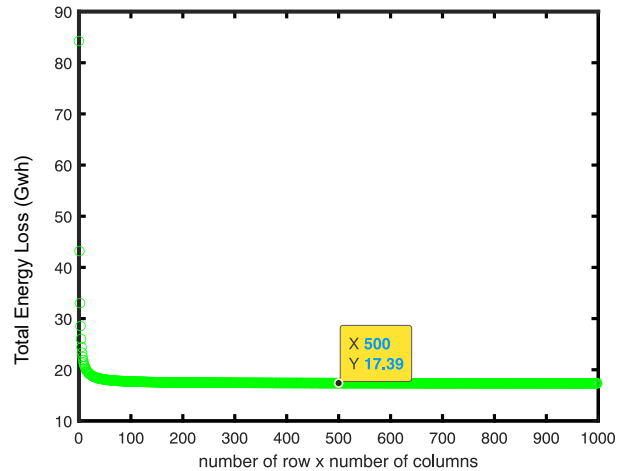


Fig. 31. The figure illustrates the converging value of all the discrete loading point (blue and circles).

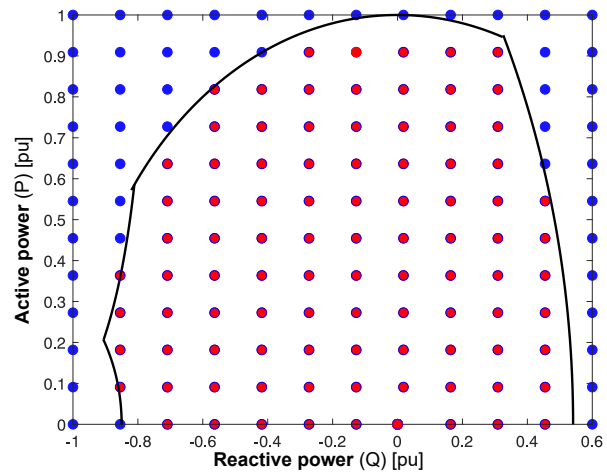


Fig. 32. The figure illustrates the discrete loading points outside the capability diagram (blue) and the discrete loading points inside the capability diagram (red). This figure has a resolution equivalent to a 11x11 matrix. i.e 121 discrete loading points evenly distributed throughout the figure.

of discrete loading points, would not affect the TEL, i.e TEL has reached a converging value.

3) *total energy loss modeled as distribution circles*: One interesting study could be to look at the different loading points distributed as circles moving away from an arbitrary operating point. one could for example choose an arbitrary loading point, where the reactive power is equal to 0 pu and the active power is equal to 0.5 pu. One can then calculate the TEL as one moves further away from this operating point, i.e gradually encompass an increasing number of discrete loading points, by increasing the radius of the circles. This can be seen in figure 35

The figures show that as one moves away from this point the TEL converges. This arbitrary point might not be much of interest. This arbitrary point is used to illustrate that the TEL converges to the TEL of the entire capability diagram as one increases the radius. What is of more interest, is to see



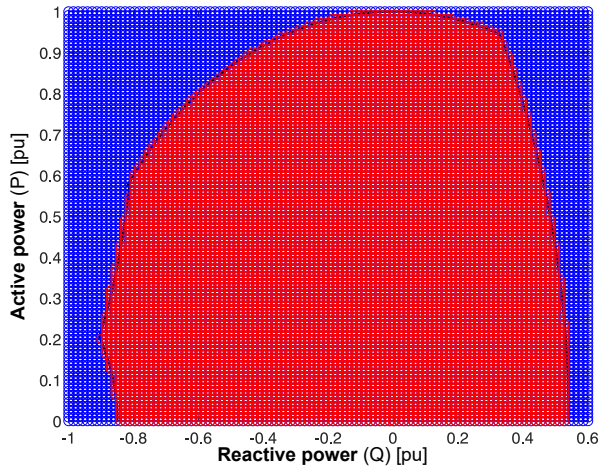


Fig. 33. The figure illustrates the discrete loading points outside the capability diagram (blue) and the discrete loading points inside the capability diagram (red). This figure has a density equivalent to a  $110 \times 110$  matrix. i.e 12100 discrete loading points evenly distributed throughout the figure.

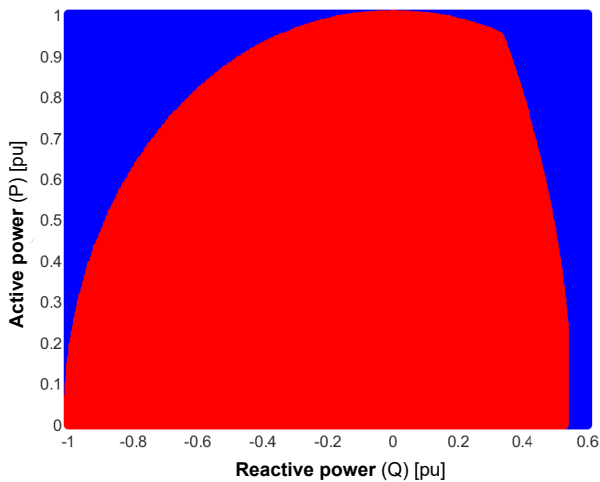


Fig. 34. The loading points outside the capability diagram (blue) and the discrete loading points inside the capability diagram (red). This figure has a density equivalent to a  $1100 \times 1100$  matrix. i.e 1210000 discrete loading points evenly distributed throughout the figure.

what happens when one moves further away from the nominal operating point. The nominal operating point for generator G1 is 0.33 pu (Q) and 0.95 pu (P). This can be seen in figure 36. In addition to the nominal operating point, a third point was studied. The third operating point under study was 0 pu (Q) and 1 pu (P). This is illustrated in figure 37. These three points are studied to see how the TEL differs as one increases the radius of the distribution circles.

The TEL was modeled as a function of the distribution circle radius. This was done for all three points. what can be seen is that the total energy losses start at different values. This is because the algorithm starts by calculating the TEL with a very small radius. This is because when the radius is very small one considers only a few discrete loading points. This is the same as considering the total energy loss for the point (0,0.5),

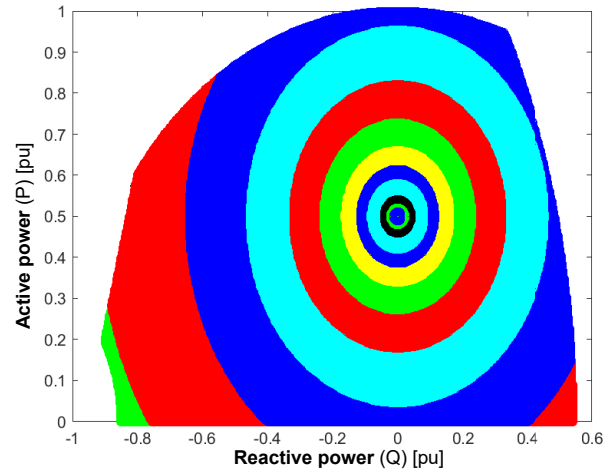


Fig. 35. The figure illustrates the discrete loading points for different distribution circles. The distribution circles has their center at the point (0,0.5).

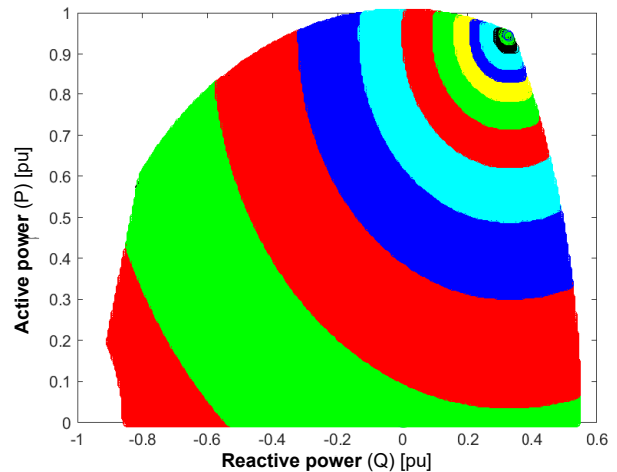


Fig. 36. The figure illustrates the discrete loading points for different distribution circles. The distribution circles has their center at the nominal point (0.33,0.95).

(0.33,0.95) and (0,1). If one compares the starting values of figure 38, 39 and 40 with the total energy loss in figure 28, one can see that the starting value for the figures is equivalent to the total energy losses at these points. One can also see that as one increases the distribution radius the losses converge to a value equal to that of the TEL of the capability diagram. This is because the radius of the distribution circle becomes so big that it encompasses the entire capability making it equivalent to the TEL of the entire capability diagram.

The cost was also modeled as a function of the distribution radius of the circles. The formula for the TEL ( $\bar{E}_{loss}$ ) can be seen in equation 46 and the cost is given by equation 56. The cost is modeled in regards to the Norwegian market price, which is 14.4 øre. The TEL is divided by 8760 to convert the energy to power and is multiplied with  $10^3$  and 14.4 øre to convert it to MW\*øre. The cost for the operating points (0,0.5), (0.33,0.95) and (0,1) can be seen in figure 41, 42 and



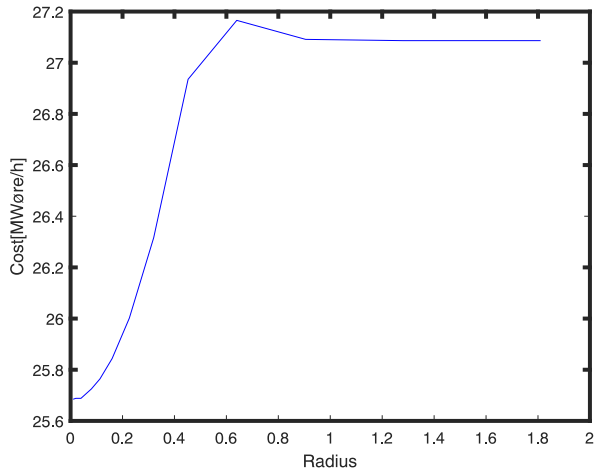


Fig. 41. The figure illustrates the converging value of the cost as one increases the radius of the distribution circles, starting from the operating point (0,0.5). The figure starts with a cost of 25.7 MWøre/h and converges to 27.0872 MWøre/h, which is the cost when the discrete loading points covers the entire capability diagram.

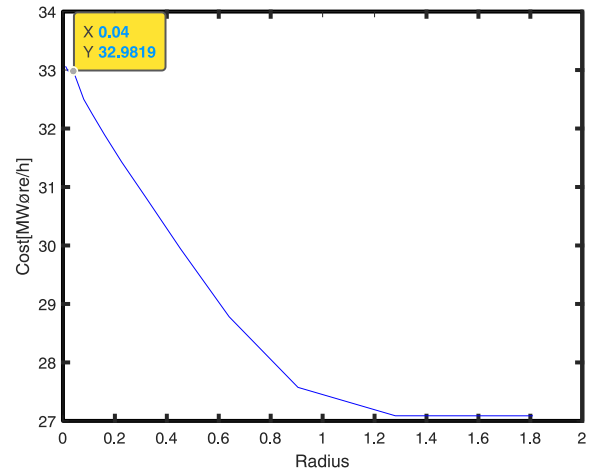


Fig. 43. The figure illustrates the converging value of the cost as one increases the radius of the distribution circles, starting from the operating point (0,1). The figure starts with a cost of 32.9819 MWøre/h and converges to 27.0872 MWøre/h, which is the cost when the discrete loading points covers the entire capability diagram.

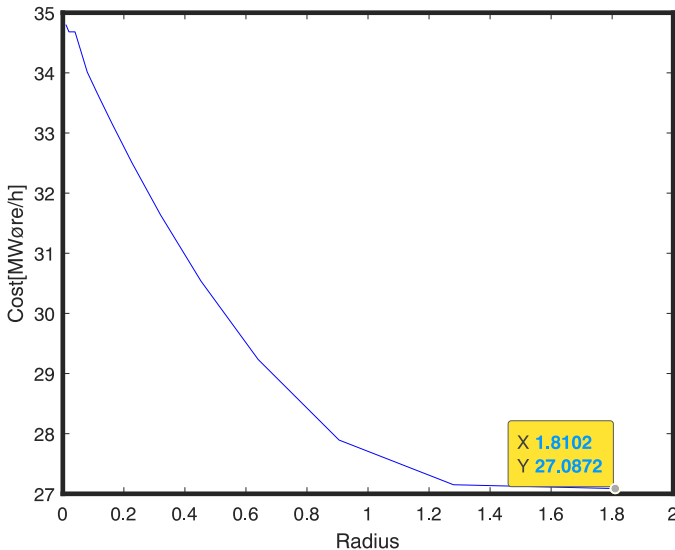


Fig. 42. The figure illustrates the converging value of the cost as one increases the radius of the distribution circles, starting from the nominal operating point (0.33,0.95). The figure starts with a cost of 34.7 MWøre/h and converges to 27.0872 MWøre/h, which is the cost when the discrete loading points covers the entire capability diagram.

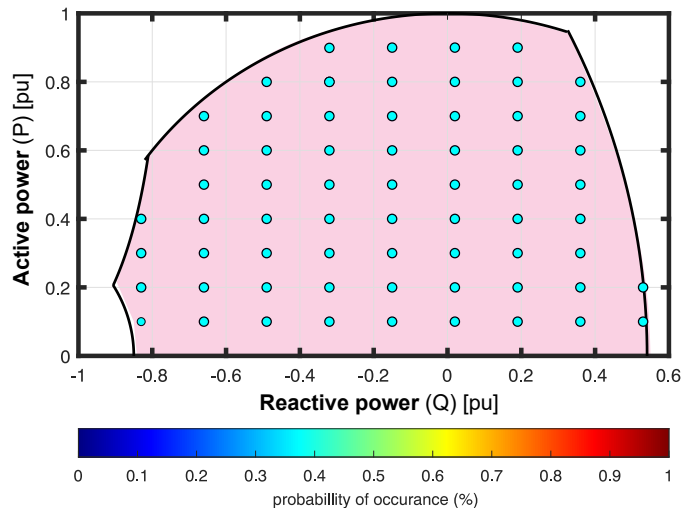


Fig. 44. The figure illustrates an artificially made uniform load distribution and the likelihood of a loading point to occur in a certain region, which is the entire capability diagram in this case.

the discrete loading points. This can also be seen in figure 51.

5) *comparing the illustration models distribution circles and 2D histogram:* The illustration model distribution circle is not as good of an illustration model as the 2D histogram. This is because the illustration model uses a scatter plot that shows all the discrete loading points. As previously the discrete loading points are presented in a scatter plot that highlights the density of the occurring loading points. The probability of occurrence is determined based on the proximity of the discrete load points. I.e. the histogram does not show the probability of an exact loading but rather the likelihood of a loading point to occur in a certain region. This model is very descriptive and gives a clear overview of

where the generator operates the most, and which kind of load distribution/operational regime that is present.

The illustration model distribution circle is a relatively good illustration model. The illustration model can be used to illustrate the TEL and TEP. The drawback is that the last distribution circle is the only circle that encompasses the entire load distribution/operational regime. This is because this is the only circle that encompasses the entire capability diagram. What is of interest is the discrete loading points throughout the entire capability diagram. In other words what is of interest is the "overall efficiency" of the entire load distribution, not a specific part of the load distribution. If the distribution circle does not encompass the entire operational regime, it does not calculate the TEP and TEL of the entire distribution.

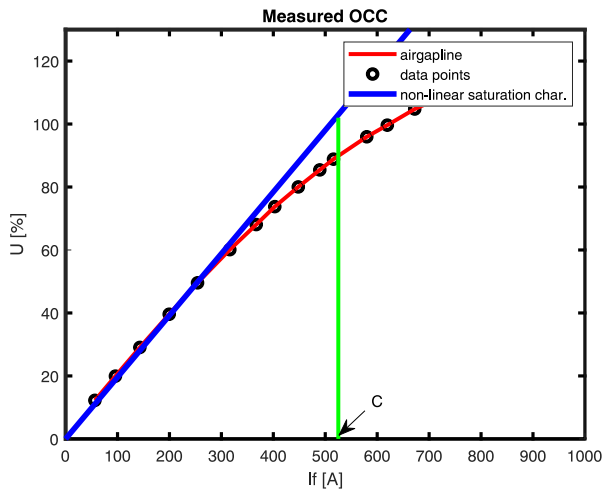


Fig. 45. The open circuit characteristic of Åbjøra given by the manufacturers.

## VII. RESULTS

In this section, a case study is made, where the efficiency and field current is calculated analytically using the methods presented in this report. The calculated values are compared with the measured efficiency and field current from an actual industry generator. The methods are experimentally validated using the measured efficiency and field current at eight different loading points. The industry generator under study is a Norwegian hydro-generator called Åbjøra (G2). The rated data for this generator can be seen in Table III. The calculation models AAE and WAE are also compared for different load distributions. This is done to observe how the calculation models perform for different operational regimes. The characteristic behavior of the calculation models is also studied. This is done to see how the calculation models behave for different active power levels and an increasing number of discrete loading points.

### A. Quantifying the Saturation from OCC

One must first consider saturation when calculating the efficiency of a generator. In this case, the open circuit characteristics are given. The open-circuit characteristic of this generator can be seen in figure 45. The method used for considering saturation is the method, which stems from Machowski's equation. Were equation 30 is used as the saturation increment, when the generator reaches a threshold voltage of  $E_p = 0.55pu$ .

The replicated OCC can be seen in figure 46. The figure is scaled in regards to base current 525.15 A which is the field current that results in the rated voltage on the airgap line. It is illustrated as (C) in figure 45. The replicated figure illustrates an extrapolation of the measurement points (black dots) of figure 45, in addition to the air gap line and the saturation curve of the generator. The threshold voltage  $U_t$  and the equation used to plot the air gap line and saturation curve is also illustrated in figure 46. The values and quantities used to plot the air gap line and the non-linear saturation characteristics can be seen in Table VII.

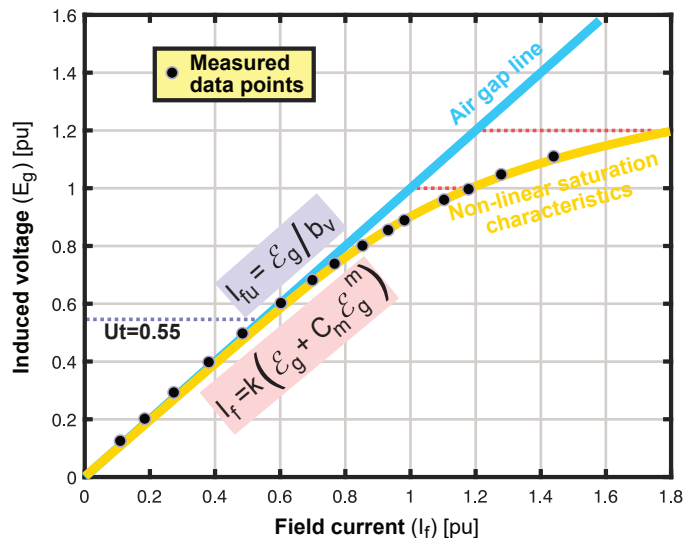


Fig. 46. The replicated air gap line and non-linear saturation characteristics of Åbjøra.

TABLE VII  
COEFFICIENTS USED TO PLOT THE OCC SHOWN IN FIGURE 46

Symbols	$b_v$	$C_m$	$\varepsilon_g$	$m$	$k$
Values	1	0.160	0 - 1.8	7	1.0308

### B. Experimental Validation of Efficiencies and Saturation Model

Eight measured loading points from the industry generator Åbjøra were used to validate the algorithm. I.e this was done to validate the chosen methods and assumptions. The measured quantities at these loading points were compared with the calculated quantities. This was done to qualitatively validate the illustration models and the saturation modeling. This can be seen by studying the iso efficiency curves and the eight loading points in figure 49. The measured loading points and key quantities can be seen in Table VIII.

As previously stated, quantifying saturation is a rigorous task. To quantify the saturation, one must accurately quantify the field current at different loading points. The measured field current at different loading points is therefore compared with the calculated field current. This is done to validate the saturation model and illustrate its accuracy. The validation of the saturation model can be seen in Table IX.

1) *The V-curve family of Åbjøra:* Once the saturation model is validated one can determine the V-curve family of the generator. The armature current is directly proportional to the complex power output, the field current must be calculated for each operating point considering saturation as previously described. For this generator the  $X_d$  is 1.06 pu,  $X_q$  is 0.676 pu and  $X_p$  is 0.141 pu and  $R_a$  is 0.002 pu. If one applies the equation for the armature current and the equation for the field current (31) one can obtain the Mordey diagram also know as the V-curve family. This can be done by relating the armature current to the field current, for several constant active powers. Figure 47 presents the Mordey diagram, for powers varying from 0 to 103 MW in steps of 25.7 MW. This means

TABLE VIII  
THE MEASURED LOAD POINTS, AND IMPORTANT QUANTITIES AT THESE LOAD POINTS.

Output	#1	#2	#3	#4	#5	#6	#7	#8
$S$	1.000 pu	0.750 pu	0.500 pu	0.250 pu	1.000 pu	0.750 pu	0.500 pu	0.250 pu
$\cos(\varphi)$	0.900	0.900	0.900	0.900	1.000	1.000	1.000	1.000
$P$	0.900 pu	0.675 pu	0.450 pu	0.225 pu	1.000 pu	0.750 pu	0.500 pu	0.250 pu
$Q$	0.436 pu	0.327 pu	0.218 pu	0.109 pu	0.000 pu	0.000 pu	0.000 pu	0.000 pu
$I_a$	5406.1 A	4054.6 A	2703.0 A	1351.5 A	5406.1 A	4054.6 A	2703.0 A	1351.5 A
$I_f$	1065.00 A	936.12 A	816.18 A	711.38 A	873.17 A	776.61 A	698.70 A	646.84 A
$P_f$	173.65 kW	133.66 kW	101.61 kW	77.19 kW	116.29 kW	91.99 kW	74.48 kW	63.81 kW
$P_{ex}$	15.88 kW	13.02 kW	10.72 kW	8.87 kW	11.65 kW	9.92 kW	8.68 kW	7.92 kW
$P_{br}$	2.13 kW	1.87 kW	1.63 kW	1.42 kW	1.75 kW	1.55 kW	1.40 kW	1.29 kW
$P_a$	187.46 kW	105.45 kW	46.86 kW	11.72 kW	187.46 kW	105.45 kW	46.86 kW	11.72 kW
$P_s$	89.16 kW	50.15 kW	22.30 kW	5.57 kW	89.16 kW	50.15 kW	22.30 kW	5.57 kW
$P_c$	211.92 kW	211.92 kW	211.92 kW	211.92 kW	211.92 kW	211.92 kW	211.92 kW	211.92 kW
$P_{be}$	240.90 kW	240.90 kW	240.90 kW	240.90 kW	240.90 kW	240.90 kW	240.90 kW	240.90 kW
$P_{wf}$	172.92 kW	172.92 kW	172.92 kW	172.92 kW	172.92 kW	172.92 kW	172.92 kW	172.92 kW
$P_{loss}$	1094.02 kW	921.89 kW	808.85 kW	730.51 kW	1032.05 kW	884.81 kW	779.0 kW	172.92 kW
$\eta$	98.834 %	98.680 %	98.250 %	96.944 %	99.008 %	98.868 %	98.509 %	97.294 %

TABLE IX  
VALIDATION OF THE SATURATION MODEL AND AN ILLUSTRATION OF ITS ACCURACY.

Output	#1	#2	#3	#4	#5	#6	#7	#8
Measured $I_f$	1065.00 A	936.12 A	816.18 A	711.38 A	873.17 A	776.61 A	698.70 A	646.84 A
Calculated $I_{fu}$	907.99 A	794.05 A	689.23 A	597.70 A	747.18 A	657.57 A	586.96 A	541.21 A
Calculated $I_f$	1064.88 A	934.23 A	815.01 A	711.11 A	857.50 A	764.76 A	691.88 A	644.67 A
Deviation $I_f$	-0.01 %	-0.20 %	-0.14 %	-0.03 %	-1.79 %	-1.52 %	-0.97 %	-0.34 %

that the active power is held constant and the reactive power is gradually changed, which changes the field current. Once the reactive power is gradually increased from minimum to maximum. The active power is increased with a step of 25.7 MW. The lowest point of all the V-curves for various power levels also called the unity power factor compounding curve is around 600 A. The curves on each side of the unity PF compounding curve also called compounding curves have a power factor equal to -0.9 and 0.9. This is also illustrated in the figure 47.

As previously stated the V-curve family does not show the power factor of the generator for all the different loading points. The capability diagram and power factor lines are often used to illustrate the different power factors of the generator for different loading points. Therefore the capability diagram in addition to the power factor at different loading points is plotted. This can be seen in figure 48.

The efficiency map for the different loading points can be seen in the figure 49. From the iso-efficiency curves, one can see that the iso-efficiency curve at the nominal operating point is 98.83 %, which is the rated efficiency for the generator. This indicates that the iso-efficiency curves are correct. In addition to this one can notice that the measured loading point is aligned with its corresponding efficiency.

The pu power loss curves for the different loading points can be seen in figure 50. The curves indicate the pu power losses if the generator were to operate at a certain loading point for a year. This would for example mean that if the generator operated at (0.2,0.4) for an entire year the pu power

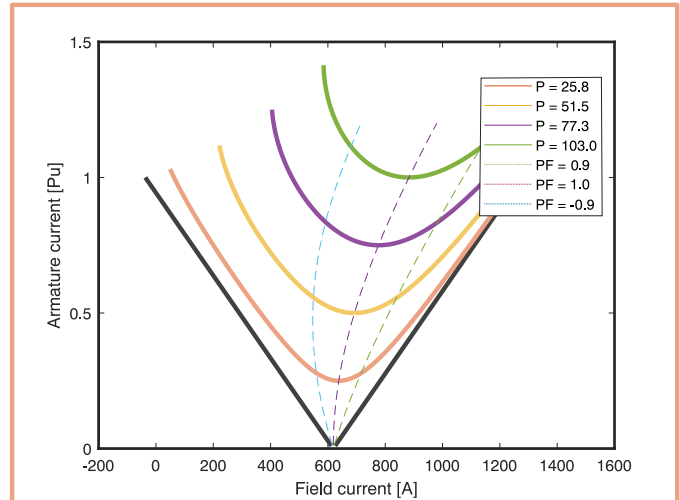


Fig. 47. The figure illustrates the v-curve family of Åbjøra. The figure illustrates the relationship between the armature current and the field current, for several constant active powers. The figure presents the v-curve family, for powers varying from 0 to 103 MW in steps of 25.7 MW. This means that the active power is held constant and the reactive power is gradually changed, which changes the field current.

losses would be 0.0075 pu.

### C. Comparing the Different Load Distribution

This subsection presents a calculation of the WAE and AAE for three different load distributions. The first load distribution under study is a concentrated load distribution

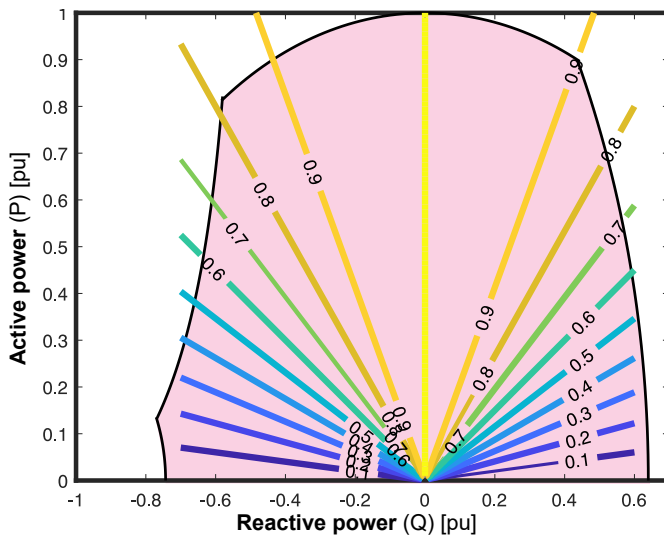


Fig. 48. The figure illustrates different  $\cos(\phi)$  at different loading points.

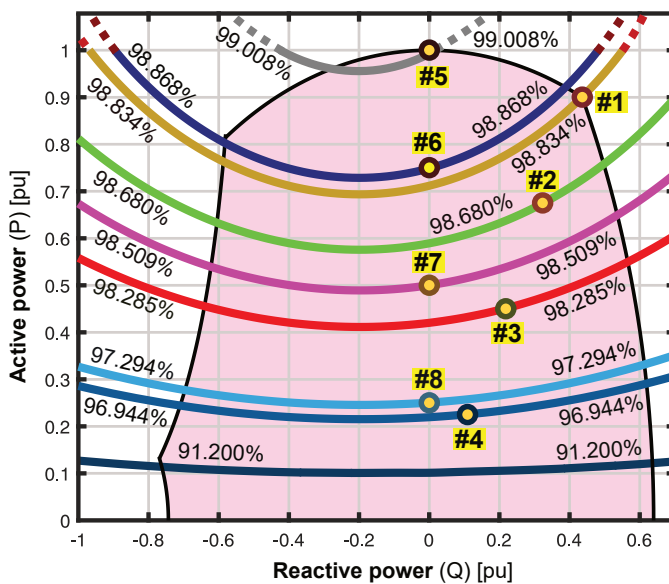


Fig. 49. Mapping of the calculated iso-efficiency curves of the capability diagram of the synchronous machine (G2), and assessed against eight measured operating points (referring to Table VIII).

from Åbjøra's production data. The second load distribution is a uniform load distribution, like the one illustrated in figure 10, after the Energiewende. The third load distribution is a synchronous condenser distribution, like the one illustrated in figure 24. The uniform load distribution and synchronous condenser distribution are artificially made because these kinds of datasets are not readily available. This comparison is done to illustrate how the AAE and WAE differ for different load distributions. It is also done to test the calculation models for more complex datasets.

The University of Southeast Norway provided production data from Åbjøra. The histogram and the bar plot of the production data are illustrated in figure 51. The figure depicts the duration and density of the discrete loading point. The sub-figure in the top left corner illustrated as a bar plot is very

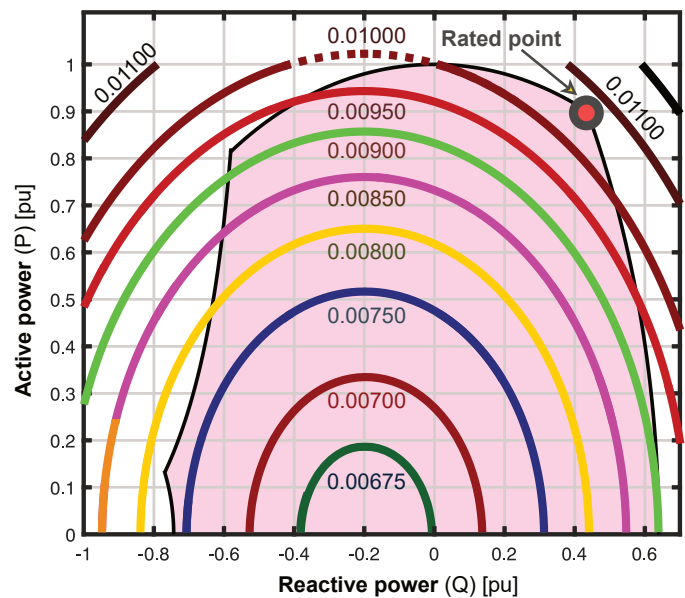


Fig. 50. Mapping of the calculated power loss contours over the capability diagram of the synchronous machine (G2) in per unit with 103 MVA as the power base.

illustrative and gives a better overview of the load distribution and their concentration, in comparison to the other sub-figures in figure 51. From the figure, one can see that most of Åbjøra's production is around 0.93 pu active power and the range of reactive power is very small. The reactive power ranges from -0.08 pu to 0.175 pu. This illustrates that the loading points are concentrated around a relatively small area. The density of the different loading points and the probability of occurrence can be seen in the 2D histogram, also illustrated in figure 51. The contours are also plotted to highlight where the loading points are concentrated. The WAE and the AAE in addition to other key parameters for this particular load distribution are illustrated in Table X.

As previously stated production dataset consisting of loading points that are partly or almost completely uniformly distributed is not readily available. The Energy transition is still in its infancy, which means that renewable energy sources are not as prevalent in Norway. Figure 52 illustrates the artificially made uniform load distribution. The load distribution has equal density across the entire capability diagram. A relatively simple case study is made where the number of discrete loading points is 641. The WAE and the AAE in addition to other key quantities for this particular load distribution are illustrated in Table X.

The synchronous condenser distribution is also illustrated in figure 52. In this distribution, a lot of the loading points are concentrated around 0. Forcing the generator to operate as a synchronous condenser. The synchronous condenser distribution in figure 52 operates below 0.02 pu 60.5% of the time. The WAE and the AAE in addition to other key quantities for this particular load distribution are illustrated in Table X.

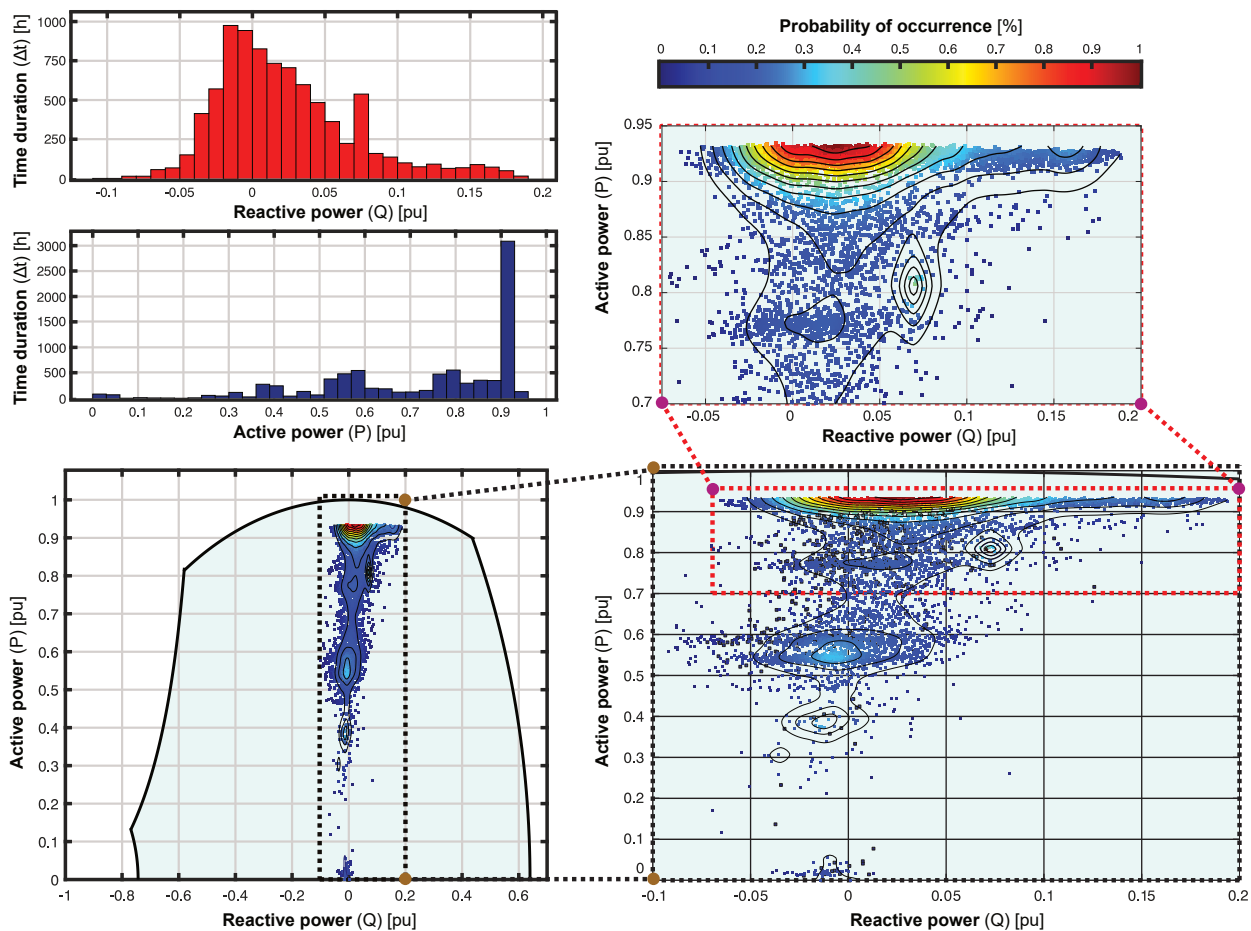


Fig. 51. Load distributions for a whole year of the studied hydropower plant. The minimum and maximum reactive power ranges from -0.08 to 0.2 pu. The minimum and maximum active power are varying from 0 to 1 pu. The measurements were recorded every hour, starting from 06. January 2020 15:00, ending at 31. December 2021 (i.e., 8610 h in total). The generator were operated 3087 h around the vicinity of the  $P_{max}$  region. Contour lines are added to indicate the density peaks. a): One-dimensional histogram of number of hours ( $\Delta t$ ). b): Two-dimensional histogram of probability of occurrence in percent (%).

TABLE X  
IMPORTANT QUANTITIES FOR DIFFERENT LOAD DISTRIBUTION/OPERATIONAL REGIMES.

Distribution	E	$E_{loss}$	$\bar{P}$	$\bar{P}_{loss}$	$\eta_w$	$\eta_a$	$\eta_a - \eta_w$	T
Concentrated load distribution	663.558 GWh	7.85 GWh	0.7354 pu	0.0087	98.17 %	98.83 %	+0.67 %	8610
Uniform load distribution	412.11 GWh	7.25 GWh	0.457 pu	0.0080 pu	96.84 %	98.27 %	+1.43 %	641
Synchronous condenser distribution	165.98 GWh	6.82 GWh	0.1840 pu	0.0076	62.87 %	96.05 %	+33.18 %	1517

#### D. The Characteristic Behaviors of the Calculation Models

In this subsection, the calculation models AAE and WAE are compared for different active power thresholds. In addition to this, an evenly distributed case was studied as a function of the number of elements ( $N$ ) inside the capability diagram, i.e. an increasing number of discrete loading points. This is done to study the characteristics behavior of the calculation models for different active power levels and increasing discrete loading points.

1) *Uniform distribution with Power Constraints*: Figure 53 illustrates the AAE and WAE for different active power thresholds. The active power threshold is increased from 0.001-1 pu, where all the uniformly discrete loading points are below this threshold. Figure 54 also illustrates the AAE and WAE for different active power thresholds. In this case

the threshold starts at 0.999 and goes to 0. All of the discrete loading points are uniformly distributed and above the active power threshold.

2) *Uniform load distribution with an increasing number of elements*: The uniformly distributed case was studied as a function of the number of elements ( $N$ ) inside the capability diagram. This can be seen in figure 55. As  $N$  is increasing, both the AAE and the WAE are shown to converge toward asymptotic values.

## VIII. DISCUSSION

This section consists of some reflected thoughts around the results and their meaning. This section starts by describing some observations and analysis of the saturation model, iso-efficiency curves, and the pu power loss curves. This section

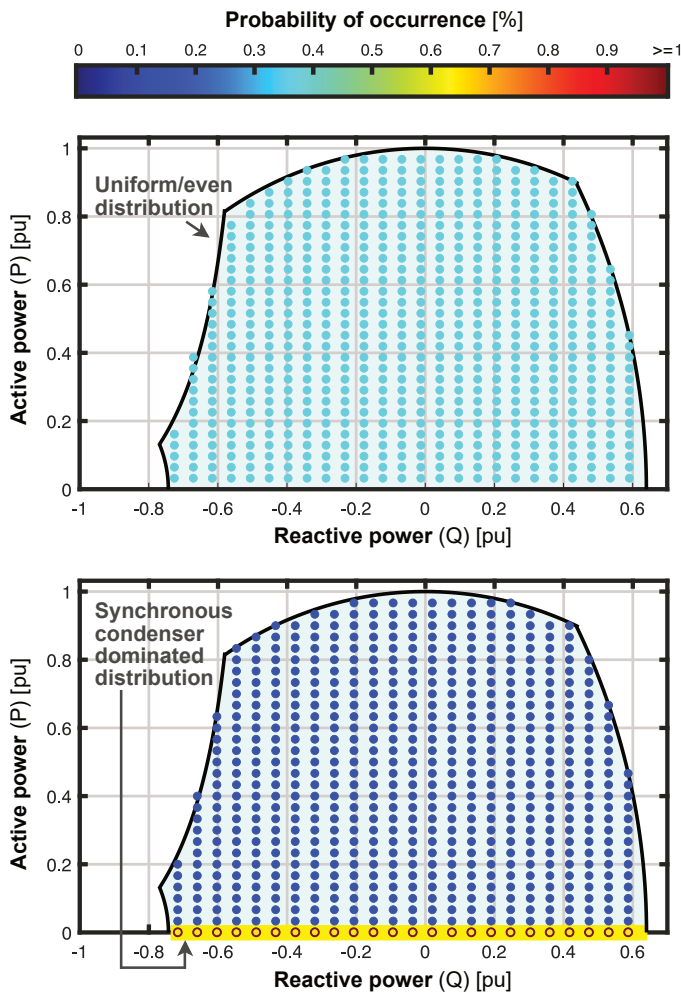


Fig. 52. The figure illustrates and artificially made uniform load distribution and synchronous condenser dominated distribution. The uniform load distribution has 641 discrete loading points. synchronous condenser dominated distribution has a 60.5 % probability for a loading point to occur below 0.02 pu in active power and has a 39.5% probability of occurrence for loading points outside this region. It is assumed an even distribution above 0.02 pu active power.

also explains the difference in results between the calculation models for different load distributions. In addition to this, some reflected thoughts and comments are made regarding the characteristic behavior of the calculation model for different active power thresholds in uniform load distributions. The calculation model for an increasing number of elements in a uniform load distribution is also studied and analyzed.

#### A. Efficiency Calculation and Saturation Model

An iso-efficiency map using the saturation model was plotted together with the measured efficiencies in figure 49. The calculated non-concentric curves show a good agreement with the measured operating points of Table VIII, as indicated in figure 49. The pu power loss curves are also plotted in the figure 50. This additional map is needed to conduct the proposed AAE, which is different from the alternative WAE. The most sensitive loss component was the saturation model, which predicts  $I_f$ . In Table IX, the accuracy of this model

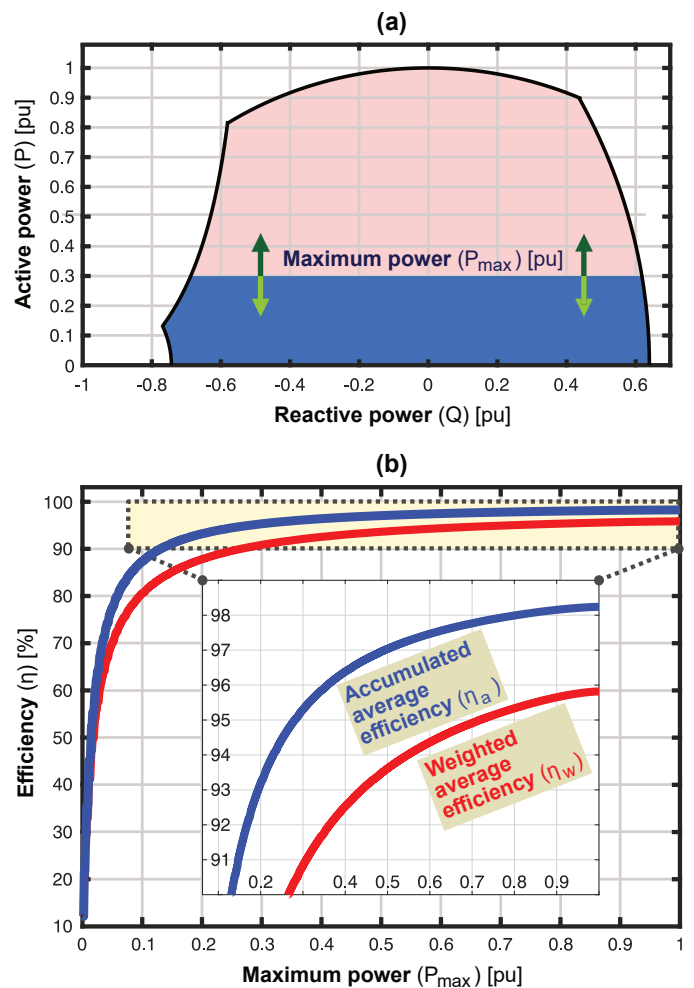


Fig. 53. The figure Compares the WAE to the AAE for different active power thresholds. The active power threshold is increased from 0.001-1 pu until the loading points are uniformly distributed throughout the entire capability diagram. (a): The dark blue area covering the evenly distributed load points. (b): Efficiencies ( $\eta_w$  and  $\eta_a$ ) plotted in terms of  $P_{max}$ , converging toward the values 98.24 % ( $\eta_a$ ) and 95.923 % ( $\eta_w$ ) as  $P_{max}$  approaches 1 pu. The number of elements (N) where 171 075.

was assessed against the measurements, revealing a worst-case deviation of 1.79 %, occurring in measurement number #5. The reason that the iso-efficiency curves are so perfectly aligned with the measured loading point is due to the accuracy of the saturation modeling. As previously stated the saturation modeling is the most sensitive loss component, which means that if the field currents saturation characteristic is not accurately model. The discrepancy between iso-efficiency curves and measured loading points will be prevalent in the iso-efficiency map. This also applies to the pu power loss curves.

#### B. Reason for the Disparities in the Results and its Consequences

1) *Disparities between the calculation models for a concentrated load distribution:* Today's generators operate with a concentrated load distribution which means that most loading point is concentrated around a relatively small area. Section VII shows the load distribution of Åbjørås production data. This is illustrated in figure 51. From the histogram that depicts



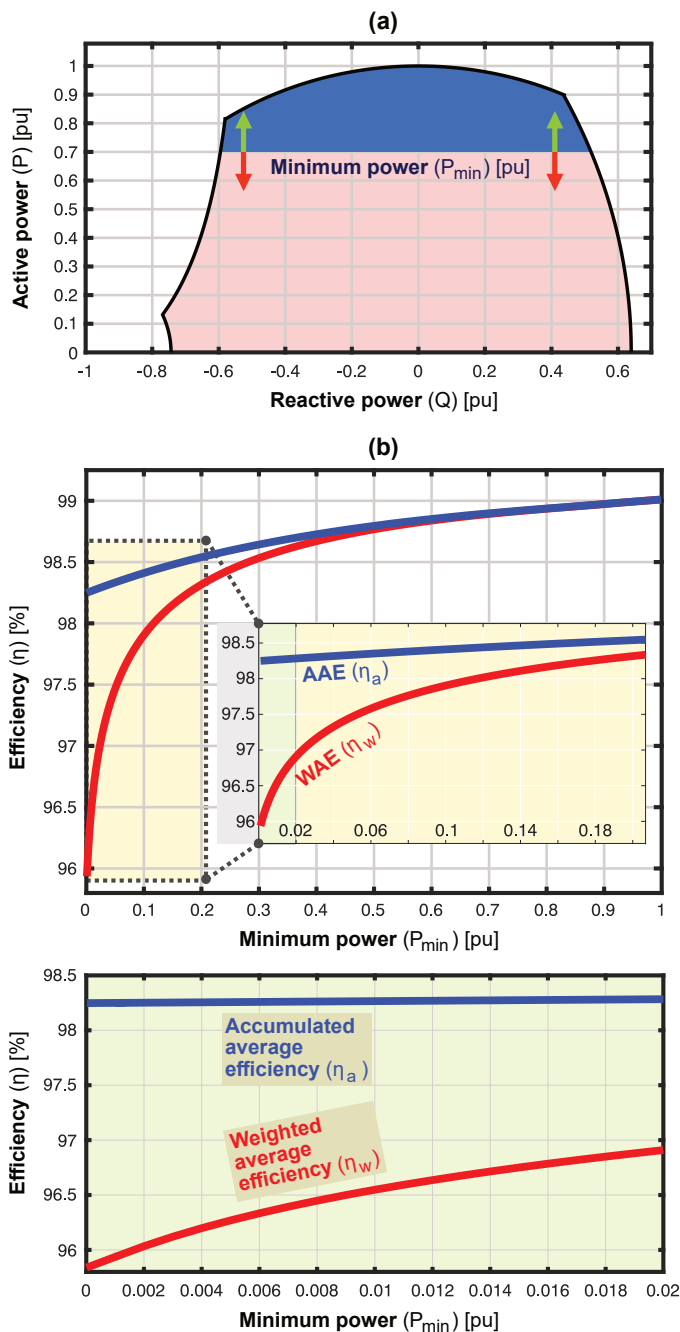


Fig. 54. The figure Compares the WAE to the AAE for different active power thresholds. The active power threshold is decreased from 0.999-0 pu until the loading points are uniformly distributed throughout the entire capability diagram. **a)** Definition of the minimum power ( $P_{min}$ ) with the dark blue area covering the evenly distributed load points. **b)** Efficiencies ( $\eta_w$  and  $\eta_a$ ) plotted in terms of  $P_{min}$ , converging toward the values the values 98.24 ( $\eta_a$ ) and 95.923 ( $\eta_w$ ) as  $P_{min}$  approaches 0 pu. The number of elements (N) where 171 075.

the duration one can see that most of the loading points are concentrated around the generators,  $P_{max}$  value. One can also see that reactive power production and consumption do not vary drastically. It ranges from -0.08 to 0.175 pu. This is not very clear in the 2D histogram illustrated in the sub-figure below. The 2D histogram shows the density of the discrete loading points, while the other figure shows for example that

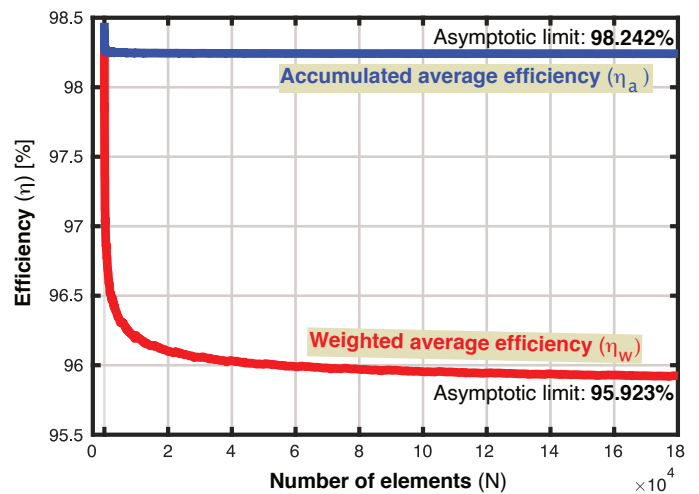


Fig. 55. The figure Compares the WAE to the AAE in a uniformly distributed load distribution. The number of discrete loading points is gradually increased until both values converge.

the generator operates 3087 hours around  $P_{max}$ . In other words, the figure shows that the generator operates 3087 hours out of 8610 hours around nominal power. One can see that the generator operates for very few hours around zero active power. The generator usually operates at zero, because it is turned off, not because it is operated as a synchronous condenser. The generator is not operating at very low active powers, which means that one gets a high efficiency. The 2D histogram that shows the density illustrates that most of the loading points are concentrated around  $P_{max}$ , which results in high efficiency and high weights for the efficiencies around nominal power. This gives a high WAE. The calculation model AAE is based on the accumulation of active power productions and losses. Because most of the loading points are at high active powers, the accumulated value must also be high. This gives a high AAE. This kind of load distribution gives high efficiency for both the WAE and AAE, which results in small disparities between the calculation models. The disparities is 0.67% and illustrated in Table [X](#)

2) *Disparities between the calculation models for a uniform load distribution:* Figure [10](#) shows the probability and distribution of loading point when there is a large integration and prevalence of renewable energy sources. The introduction of renewable energy sources gives a lot more loading points below eg. 0.6 pu active power, as explained in Section [III](#). The renewable energy sources will affect the operational range and the duration of the loading points. The duration of the loading points will be more evenly distributed. These datasets are not readily available, therefore an artificially made uniform load distribution was made. This was done to mimic the characteristics of a load distribution that is more or less evenly distributed and covers most if not the entire capability diagram, like the one illustrated in figure [10](#). The artificially made uniform load distribution was made to quantify the ramifications of uniformly distributed load distributions and their effect on the calculation models WAE and AAE.

The artificially made uniform load distribution is illustrated in figure [52](#). The load distribution is evenly distributed, i.e the

density is the same everywhere in the capability diagram. This creates a lower efficiency because it affects the probability of a loading point (low weight). In addition to low weights there is an increase of relatively low energy conversion efficiency because the generator produces a lot less active power, by not being concentrated around  $P_{max}$ . All this results in a lower WAE. As previously mentioned the weight plays a considerable role in the WAE calculation resulting in a lower WAE for the uniformly distributed case in comparison to concentrated load distribution. This can be seen quantitatively using equation 58. The weight is multiplied by the efficiency of a particular loading point. This means that if the likelihood of a loading point is low, the WAE is lowered.

By comparing the WAE of Åbjøra's production data with the uniform load distributions WAE one can see the significance of the weight in the calculation model. This has been quantitatively deduced and illustrated in Table X.

As previously stated, The AAE is independent of the weight and is lowered due to the increasing number of elements closer to the boundary of the synchronous condenser operations, where the efficiency is steeply approaching zero. This is quantitatively illustrated in Section VI-G, where the weight is factored out and removed. Since the weight does not affect AAE, one gets a higher "overall efficiency" in comparison to the WAE. Another reason for the higher efficiency is the fact that the active power production is accumulated. Summing the active power production, causes the high active power operations to mitigate or compensate for the low active power production giving a higher overall active power production and efficiency. This is also illustrated in the worked example in Section VI-G3, which demonstrates the working principles of equation 57 and 58. This results in a disparity of 1.43 % between the calculation models. This disparity is illustrated in Table X.

$$\eta_a = \frac{\sum_i^n P_{Prod(i)}}{\sum_i^n P_{Prod(i)} + \sum_i^n P_{Loss(i)}} \quad (57)$$

$$\eta_w = \sum_i^n A_i * \eta_i \quad (58)$$

3) *Disparities between the calculation models for synch. condenser load distribution:* In the worked example in Section VI-G3, three loading points were considered. The loading points were used to illustrate what happens to the efficiency of the different calculation models when the generator operates one-third of its yearly operating time at zero active power. It was illustrated that the efficiency dropped  $\frac{1}{3}$  as a consequence. In Section VII, a more realistic and complex load distribution is considered. The section illustrates a synchronous condenser distribution that is artificially made. This was done to mimic the characteristics of a load distribution where the generator operates as a synchronous condenser most of the time, like the one illustrated in figure 24. The WAE calculation of the synchronous condenser distribution illustrated in figure 52 gave a value equal to 62.87%, while the AAE gave a value equal to 96.05%. This gives a difference of 33.18%. This is illustrated in Table X.

The primary reason for the disparities is that calculation models WAE calculates the efficiency for a particular loading point and multiplies it with the weight, then sums all the efficiencies. If the generator operates at low active power for long periods, then one gets a summation of mostly zero or very low efficiency, which gives a low WAE. The calculation model AAE focuses on summing the active powers rather than the efficiency. As previously stated if one considers the loading points individually and calculates their corresponding efficiency one gets a summation of mostly zero efficiencies. This is because more elements will now be placed closer to the boundary of the synchronous condenser operations, where the efficiency is steeply approaching zero. The working principles behind this disparity are quantitatively deduced in the worked example in equation 54 and 53.

From the results section, one can see that the calculation model AAE supersedes the WAE for all the operational regimes investigated. The biggest advantage of the calculation model is when the generator has a synchronous condenser distribution. I.e when the generator produces little or no active power for relatively long periods. This gives vast differences in efficiency between the calculation models.

If one looks at Table X one can see that the weight plays a role in the WAE calculation, but very low active powers play the most significant role when it comes to the WAE. This means that operating the generator as a synchronous condenser is the "worst-case scenario" in regards to the "overall efficiency" of the generator. In other words, operating the generator as a synchronous condenser for long periods will give the lowest efficiency compared to the other load distributions.

4) *Uniform distribution with Power Constraints:* In figure 53 one can see that the deviation is greatest around 0.1-0.3 pu active power. This is because of the reason previously stated, the calculation model AAE accumulates the active power production, where the high active power operations increase the "overall efficiency". This causes the calculation model to differ in their results. This is because the WAE model gives low efficiency for relatively low active power operations. As one increases the threshold to 1, one can see that the WAE and AAE converge to the values 98.24% ( $\eta_a$ ) and 95.923% ( $\eta_w$ ). This is because the threshold is increased until the discrete loading points cover the entire capability diagram.

In figure 54 the active power threshold is reduced from 0.999-0, the calculation models are the same for very high active powers. As one lowers the threshold, the calculation models start to diverge. This is primarily due to two reasons. The first reason is that lowering the threshold increase the number of the discrete loading point. This reduces the weight. The second reason is due to the inclusion of more and more relatively low active power operations by gradually lowering the active power threshold.

5) *Uniform load distribution with an increasing number of elements:* The evenly distributed case was studied as a function of the number of elements ( $N$ ) inside the capability diagram. This can be seen in figure 55. The AAE and the WAE are shown to converge toward asymptotic values as  $N$  increases. The deviation between the AAE and WAE is found

to be 2.32%. The AAE and WAE behave similarly with very few elements, but the weighting in the WAE model causes the calculation models to diverge with increasing  $N$ . This is because the weight becomes lower for increasing discrete loading points, and as previously stated the weight plays a significant role in the WAE calculation. In addition to this is more elements will now be placed closer to the boundary of the synchronous condenser operations, where the efficiency is steeply approaching zero. Increasing the discrete loading point beyond a certain point does not affect WAE. This is because the discrete loading points are distributed throughout the entire capability diagram. The density is so compact that the weight remains constant. This causes the WAE to converge. The AAE is independent of the weight and converges due to the increasing number of elements closer to the boundary of the synchronous condenser operations, where the efficiency is steeply approaching zero.

6) *Proposed solution and implementations*: Bortoni technical report states that the generator G1 has a WAE of 64.84%. This is because the generator operates at low active power for long periods. In the technical report, it is stated that. "One can observe that about 40% of the time, the active power is higher than 0.6 pu, with efficiencies greater than 97%, on the other hand, the active power is below 0.02 pu about 50% of the time, with efficiencies lower than 55%. One must also take into consideration that those values are weighted by their probabilities of occurrence, resulting in a considerable reduction of the WAE in comparison to the rated efficiency of 98.4%. As previously stated this can also be seen illustratively by looking at figure 25. The technical report proposes a lower limit of active power generation equal to 0.6 pu. By doing this one gets a WAE efficiency equal to 98.01%, which is relatively close to the generator's rated efficiency of 98.4%.

The technical report offers a proposed solution but does not state how the solution is implemented. This is vital for the validity of the proposed solution. The implementation would most likely involve expensive power electronics. This is because forcing the generator to operate above a 0.6 pu active power limit reduces its reactive power capability. This is because the reactive power operating range of the generator becomes smaller as one moves further up in the capability diagram. Germany's "Energiewende" illustrates that a wider operating range is necessary when a lot of renewable energy sources are connected to the grid. In other words, using a threshold of 0.6 pu would limit the operating range of the generator and result in not utilizing the full operating capacity of the generator. From a technical-economic perspective, the best solution is to utilize most of the operating capacity if not all of the operating capacity provided by the generator. The accumulated average efficiency gives a viable solution to the challenges caused by the energy transition and prevents the utilization of an active power threshold when the generators operate as a synchronous condenser.

7) *A technical-economic perspective*: If one compares the WAE and AAE for uniform load distribution one can see that the AAE gives approximately 1.43% higher efficiency. This can be seen in Table X. This number may seem small and insignificant, but a 1.43% difference in efficiency could rep-

resent a large difference in generation cost. In other words, the difference is not quantitatively large, but from a technical and economical perspective this difference could be significant. The same applies to the concentrated load distribution where the difference is 0.67%. The significance of this could be further studied. An example could be a cost-benefit analysis that quantifies the economical implications.

The generator range in reactive power production and consumption can be vast when the generator is operating as a synchronous compensator. This stresses the excitation system and gives relatively large losses related to the excitation system. In other words, one gets huge excitation losses when the generator is running purely as a synchronous compensator and if one also considers the fact that it is running as a synchronous compensator for long periods.

Its common practice to design a machine for a specific application. It is observed that, the larger the diameter of the machine is, the larger the losses will be. It is also observed that the losses related to the armature current vary drastically depending on the size of the machine. This means that it is better to design the machine in regards to a specific purpose or an expected "overall efficiency". For this to happen one needs to design a generator using a calculation model that is applicable for all kinds of load distribution. Making a calculation model like AAE highly relevant in regards to the design of future hydro generators.

## IX. CONCLUSION

This report has comprehensively explored a wide variety of realistic operating points of hydro generators due to the ongoing energy transition. In Section III, the different operational regimes resulting from increased grid-integration of renewable energy sources are explored. It is highlighted that the classical operation mode with base, average, and peak condition, is no longer valid. New calculation schemes are necessary to accurately quantify the "efficiency" of a generator, in other words, to accurately quantify the impact of new operational regimes. This is because these new operational regimes were not considered during their past development, it is a new phenomenon caused by the integration of renewable energy. The integration of new power sources such as solar power panels and wind farms creates a fundamental change in the power grid's load regime, seen from the hydro-generator operators. These changes cause a higher variation in production, which results in huge electromechanical stresses on the machine and a drastic increase in losses (due to rapid power ramping and different inefficient operating conditions). The increased thermo-mechanical loading and load variation cause significant stresses on the generator and excitation system. Consequently, the losses concerning the field current and magnetic saturation play a significant role in determining the losses and the efficiency of the hydro-generator during different loading points.

A new method to determine the "overall efficiency" of synchronous generators under intermittent operation is proposed, incorporating the machine's magnetic saturation. Section VI introduces a procedure where one considers the magnetic

saturation of a generator using the most appropriate method based on the available data. It is emphasized that determining saturation is a rigorous task. Moreover, this is because there are a wide variety of methods and approaches to determine and quantify the saturation. Therefore one must choose the procedure based on semi-heuristic reasoning, judiciously chosen approximations, available data, and accuracy of the method/results. The losses concerning the field current and magnetic saturation introduced in this report are fairly accurate and have a maximum deviation of 1.79 % in comparison to the measured nominal field current.

Section VI-E explains the underlying theory and assumption regarding the practical stability limit. By starting from the relationship which shows the active and reactive power of the generator dependency on the power angle  $\delta$ . The breakover angle can be determined for which active power is a function of the power angle  $\delta$ . In this subsection, it was concluded that if the mechanical power from the generator were to be increased beyond  $P_{max}$ , i.e the generator crosses its break-over angle. The electromechanical torque would no longer be in balance with the mechanical torque and the generator would slip out of synchronism. Two different methods were used to validate the results of the calculations.

Section VI-H5 introduces a procedure where one considers the density and distribution of the loading points. In this section, the density is increased so much that the total energy losses (TEL) reach a converging value. In this section, it was concluded that increasing the number of discrete loading points beyond this converging value had little to no difference in the TEL. The TEL was also investigated using different zones. Bortoni calculates the weight using zones of "exact loading points". In other words, the zone consist of all the discrete loading points rounded up to exact values. This report presented an implementation of different zones for AAE. This was used to capture the discrete loading points and quantify their probability of occurrence, and the total energy losses inside these zones. The discrete load operation was divided into zones of different sizes and shapes. After studying the different zones a conclusion of the most appropriate zone was made.

It is shown that the proposed AAE is more effective and adaptable than the alternative WAE for all the different load distributions that were investigated. The AAE is therefore, a possible tool to quantify a generator's overall efficiency accurately in future operating regimes. To legitimize the results, the efficiency and loss map has been validated by eight handpicked load-point measurements. Once the method was validated the AAE and the WAE were compared. The following findings comparing the AAE and the WAE have been identified.

- 1) A load distribution dominated by synchronous condenser generation yields a difference as high as 33.18 %, while an even distribution deviates by 1.43 % in their respective efficiencies;
- 2) A concentrated load distribution found from a full year of measurements on the studied generator revealed a discrepancy of 0.67 %, which could be a significant deviation considering what the operating regime would mean in terms of economic implications;

- 3) It is perceived that there are technical and economical implications of the significant reduction in the WAE against the AAE, as it is much more heavily influenced by the weight coefficients and by intervals of lower active power.

The additional costs for intermittent operation of hydro generators should not merely be investigated in terms of losses, but also its implication on the generator's lifetime. The burden is not only influenced by the static load points, but also by the rapid transitions between them. Future work should also investigate how the loading regime could be better incorporated into the design of future hydro generators.

These kinds of studies are projected to have a significant impact. The information harvested in these kinds of projects lays the foundation for the design and operation of future hydropower plants. Therefore actual data and comprehensive studies on these kinds of issues are highly relevant for policymakers to make wise decisions paving the way for a sustainable energy transition.

## X. FURTHER WORK

In this section, some reflected comments about the entire study are made. The possibility for further work is also discussed. Its common practice to design a machine for a specific application. It is observed that, the larger the diameter of the machine is, the larger the losses will be. It is also observed that the losses related to the armature current vary drastically depending on the size of the machine. Future work should investigate how the loading regime could be better incorporated into the design of future hydro generators. One can use the calculation model AAE to calculate the overall efficiency using the entire operational regime. One can then design the machine in regards to the AAE. A lot of the algorithms developed in this report are not fully automated, a possibility could be to automate the entire process for calculating the AAE and other important quantities. A more comprehensive study could be done on the different calculation models presented in this report. A more detailed study on the calculation model's response to different load distribution could also be made. This report is submitted to the University of Southeast Norway for further study. The methods deduced and developed for the two calculation models, as well as algorithms developed in this report, are also submitted.

1) *Estimating the losses in a generator at nominal operation:* One of the necessary input parameters is the losses in the generator at the nominal operating point. In other words  $P_{an}$ ,  $P_{fn}$ ,  $P_{sn}$ ,  $P_{brn}$ ,  $P_{ex}$ ,  $P_b$ ,  $P_{wf}$  and  $P_{cn}$ . One can implement an algorithmic procedure that calculates these losses based on standard parameters/rated data of the generator. There is a method developed by a professor called Erling Westgaard which calculates the dimension of a generator and the losses in a generator based on educated guesses and rules of thumbs. The book is called "dimensjoneringseksempel for synkronmaskin" [44]. The book illustrates the design procedure for a hydro generator above 5 MVA. The book also illustrates a calculation procedure for determining generator losses at the nominal operating point. The calculation procedure developed

TABLE XI  
THE KNOWN DATA VALUES IN WESTGAARD'S METHOD

Data	Values
S	47 MVA
n	166.67
n <sub>r</sub>	441
cos( $\phi$ )	0.9

in the book can be used to estimate generator losses at the nominal operating point. The design procedure by Westgaard takes into account that certain data values are known or specified. These values can be seen in Table XI.

Westgaard's method also takes into account three important criteria that must be fulfilled. The first criterion is that the synchronous reactance of the generator is lower or equal to 1.1 pu. The second criterion states that the moment of inertia  $GD^2$  must be equal to or greater than  $225 \text{ tm}^2$ , and the third criterion is that the temperature rise in the stator and field winding's must not exceed  $60 \text{ }^\circ\text{C}$ . If these values are known and the criteria are fulfilled the design procedure can begin. By using this procedure one can calculate/ estimate almost all the dimensions of the generator, in addition to important quantities like rated armature current and terminal voltage.

In most cases, the rated generator losses are given in the datasheet of the generator. The calculation model AAE can be used on a particular generator's expected yearly production. The AAE of the existing generator can be used to determine the design parameters of future generators. Erling Westgaard's "dimensjoneringseksempel for synkronmaskin" can be used to roughly estimate the dimensions of a generator giving an efficiency equivalent to the AAE. The designed parameters can then be finely tuned using the book "Design of rotating electrical machines" [45], which is written by Juha Pyrhönen. The book illustrates the design procedure for different electrical machines. The design procedure developed in the book is very precise and can be used to finely tune the design parameters. The design parameters can be calculated using the software MATLAB. Once the design parameters are established one can build the model in COMSOL Multi-Physics where one can tune the parameters even more and stress test the generator.

2) *Automatising the implementation of saturation data and the Algorithmic procedure:* In Section VI the Anderson and Faoud method was introduced. This method uses the open circuit characteristic (OCC) to calculate the saturation factors  $S_{1,0}$  and  $S_{1,2}$ , which is respectively the saturation factor at the rated terminal voltage and 20% overvoltage. These saturation factors are often given in the industry. Sometimes the saturation factors are given instead of the OCC. An illustration of a dataset consisting of saturation factors for several different generators is placed in the appendix and can be seen in figure 56. One can develop an algorithm that extracts the saturation factors of the different generators from for example an excel document and plots the OCC of that particular generator. This can be done by reverse-engineering the Anderson and Faoud method to deduce the saturation curve. The easiest procedure would be to implement the saturation factor directly using the Anderson and Faoud method.

The dataset in figure 56 illustrates several important rated quantities like the synchronous reactance in the d-axis and q-axis, and the generators rated voltage and armature current, but not the rated generator losses, which illustrates the importance of being able to implement an algorithm like the one developed by Erling Westgards. This particular dataset has all the necessary input to run the WAE and AAE algorithm except for the generator losses at the nominal operating point, and its yearly production data.

The algorithms developed for calculating the fitting equation constants, capability diagram, iso-efficiency curve, total energy loss curves, and AAE are only partly automated. One could further this study by atomizing the entire process. This means that the algorithm would take specific inputs and calculate the level of saturation, capability diagram, iso-efficiency curve, total energy loss curves, and AAE (output). In other words combine all the different individual algorithm as one complete algorithm, which output eg. the iso-efficiency curves, total energy loss curves, and AAE.

3) *A more comprehensive study:* A more comprehensive study could be done on the different calculation models presented in this report. In addition to this, a more detailed study on the different load distribution could also be made. Once data with operating range like "Energiewende" are more readily available a study on uniform load distribution could be made using actual industry data. This could give an additional validation of the significance of the calculation models. As previously stated this report is submitted to the University of Southeast Norway. This is done to conduct further studies on the calculation model AAE. This calculation model will be tested for different operational regimes and possibly developed further. Another approach would be to implement a new calculation model that is even better than the ones presented in this report.

## XI. ACKNOWLEDGEMENT

I would like to express my gratitude to my supervisors Jonas Kristiansen Nøland and Thomas Øyvang for providing me with excellent guidance throughout my fifth year here at NTNU. I would also like to thank Trond Leiv Toftevaag for providing additional feedback and being a good sparring partner regarding the fundamentals.

## REFERENCES

- [1] E. d. C. Bortoni, "Efficiency map and weighted average efficiency for synchronous machines for hydropower plants," *Technical report, Universidade Federal de Itajuba (UNIFEI)*, 2019.
- [2] Y. C. Karekezi, T. Øyvang, and J. K. Nøland, "The energy transition's impact on the accumulated average efficiency of large hydrogenerators," *IEEE Trans. Energy Convers. (under review)*, vol. PP, no. 99, pp. 1–10, 2021.
- [3] J. Machowski, "Power system dynamics : stability and control," Chichester, 2008.
- [4] T. Øyvang, J. K. Nøland, R. Sharma, G. J. Heggliid, and B. Lie, "Enhanced power capability of generator units for increased operational security using nmpc," *IEEE Trans. Power Syst.*, pp. 1–1, 2019.
- [5] J.-H. Braam, "Development, test and validation of new generator product line for current and future operational regimes," *CIGRE*, 2018.
- [6] ENSOE, "Requirements for Generators (RFG)," *ENTSO-E*, 2016.
- [7] A. Joswig and M. Baca, "Extended requirements on turbo-generators and solutions for flexible load operation," in *Proc. XXII Int. Conf. Elect. Mach. (ICEM)*, Sep. 2016, pp. 2649–2654.

- [8] B. B. Contributor, *Brazilian Companies Increase Investments In Renewable Energy*. [Online]. Available: <https://www.hartenergy.com/exclusives/brazilian-companies-increase-investments-renewable-energy-177301>
- [9] A. Nami, "Power electronics for future power grids: Drivers and challenges," in *2018 20th European Conference on Power Electronics and Applications (EPE'18 ECCE Europe)*, 2018, pp. P.1–P.2.
- [10] J.-H. Braam, "Development, test and validation of new generator product line for current and future operational regimes," 2018.
- [11] B. Zhu, X. Zheng, S. Shen, Y. Jiang, Z. Zhang, Y. Huang, C. Tong, Y. Su, L. Yang, and Z. Lin, "Development path of future power grid with high proportion of renewable energy in the context of electricity spot market," in *2020 IEEE 4th Conference on Energy Internet and Energy System Integration (EI2)*, 2020, pp. 3827–3831.
- [12] F. Ayadi, I. Colak, I. Garip, and H. I. Bulbul, "Impacts of renewable energy resources in smart grid," in *2020 8th International Conference on Smart Grid (icSmartGrid)*, 2020, pp. 183–188.
- [13] W. Yang, P. Norrlund, L. Saarinen, A. Witt, B. Smith, J. Yang, and U. Lundin, "Burden on hydropower units for short-term balancing of renewable power systems," *Nature communications*, vol. 9, no. 1, pp. 1–12, 2018.
- [14] J. K. Nøland, S. Nuzzo, A. Tessorolo, and E. F. Alves, "Excitation system technologies for wound-field synchronous machines: Survey of solutions and evolving trends," *IEEE Access*, vol. 7, pp. 109 699–109 718, 2019.
- [15] E. Agneholm, "REPORT ON COORDINATION OF GRID CODES AND GENERATOR STANDARDS: Consequences of diverse grid code requirements an synchronous machine design and standards," *Technical report PES-TR69*, pp. 1–88, Feb 2019.
- [16] T. Øyvang, J. K. Nøland, G. J. Heggliid, and B. Lie, "Online model-based thermal prediction for flexible control of an air-cooled hydrogenerator," *IEEE Trans. Ind. Electron.*, vol. 66, no. 8, pp. 6311–6320, Aug 2019.
- [17] W. Tang, J. Hu, Y. Chang, and X. Kong, "Short-circuit current of grid-connected voltage source converters: Multi-timescale analysis method," in *Proc. IEEE PES GM*, July 2017, pp. 1–5.
- [18] IEEE, "Ieee standard for cylindrical-rotor 50 hz and 60 hz synchronous generators rated 10 mva and above," *IEEE Std C50.13-2014 (Revision of IEEE Std C50.13-2005)*, pp. 1–63, May 2014.
- [19] A. Joswig, K. Walli, and M. Baca, "Synchronous rotating equipment as backbone for renewables," in *VDE High Voltage Technology 2018; ETG-Symposium*. VDE, 2018, pp. 1–6.
- [20] *Short Circuit Ratio*. [Online]. Available: [https://en.wikipedia.org/wiki/Short\\_circuit\\_ratio](https://en.wikipedia.org/wiki/Short_circuit_ratio)
- [21] K. Mayor, L. Montgomery, K. Hattori, and J. Yagielski, "Grid code impact on electrical machine design," in *Proc. IEEE Power Energy Soc. Gen. Meeting*. IEEE, 2012, pp. 1–8.
- [22] N. R. E. Laboratory and I. P. S. O. C. Limited, "Ramping up the ramping capability," Tech. Rep., September 2020.
- [23] L. Rouco, K. Chan, J. Oesterheld, and S. Keller, "Recent evolution of european grid code requirements and its impact on turbogenerator design," in *Proc. IEEE Power Energy Soc. Gen. Meeting*. IEEE, 2012, pp. 1–9.
- [24] W. E. Council and CAISO, "Five steps to energy storage," Tech. Rep., 2020.
- [25] J. K. Nøland, M. Leandro, A. Nysveen, and T. Øyvang, "Future operational regimes of bulk power generation in the era of global energy transition: Grid codes, challenges and open issues," in *Proc. IEEE Power Energy Soc. Gen. Meet. (PESGM)*, 2020, pp. 1–5.
- [26] O. Rahman, K. M. Muttaqi, and D. Sutanto, "High temperature superconducting devices and renewable energy resources in future power grids: A case study," *IEEE Transactions on Applied Superconductivity*, vol. 29, no. 2, pp. 1–4, 2019.
- [27] D. Fenwick and W. Wright, "Review of trends in excitation systems and possible future developments," in *Proc. of the Institution of Electrical Engineers*, vol. 123, no. 5. IET, 1976, pp. 413–420.
- [28] F. Yao, Q. An, X. Gao, L. Sun, and T. A. Lipo, "Principle of operation and performance of a synchronous machine employing a new harmonic excitation scheme," *IEEE Trans. Ind. Appl.*, vol. 51, no. 5, pp. 3890–3898, 2015.
- [29] S. Nuzzo, M. Galea, C. Gerada, and N. Brown, "Analysis, modeling, and design considerations for the excitation systems of synchronous generators," *IEEE Trans. Ind. Electron.*, vol. 65, no. 4, pp. 2996–3007, April 2018.
- [30] Z. Zhang, Y. Liu, B. Tian, and W. Wang, "Investigation and implementation of a new hybrid excitation synchronous machine drive system," *IET Elect. Power Appl.*, vol. 11, no. 4, pp. 487–494, 2017.
- [31] IEEE, "Discussion on "review of trends in excitation systems and possible future developments"," *Electrical Engineers, Proceedings of the Institution of*, vol. 123, no. 12, pp. 1363–1364, December 1976.
- [32] D. C. Ludois, J. K. Reed, and K. Hanson, "Capacitive power transfer for rotor field current in synchronous machines," *IEEE Transactions on Power Electronics*, vol. 27, no. 11, pp. 4638–4645, Nov 2012.
- [33] IEEE, "IEEE standard for salient-pole 50 hz and 60 hz synchronous generators and generator/motors for hydraulic turbine applications rated 5 mva and above," *IEEE Std C50.12-2005 (Previously designated as ANSI C50.12-1982)*, pp. 1–45, Feb 2006.
- [34] —, "IEEE standard definitions for excitation systems for synchronous machines," *IEEE Std 421.1-2007 (Rev of IEEE Std 421.1-1986)*, pp. 1–38, July 2007.
- [35] F. Evestedt, *Improving the Functionality of Synchronous Machines using Power Electronics*. Licentiate thesis, Division of Electricity, Angstrom Laboratory, Uppsala University, Uppsala, Sweden, 2017.
- [36] P. Kundur, "Power system stability and control," Toronto, 1993.
- [37] Y. C. Karekezi, *A In-Depth Study of Hydro-Generator Losses and Efficiencies for Different Load Operations: Quantifying the Impact of the Energy Transition*, December 2020.
- [38] C. A. P. Gaona, F. B. García, P. F. Marín, M. R. Cuevas, R. G. Arrabé, and C. C. López, "Rapid de-excitation system for synchronous machines with indirect excitation," Feb. 11 2010, US Patent App. 13/201,971.
- [39] R. Thornton-Jones, I. Golightly, N. Gutteridge, C. Huizer, and D. Navratil, "Review of generator and excitation system specification and test requirements to satisfy multiple international grid code standards," in *Proc. IEEE Power and Energy Soc. Gen. Meeting*, July 2012, pp. 1–6.
- [40] F. Bensmaine, A. Barakat, S. Tnani, G. Champenois, and E. Mouni, "Dual control of synchronous generator for terminal voltage regulation-comparison with a single control," *Electric Power Systems Research*, vol. 91, pp. 78–86, 2012.
- [41] S. Sourish Sanyal Sohorab Hossain Sujit Dhar, "Computer-aided analysis of saturation in synchronous machines," 2017.
- [42] H. Gorginpour, "Optimal design of brushless ac exciter for large synchronous generators considering grid codes requirements," *IET Gen., Trans. Dist.*, vol. 12, no. 17, pp. 3954–3962, 2018.
- [43] K. N. D. Pejovski, B. Velkovski, "Matlab model for visualization of pq diagram of a synchronous generator," *Researchgate*, 2016.
- [44] E. H. Westgaard, "Dimesjoneringseksempel for synkronmaskin," Trondheim, 1965.
- [45] J. Pyrhonen, V. Hrabovcova, and T. Jokinen, *Design of Rotating Electrical Machines*, 1st ed. New York: Wiley, 2009.

## LISTINGS

1	Code for the OCC remake shown in figure 12 .	37
2	Code for the theoretical and practical stability limit shown in figure 20 . . . . .	37
3	Code for contour plot of the practical stability limit shown in figure 20 . . . . .	38
4	Code for the final capability diagram (G1) shown in figure 21 . . . . .	39
5	Code for the iso-efficiency curves of G1 illustrated in fig. 27 . . . . .	40
6	Code for the energy prod. and loss illustrated in figure 29 and 28 . . . . .	41
7	Code for the converging value shown in figure 31 . . . . .	42
8	Code for the three different densities inside the cap. . . . .	44
9	Code for the distribution circles. . . . .	46
10	Additional function that plots circles . . . . .	48
11	Additional function that clean vector of zero . . . . .	49
12	Additional function that plots datapoints inside cap. . . . .	49
13	Additional function that plots datapoints inside the circle . . . . .	50
14	Code for the scatter plot in figure 44 . . . . .	52

15	Code for the measured OCC in figure 45	. . . .	52
16	Code for the replicated OCC in figure 46	. . . .	53
17	Code for the V-curve family shown in figure 47	. . . .	53
18	Code for the efficiency map in figure 49	. . . .	54
19	Code for the energy loss map in figure 50	. . . .	55
20	Code for the 2D histogram in figure 51	. . . .	56
21	Code for the synch. cond dis. in Fig. 52	. . . .	56
22	Code for the uniform load dis in figure 52	. . . .	57
23	Code for the max active power threshold in figure 53	. . . . .	57
24	Code for the min active power threshold in figure 54	. . . . .	58
25	Code for increasing number of elements shown in figure 55	. . . . .	59
26	Function that calculates WAE and AAE for AAbjora	. . . . .	60
27	Function that plots AAbjoras capability diagram	. . . . .	61
28	Function that plots datapoints ins. cap. of AAbjora	. . . . .	62
29	Function that plots field current using the fitting function method	. . . . .	63
30	Function that plots the approximated field current	. . . . .	64

AM	AN	AO	AP	AQ	AR	AS	AT	AU	AV	AW		
(mettet Rs20 p.u	R0 p.u	Tekst (Valgmulig	S(1,0) p.u	S(1,2) p.u	Uf0	V (fe H	Ws/VA	Gr^2	kgm^	"1" Ak		
Nullsystem	Resistans	Nullsystem	Rotortype	Antall	Metningsfaktor ved 1.0	Metningsfaktor ved 1.2 p.u.	feltsp	Feltspenning (luftgapslinje)	ved merkesp			
JLLSYS	RESISTAN	NULLSYS	ROTORT	ANTA	METN_FAKT	FELTSP	METN_FAKT_FELTSP	S12	FELTSP_I	TREGHET	TREGHETS	METN
0,100	0,0070	0,0039	Utpregede	6	0,087		0,318	40,0	0,6	867,5		
0,106	0,0091	0,0056	Utpregede	8	0,079		0,271	28,8	1,3	3298,2		
0,075	0,0151	0,0110	Sylindrisk	4					0,3	256,0		
0,067			Sylindrisk	4					0,5	380,0		
0,112	0,0166		Sylindrisk	9					0,8	3456,3		
0,045			Sylindrisk	6					0,5	1125,0		
0,133			Sylindrisk	8					0,7	3560,5		
0,063	0,0096		Sylindrisk	5					0,6	1500,0		
0,047			Utpregede	5					0,8	2200,0		
0,009			Sylindrisk	3					0,8	846,1		
0,049	0,0061		Sylindrisk	6					0,7	2840,0		
0,184			Sylindrisk	16					0,4	12500,0		
0,086	0,0052	0,0026	Utpregede	20	0,053		0,208	66,5	2,3	155119,3		
0,048	0,0035	0,0020	Utpregede	6	0,087		0,399	45,3	1,1	7125,0		
	0,0043		Utpregede	3					1,1	2100,0		
0,090	0,0044	0,0027	Utpregede	8	0,063		0,262	69,9	1,2	17665,4		
0,062	0,0050	0,0027	Utpregede	20	0,125		0,561	124,9	1,6	147478,1		
0,062	0,0050	0,0027	Utpregede	20	0,125		0,561	124,9	1,6	147478,1		
0,069	0,0038	0,0023	Utpregede	10	0,099		0,468	81,6	1,6	44435,9		
0,069	0,0038	0,0023	Utpregede	10	0,099		0,468	81,6	1,6	44435,9		
0,065	0,0038	0,0021	Utpregede	10	0,154		0,883	59,2	1,9	53877,4		
0,063	0,0036		Utpregede	8					1,2	24800,0		
0,089	0,0044	0,0028	Utpregede	10	0,062		0,248	66,1	2,7	100000,0		
0,142	0,0044	0,0027	Utpregede	6	0,038		0,159	59,7	2,8	37337,0		
0,142	0,0044	0,0027	Utpregede	6	0,038		0,159	59,7	2,8	37337,0		
0,100	0,0057	0,0041	Utpregede	30	0,073		0,292	252,5	2,4	791786,4		
0,098	0,0031	0,0019	Utpregede	9	0,061		0,252	46,5	2,0	61750,0		
0,122	0,0041	0,0066	Utpregede	12	0,108		0,527	101,1	1,7	95000,0		
0,044	0,0024	0,0014	Utpregede	4	0,061		0,248	30,3	2,9	17800,1		
0,001	0,0026	0,0010	Utpregede	8	0,041		0,144	57,4	1,7	42750,0		

Fig. 56. The figure illustrates a dataset of different saturation factor for different generators.



APPENDIX A  
MATLAB CALCULATIONS

A. Code for OCC remake shown in Fig. 12

Listing 1. Code for the OCC remake shown in figure 12

```

1
2 %Data
3 Xq_pu= 0.72
4 Xp_pu= 0.2
5 Xd_pu=1.09
6
7
8 n=7
9 C=0.175
10 k=1.12
11 V=0:0.01:1.5
12 If=(V+C.*V.^n).*k
13 %If2=V+C2.*V.^n
14
15
16 xad=1.09-0.2
17 Ep=xad*If
18 figure(1)
19 clf
20 plot(If,Ep,'b'), hold on
21 plot(If,V,'-')
22 %plot(If,x)
23 %plot(If,x2)
24 %plot(If,x1)
25 plot([0 4],[0.89 0.89],'Linewidth',1)
26 plot([1.0 1.0],[0 2],'Linewidth',1)
27 plot([1.2 1.2],[0 2],'Linewidth',1)
28 plot([1.087 1.087],[0 2],'Linewidth',1)
29 plot([0 4],[1.085 1.085],'Linewidth',1)
30 plot([1.5816 1.5816],[0 2],'Linewidth',1)
31 xlabel('If')
32 ylabel('U')
33 axis([0 4 0 2])
34 %plot(If,V,'o',If2,V,'o')

```

B. Code for the theoretical and practical stability limit shown in figure 20

Listing 2. Code for the theoretical and practical stability limit shown in figure 20

```

1 %% Capability diagram of the hydro
  generator:
2
3
4 %% Plot Capabilitydiagram
5 Xd_pu=0.8;
6 Xq_pu=0.6;
7 V=1;
8 %Pmax =0.9
9 th = (71.1:0.905:180);
10 Sn1 = 1; %or whatever radius you want
11 x = Sn1*cosd(th) ;

```

```

12 y = Sn1*sind(th) ;
13
14
15 A_x=-1/Xq_pu;
16 B_x=-1/Xd_pu;
17
18 %small circle E=0
19 E0=0.0
20 th1 = (0:0.1:180);
21 R=(0.5*(V^2)*(Xd_pu-Xq_pu))./(Xd_pu.*
  Xq_pu)+E0
22 c=(0.5*(V^2)*(Xd_pu+Xq_pu))./(Xd_pu.*
  Xq_pu)-E0
23 x1= R*cosd(th1) - c;
24 y1= R*sind(th1);
25
26
27 %small circle E=0.1
28 E1=0.1
29 th1 = (0:0.1:180);
30 R=(0.5*(V^2)*(Xd_pu-Xq_pu))./(Xd_pu.*
  Xq_pu)+E1
31 c=(0.5*(V^2)*(Xd_pu+Xq_pu))./(Xd_pu.*
  Xq_pu)-E1
32 x1_01= R*cosd(th1) - c;
33 y1_01= R*sind(th1);
34
35
36 %small circle E=0.2
37 E2=0.2
38 th1 = (0:0.1:180);
39 R=(0.5*(V^2)*(Xd_pu-Xq_pu))./(Xd_pu.*
  Xq_pu)+E2
40 c=(0.5*(V^2)*(Xd_pu+Xq_pu))./(Xd_pu.*
  Xq_pu)-E2
41 x1_02= R*cosd(th1) - c;
42 y1_02= R*sind(th1);
43
44 %64.5
45 %third semi circle Emax
46 th2 = (64.5:0.8:96);
47 R=2.20757
48 y2= R*cosd(th2);
49 x2= R*sind(th2) +A_x;
50
51
52 %%
53
54 figure(1)
55 clf
56 plot(x,y,'k','linewidth',1.5), hold on
57 %plot([-0.326 0.326],[0.95 0.95],'
  Linewidth',1)%Pmax
58 %plot([0 0],[0 1],'Linewidth',1)%
  origoaxis
59 % %plot([0 0.326],[0 0.95],'Linewidth',1)
  %Sn
60 %plot(A_x,0,'o')

```

```

61 %plot(B_x,0,'o')
62 plot(x1,y1)%first semi-circle
63 plot(x1_01,y1_01)%second semi-circle
64 plot(x1_02,y1_02)%third semi-circle
65 % %plot([A_x 0.326],[0 0.95],'Linewidth
    ',1)%second line
66 plot(x2,y2,'k','linewidth',1.5)%third
    semi circle Emax
67 xlabel('Q [pu]')
68 ylabel('P [pu]')
69 axis([-1.8 0.6 0 1])
70
71
72 % The Practical stability limit
73 eq=0:0.1:1
74
75 %Calculation of delta
76 %derivate P in regard to delta to get the
    maximum delta
77 a=(eq.*Xq_pu)./(V.*(Xd_pu-Xq_pu))
78 b=sqrt(a.^2+8)
79 cosdelta=(1/4).*(-a+b)
80 delta=acosd(cosdelta)
81
82 %Calculate the active power and reactive
    power
83 %with eq ranging from 0-1 and use max
    delta
84 c=(eq*V)/(Xd_pu).*sind(delta)
85 d=(0.5*V.^2).*((Xd_pu-Xq_pu)./Xd_pu*Xq_pu
    ).*sind(2*delta)
86 P=c+d
87 e=2*d
88 f=((V.^2)./Xd_pu)
89 Q=((eq.*V)./Xd_pu).*cosd(delta)-f-e
90
91 %In order to get the PLS multiply with a
    stability margin
92 %25 percent stability margin
93 stabm=0.75
94 stabm=0.75
95 S=(j*Q+P).*stabm
96
97 plot(imag(S),real(S),'-')

```

C. Code for contour plot of the practical stability limit shown in figure 20

Listing 3. Code for contour plot of the practical stability limit shown in figure 20

```

1
2 %% Plot Capabilitydiagram
3 Xd_pu=0.8;
4 Xq_pu=0.6;
5 V=1;
6 %Pmax =0.9
7 th = (71.1:0.905:180);
8 Sn1 = 1; %or whatever radius you want

```

```

9 x = Sn1*cosd(th) ;
10 y = Sn1*sind(th) ;
11
12
13 A_x=-1/Xq_pu;
14 B_x=-1/Xd_pu;
15
16 %small circle E=0
17 E0=0.0
18 th1 = (0:0.1:180);
19 R=(0.5*(V^2)*(Xd_pu-Xq_pu))./(Xd_pu.*
    Xq_pu)+E0
20 c=(0.5*(V^2)*(Xd_pu+Xq_pu))./(Xd_pu.*
    Xq_pu)-E0
21 x1= R*cosd(th1) - c;
22 y1= R*sind(th1);
23
24
25 %small circle E=0.1
26 E1=0.1
27 th1 = (0:0.1:180);
28 R=(0.5*(V^2)*(Xd_pu-Xq_pu))./(Xd_pu.*
    Xq_pu)+E1
29 c=(0.5*(V^2)*(Xd_pu+Xq_pu))./(Xd_pu.*
    Xq_pu)-E1
30 x1_01= R*cosd(th1) - c;
31 y1_01= R*sind(th1);
32
33
34 %small circle E=0.2
35 E2=0.2
36 th1 = (0:0.1:180);
37 R=(0.5*(V^2)*(Xd_pu-Xq_pu))./(Xd_pu.*
    Xq_pu)+E2
38 c=(0.5*(V^2)*(Xd_pu+Xq_pu))./(Xd_pu.*
    Xq_pu)-E2
39 x1_02= R*cosd(th1) - c;
40 y1_02= R*sind(th1);
41
42 %64.5
43 %third semi circle Emax
44 th2 = (64.5:0.8:96);
45 R=2.20757
46 y2= R*cosd(th2);
47 x2= R*sind(th2) +A_x;
48
49
50 %%
51
52 figure(1)
53 clf
54 plot(x,y,'k','linewidth',1.5), hold on
55 %plot([-0.326 0.326],[0.95 0.95],'
    Linewidth',1)%Pmax
56 %plot([0 0],[0 1],'Linewidth',1)%
    origoaxis
57 % %plot([0 0.326],[0 0.95],'Linewidth',1)
    %Sn

```

```

58 %plot(A_x,0,'o')
59 %plot(B_x,0,'o')
60 plot(x1,y1)%first semi-circle
61 plot(x1_01,y1_01)%second semi-circle
62 plot(x1_02,y1_02)%third semi-circle
63 % %plot([A_x 0.326],[0 0.95],'Linewidth
    ',1)%second line
64 plot(x2,y2,'k','linewidth',1.5)%third
    semi circle Emax
65 xlabel('Q [pu]')
66 ylabel('P [pu]')
67 axis([-1.8 0.6 0 1])
68
69
70
71 %% Data inputs
72 %P=1;
73 V=1;
74 Xd=0.8 ;
75 Xq=0.6;
76 a=V/Xd;
77 b=(0.5*V^2)*((Xd-Xq)/Xd*Xq);
78 c=((V^2)/Xd);
79
80
81 % Eq_P=(P-(b.*sind(2.*delta)))/(a.*sind(
    delta));
82 % Eq_Q=(Q+c+(2.*b.*d.^2))/(a.*cosd(delta
    ));
83
84 %delta_SP=[]
85 for i =drange(1,11)
86     P=(0-1/10)+i/10;
87     for s =drange(1,17)
88         Q=(-1-1/10)+s/10;
89         counter=s
90         for k= drange(1,80000)
91             delta=k/1000;
92             d=sind(delta);
93             Eq_P=(P-(b.*sind(2.*delta))
                )/(a.*sind(delta));
94             Eq_Q=(Q+c+(2.*b.*d.^2))/(a.*
                cosd(delta));
95             if round(Eq_P,2)==round(Eq_Q
                ,2)
96                 break
97             end
98         end
99         delta_SP(i,s)=delta
100     end
101 end
102
103
104 delta_SP(1,1:end)=0
105 P1=0:0.1:1;
106 Q1=-1:0.1:0.6;
107
108 [Q1,P1]=meshgrid(Q1,P1);

```

```

109 [C,h]=contour(Q1,P1,delta_SP)
110 clabel(C,h)
111
112 delta_k=40
113 Eq_P=(P1-(b.*sind(2.*delta)))/(a.*sind(
    delta));
114 q_a=((Eq_P.*V)/Xd).*sind(delta_k)
115 q_b=(V^2/Xd)
116 q_c=V.^2.*((Xd-Xq)/(Xd*Xq)).*sind(
    delta_k)
117 % Q as function of P
118 Q=q_a-q_b-q_c

```

D. Code for the final capability diagram (G1) shown in figure 27

Listing 4. Code for the final capability diagram (G1) shown in figure 21

```

1
2
3 function [x,y,x2,y2,x1_02,y1_02,x_p,y_p,
    c1]=New_capabilitydiagramG2_func(
    Xd_pu,Xq_pu)
4 %% Plot Capabillitydiagram
5 Xd_pu=Xd_pu;
6 Xq_pu=Xq_pu;
7 V=1;
8 %Pmax =0.9
9 th = (71.1:1:145.1);
10 Sn1 = 1; %or whatever radius you want
11 x = Sn1*cosd(th) ;
12 y = Sn1*sind(th) ;
13
14
15 A_x=-1/Xq_pu;
16 B_x=-1/Xd_pu;
17
18 %small circle E=0
19 E0=0.0
20 th1 = (0:0.1:180);
21 R=(0.5*(V^2)*(Xd_pu-Xq_pu))/(Xd_pu.*
    Xq_pu)+E0
22 c=(0.5*(V^2)*(Xd_pu+Xq_pu))/(Xd_pu.*
    Xq_pu)-E0
23 x1= R*cosd(th1) - c;
24 y1= R*sind(th1);
25
26
27 %small circle E=0.1
28 E1=0.1
29 th1 = (0:0.1:180);
30 R=(0.5*(V^2)*(Xd_pu-Xq_pu))/(Xd_pu.*
    Xq_pu)+E1
31 c=(0.5*(V^2)*(Xd_pu+Xq_pu))/(Xd_pu.*
    Xq_pu)-E1
32 x1_01= R*cosd(th1) - c;
33 y1_01= R*sind(th1);
34

```

```

35
36 %small circle E=0.2
37 E2=0.2
38 th1 = (0:0.1:30.5);
39 R=(0.5*(V^2)*(Xd_pu-Xq_pu))./(Xd_pu.*
    Xq_pu)+E2
40 c=(0.5*(V^2)*(Xd_pu+Xq_pu))./(Xd_pu.*
    Xq_pu)-E2
41 x1_02= R*cosd(th1) - c;
42 y1_02= R*sind(th1);
43
44 %small circle E=0.3
45 E3=0.3
46 th1 = (0:0.1:180);
47 R=(0.5*(V^2)*(Xd_pu-Xq_pu))./(Xd_pu.*
    Xq_pu)+E3
48 c=(0.5*(V^2)*(Xd_pu+Xq_pu))./(Xd_pu.*
    Xq_pu)-E3
49 x1_03= R*cosd(th1) - c;
50 y1_03= R*sind(th1);
51
52 %small circle E=0.4
53 E3=0.4
54 th1 = (0:0.1:180);
55 R=(0.5*(V^2)*(Xd_pu-Xq_pu))./(Xd_pu.*
    Xq_pu)+E3
56 c=(0.5*(V^2)*(Xd_pu+Xq_pu))./(Xd_pu.*
    Xq_pu)-E3
57 c1=c
58 x1_04= R*cosd(th1) - c;
59 y1_04= R*sind(th1);
60
61 %64.5
62 %third semi circle Emax
63 th2 = (64.5:0.8:96);
64 R=2.20757
65 y2= R*cosd(th2);
66 x2= R*sind(th2) +A_x;
67
68
69 %%
70
71 figure(1)
72 clf
73 plot(x,y,'k','linewidth',1.5), hold on
74 %plot([-0.326 0.326],[0.95 0.95],',
    Linewidth',1)%Pmax
75 %plot([0 0],[0 1],',Linewidth',1)%
    origoaxis
76 % %plot([0 0.326],[0 0.95],',Linewidth',1)
    %Sn
77 %plot(A_x,0,'o')
78 %plot(B_x,0,'o')
79 %plot(x1,y1)%first semi-circle
80 %plot(x1_01,y1_01)%second semi-circle
81 plot(x1_02,y1_02,'k','linewidth',1.5)%
    third semi-circle
82 %plot(x1_03,y1_03)%fourth semi-circle
83 %plot(x1_04,y1_04)%fifth semi-circle
84 % %plot([A_x 0.326],[0 0.95],',Linewidth
    ',1)%second line
85 plot(x2,y2,'k','linewidth',1.5)%third
    semi circle Emax
86 xlabel('Q [pu]')
87 ylabel('P [pu]')
88 axis([-1 0.6 0 1])
89 %daspect([1 1 1])
90
91 %% The practical stability limit:
92 % data inputs
93 Xd=0.8 ;
94 Xq= 0.6;
95 V=1
96 i=j
97 eq=0.2:0.01:0.63;
98
99 % Calculation of delta
100 % derivate P in regard to delta to get
    the maximum delta
101 a=(eq.*Xq)./(V.*(Xd-Xq))
102 b=sqrt(a.^2+8)
103 cosdelta=(1/4).*(-a+b)
104 delta=acosd(cosdelta)
105
106 %Calculate the active power and reactive
    power
107 % with eq ranging from 0-1 and use max
    delta
108 c=(eq.*V)./(Xd).*sind(delta)
109 d=(0.5*V.^2).*((Xd-Xq)./Xd*Xq).*sind
    (2.*delta)
110 P=c+d
111 e=(V.^2).*((Xd-Xq)./Xd.*Xq).*(sind(
    delta)).^2
112 f=((V.^2)./Xd)
113 Q=((eq.*V)./Xd).*cosd(delta)-f-e
114
115 % In order to get the PLS multiply with
    a stability margin
116 %25 percent stability margin
117 stabm=0.75;
118 S=(j*Q+P).*stabm;
119 x_p=imag(S);
120 y_p=real(S);
121 plot(x_p,y_p,'k','linewidth',1.5)
122 end

```

E. Code for the iso-efficiency curves of G1 illustrated in fig. [27](#)

Listing 5. Code for the iso-efficiency curves of G1 illustrated in fig. [27](#)

```

1 %% Data inputs
2 clear; clc;
3 Ra=0.002322; Xq=0.6; Xd=0.8; Xp=0.18;

```

```

5  b4=7.4417; b3=-22.228; b2=24.85; b1
   =-10.959; b0=2.0737; bv=1;
6
7  sn=1; ua=1; fpn=0.95; pf=0.95;
8
9  %losses along the loading
10 %s=154608; ua_o=1.04229; ia_o=0.9382;
    ifd_o=1.712;
11 s=154608; ua_o=1; ia_o=1; ifd_o=2.;
12 %s=154608;
13 P_wf=710.47/s;    % windage and friction
    loss
14 P_cn=539.87/s;    % core loss
15 P_an=327.05/s;    % stator current loss
16 P_sn=237.07/s;    % additional loss
17 P_fn=477.81/s;    % rotor current loss
18 P_brn=5.96/s;     % brush loss
19 P_exn=33.96/s;    % excitation loss
20 P_b=156.17/s;     % bearings loss
21
22 pcte=P_wf+P_b;    % constant power
23 k=0;
24 Xd_pu=0.8;
25 Xq_pu=0.6;
26 [x,y,x2,y2,x1_02,y1_02,x_p,y_p,c1]=
    New_capabilitydiagramG2_func(Xd_pu,
    Xq_pu)
27 %% Efficiency calculation
28 for i=0.01:0.001:1    % active power
    from 0 to 1
29     for j=-1:0.01:1    % reactive
        power from -1 to 1
30         ia=sqrt(i^2+j^2);
31         phi=atan(j/i);
32         delta=atan(ia*(Xq*cos(phi)-Ra*sin
            (phi))/(ua+Ra*ia*cos(phi)+Xq*
            ia*sin(phi)));
33         egu=ua*cos(delta)+Ra*ia*cos(delta
            +phi)+Xd*ia*sin(delta+phi);
34         ifu=egu/bv;
35         th=atan(ia*(Xp*cos(phi)-Ra*sin(
            phi))/(ua+Ra*ia*cos(phi)+Xp*ia
            *sin(phi)));
36         ep=ua*cos(th)+Ra*ia*cos(th+phi)+
            Xp*ia*sin(th+phi);
37         if ep>0.45
38             ifs=b4*ep^4+b3*ep^3+b2*ep^2+b1
                *ep+b0-ep/bv;
39         else
40             ifs=0;
41         end
42         ifd=ifu+ifs;
43
44         P_a=P_an*(ia/ia_o)^2;
45
46         P_s=P_sn*(ia/ia_o)^2;
47         P_f=P_fn*(ifd/ifd_o)^2;
48         P_br=P_brn*(ifd/ifd_o)^2;
49         P_ex=P_exn*(ifd/ifd_o);
50         P_c=P_cn*(ua/ua_o);
51
52         ptot=pcte+P_s+P_a+P_br+P_f+P_c+
            P_ex;
53
54         k=k+1;
55         p(k)=i;
56         q(k)=j;
57         n(k)=i/(i+ptot);    rend(k)=n(k);
58
59     end
60 end
61
62 n=n*100;
63 nPoints=101;
64 pMin=min(p); pMax=max(p);
65 qMin=min(q); qMax=max(q);
66 pVect=linspace(pMin,pMax,nPoints);
67 qVect=linspace(qMin,qMax,nPoints);
68 [pMat,qMat]=meshgrid(pVect,qVect);
69 int=scatteredInterpolant(p',q',n');
70 nMat=int(pMat,qMat);
71
72 colormap jet;    % doc colormap
73 [c,h]=contour(qMat,pMat,nMat,[91.2 94.9
    96.5 97.4 97.9 98.2 98.4], 'LineWidth',
    2);
74 clabel(c,h,'FontSize',16,'LabelSpacing',
    200,'FontName','Times New Roman')
75 ylabel('Active power (pu)','FontName','
    Times New Roman')
76 xlabel('Reactive power (pu)','FontName','
    Times New Roman')
77 axis equal;
78 axis([-1 .6 0 1]);

```

F. Code for the energy prod. and loss illustrated in figure 29 and 28

Listing 6. Code for the energy prod. and loss illustrated in figure 29 and 28

```

1  %% Data inputs
2  clear; clc;
3  Ra=0.002322; Xq=0.6; Xd=0.8; Xp=0.18;
4  b4=7.4417; b3=-22.228; b2=24.85; b1
    =-10.959; b0=2.0737; bv=1;
5
6  sn=1; ua=1; fpn=0.95; pf=0.95;
7
8  %losses along the loading
9  %s=154608; ua_o=1.04229; ia_o=0.9382;
    ifd_o=1.712;
10 s=154608; ua_o=1; ia_o=1; ifd_o=2;
11 %s=154608;
12 P_wf=710.47/s;    % windage and friction
    loss
13 P_cn=539.87/s;    % core loss

```

```

14 P_an=327.05/s; % stator current loss
15 P_sn=237.07/s; % additional loss
16 P_fn=477.81/s; % rotor current loss
17 P_brn=5.96/s; % brush loss
18 P_exn=33.96/s; % excitation loss
19 P_b=156.17/s; % bearings loss
20
21
22 pcte=P_wf+P_b; ; % constant power
23 k=0;
24
25 %% plot Capabilitydiagram
26 Xd_pu=0.8;
27 Xq_pu=0.6;
28 [x,y,x2,y2,x1_02,y1_02,x_p,y_p,c1]=
    New_capabilitydiagramG2_func(Xd_pu,
    Xq_pu)
29
30
31 %% effciecny calc
32 P=0.01:0.001:1;
33 Q=-1:0.001:1;
34
35 for i=drange(1,length(P)) % active
    power from 0 to 1
36     for j=drange(1,length(Q))
37         P1=P(i);
38         Q1=Q(j);
39         ia=sqrt(P1^2+Q1^2);
40         fi=atan(Q1/P1);
41         d=atan(ia*(Xq*cos(fi)-Ra*sin(fi))
            /(ua+Ra*ia*cos(fi)+Xq*ia*sin(
            fi)));
42         egu=ua*cos(d)+Ra*ia*cos(d+fi)+Xd*
            ia*sin(d+fi);
43         ifu=egu/bv;
44         th=atan(ia*(Xp*cos(fi)-Ra*sin(fi))
            /(ua+Ra*ia*cos(fi)+Xp*ia*sin(
            fi)));
45         ep=ua*cos(th)+Ra*ia*cos(th+fi)+Xp
            *ia*sin(th+fi);
46         if ep>0.45
47             ifs=b4*ep^4+b3*ep^3+b2*ep^2+b1
                *ep+b0-ep/bv;
48         else
49             ifs=0;
50         end
51         ifd=ifu+ifs;
52
53         P_a=P_an*(ia/ia_o)^2;
54         P_s=P_sn*(ia/ia_o)^2;
55         P_f=P_fn*(ifd/ifd_o)^2;
56         P_br=P_brn*(ifd/ifd_o)^2;
57         P_ex=P_exn*(ifd/ifd_o);
58         P_c=P_cn*(ua/ua_o);
59
60         ploss=pcte+P_s+P_a+P_br+P_f+P_c+
            P_ex;
61
62         k=k+1;
63         p(k)=P1;
64         q(k)=Q1;
65         n(k)=P1/(P1+ploss); rend(k)=n(k);
66         E(k)=((1/n(k))-1)*p(k); % losses
67     end
68 end
69
70 E=(p*8760*s*10^3)/(10^9); % production
71
72 nPoints=101;
73 pMin=min(p); pMax=max(p);
74 qMin=min(q); qMax=max(q);
75 pVect=linspace(pMin,pMax,nPoints);
76 qVect=linspace(qMin,qMax,nPoints);
77 [pMat,qMat]=meshgrid(pVect,qVect);
78 int=scatteredInterpolant(p',q',E');
79 EMat=int(pMat,qMat);
80
81 %colormap jet; % doc colormap
82 e=[14 15 16 17 18 19 20 21 22]
83 [c,h]=contour(qMat,pMat,EMat,'LineWidth',
    1);
84 clabel(c,h,'FontSize',16,'LabelSpacing',
    200,'FontName','Times New Roman')
85 title('Total energy production (Gwh)')
86 ylabel('Active power (pu)'),'FontName','
    Times New Roman')
87 xlabel('Reactive power (pu)'),'FontName',
    'Times New Roman')
88 axis equal;
89 axis([-1 .6 0 1]);

```

G. Code for the converging value illustrated in figure 31

Listing 7. Code for the converging value shown in figure 31

```

1 %%% data input
2 %rated quanteties for G1
3 Sn=160*10^6;
4 Ua_pu=1;
5 cosphi=0.95;
6 Pn=Sn*cosphi/Sn;
7 Qn=0.3259;
8 PHIn=atan(Qn/Pn)
9
10 Vn=15.8*10^3
11 %fn= 60
12 Xd_pu=0.8 ;
13 Xq_pu= 0.6;
14
15
16
17 %Potierreactance and armature resistance
18 Xp_pu= 0.18;
19 Ra=0.00232;
20

```

```

21 %nominell induced voltage
22 Egn=1.3980;
23 delta_n=26.622; %26.622
24 %rated armature current and terminal
    voltage:
25 Ian=1;
26 Uan=1;
27
28 E=Xp_pu.*Ian.*cosd(PHIn);
29 F=Ra.*Ian.*sind(PHIn);
30 G=Ra.*Ian.*cosd(PHIn);
31 H=Xp_pu.*Ian.*sind(PHIn);
32 phiportiern=atand((E-F)./(Ua_pu+G+H));
33
34 %polynomial koefisient
35 bv=1
36 b_0=0.0105
37 b_1=1.0172
38 b_2=0.0328
39 b_3=-0.218
40 b_4=0.0514
41
42
43 Egn=1.57
44 Epn=Ua_pu.*cosd(PHIn)-(Ra.*Ian.*cosd(PHIn
    +phiportiern))+Xp_pu.*Ian.*sind(PHIn+
    phiportiern)
45 Poly_Sn=b_0+(b_1.*Epn.^1)+(b_2.*Epn.^2)+(
    b_3.*Epn.^3)+(b_4.*Epn.^4)
46 Ifn=(Egn./bv)+(Poly_Sn)-(Epn./bv)
47 %Ifn=2.2
48 %Ifn=round(Ifn)
49
50 %losses in rated operation(Given):
51 P_wf=(710.47*10^3)/Sn;% Constant windage
    and friction losses
52 P_cn=(539.87*10^3)/Sn;% constant
    armature core losses
53 P_an=(327.05*10^3)/Sn;% nominal armature
    winding losses
54 P_sn=(237.07*10^3)/Sn;% nominal stray
    load losses
55 P_fn=(477.81*10^3)/Sn;% nominal field
    winding current losses
56 P_brn=(5.93*10^3)/Sn;%nominal brush
    losses
57 P_exn=(33.96*10^3)/Sn;% nominal exictor
    losses
58 P_b=(156.17*10^3)/Sn %contstant bearing
    losses
59
60 %% plot Capabilitydiagram
61 Xd=0.8 ;
62 Xq= 0.6;
63 V=1
64 i=j
65 eq=0.2:0.01:0.63;
66
67 % Calculation of delta
68 % derivate P in regard to delta to get
    the maximum delta
69 a=(eq.*Xq)./(V.*(Xd-Xq))
70 b=sqrt(a.^2+8)
71 cosdelta=(1/4).*(-a+b)
72 delta=acosd(cosdelta)
73
74 %Calculate the active power and reactive
    power
75 % with eq ranging from 0-1 and use max
    delta
76 c=(eq.*V)./(Xd).*sind(delta)
77 d=(0.5*V.^2).*((Xd-Xq)./Xd*Xq).*sind
    (2.*delta)
78 P=c+d
79 e=(V.^2).*((Xd-Xq)./Xd.*Xq).*(sind(
    delta)).^2
80 f=((V.^2)./Xd)
81 Q=((eq.*V)./Xd).*cosd(delta)-f-e
82
83 % In order to get the PLS multiply with
    a stability margin
84 %Fifteen percent stabilty margin
85 stabm=0.75;
86 S=(j*Q+P).*stabm;
87 x_p=imag(S);
88 y_p=real(S);
89
90 %% Effeciency calculation
91 %Load operations:
92 TotalEloss=[]
93 for w =drange(1,200)
94     div=w
95     P=0.0:1/div:1;
96     Q=-1:1.6/div:0.6;
97
98     [Q,P]=meshgrid(Q,P);
99     [Qdata_ins,Pdata_ins]=
    data_point_lim_func(Xd_pu,Xq_pu,Ua_pu,
    V,P,Q,div,x_p,y_p)
100 %     m_data=(Pdata_ins & Qdata_ins)~=0;
101 %     Pdata_ins=Pdata_ins(m_data);
102 %     Qdata_ins=Qdata_ins(m_data);
103 %     Q=Qdata_ins;
104 %     P=Pdata_ins;
105 %Armature current calculations
106 S=sqrt((P.^2)+Q.^2);
107 %Ibase=Sn/(sqrt(3)*Ua_pu)
108 Ia_pu=S./1;
109 PHI=atand(Q./P) ;
110
111 %field current calculations
112 A=Xq_pu.*Ia_pu.*cosd(PHI);
113 B=Ra.*Ia_pu.*sind(PHI);
114 C=Ra.*Ia_pu.*cosd(PHI);
115 D=Xq_pu.*Ia_pu.*sind(PHI);

```

```

117 delta=atand((A-B)/(Ua_pu+C+D));
118 %delta=round(delta,0)
119
120 E=Xp_pu.*Ia_pu.*cosd(PHI);
121 F=Ra.*Ia_pu.*sind(PHI);
122 G=Ra.*Ia_pu.*cosd(PHI);
123 H=Xp_pu.*Ia_pu.*sind(PHI);
124 phiportier=atand((E-F)/(Ua_pu+G+H));
125
126
127 %induced voltage and portier
    effective value
128 Eg=Ua_pu.*cosd(delta)+(Ra.*Ia_pu.*
    cosd(PHI+delta))+Xd_pu.*Ia_pu.*
    sind(PHI+delta);
129 Ep=Ua_pu.*cosd(PHI)-(Ra.*Ia_pu.*cosd(
    PHI+phiportier))+Xp_pu.*Ia_pu.*
    sind(PHI+phiportier);
130 %Ep=abs(Ua_pu+((Ra+(j*Xp_pu)).*Ia_pu)
    );
131
132
133 Poly_S=b_0+(b_1.*Ep.^1)+(b_2.*Ep.^2)
    +(b_3.*Ep.^3)+(b_4.*Ep.^4);
134 If=(Eg./bv)+(Poly_S)-(Ep./bv);
135
136
137 % Active power Losses
138 P_a=P_an.*((Ia_pu/Ian).^2); %armature
    winding losses depending on Ia
    for different load operations
139 P_f=P_fn.*((If/Ifn).^2); %field
    winding current losses depending
    on If for different load
    operations
140 P_s=P_sn.*((Ia_pu/Ian).^2); % stray
    load losses depending on Ia for
    different load operations
141 P_br=P_brn.*((If/Ifn).^2); %brush
    losses depending on If for
    different load operations
142 P_ex=P_exn.*(If/Ifn); % exictor
    losses depending on If for
    different load operations
143 P_c=P_cn.*((Ua_pu/Uan).^2); %
    Constant armature core losses
144
145
146 %Total active power losses for the
    different load operations
147 Ploss=P_a+P_f+P_s+P_br+P_ex+P_c+P_b+
    P_wf;
148
149 % Total Energy losses in a year (Kwh)
150 ElosskWh=8765.*Ploss.*(Sn/10^3);
151
152 % Expected Total losses
153 %average losses for each operation
154 %Weigth
155 A_w=(1/div)^2
156 %Average loss in giga watt
157 Eloss_avg=(A_w.*ElosskWh)/10^6;
158
159 %TotalPloss1=sum(Ploss_avg,'all');
160 TotalEloss1=sum(Eloss_avg,'all');
161 TotalEloss=[TotalEloss;TotalEloss1];
162 end
163
164 xs=0:1:div-1
165 figure(1)
166 plot(xs,TotalEloss,'go')
167 ylabel('Total Energy loss [GWh]')
168 xlabel('number of row x number of columns
    ')
169 %figure(2)
170 %plot(Qdata_ins,Pdata_ins,'ro')

```

*H. Code for the three different densities inside the cap. shown in figure [32](#) [33](#) and [34](#)*

Listing 8. Code for the three different densities inside the cap.

```

1 %% data input
2 %%rated quanteties for G1
3 Sn=160*10^6;
4 Ua_pu=1;
5 cosphi=0.95;
6 Pn=Sn*cosphi/Sn;
7 PHIn=acosd(Pn/1);
8 Qn=(Sn*sind(PHIn))/Sn;
9 Vn=15.8*10^3;
10 %fn= 60
11 Xd_pu=0.8 ;
12 Xq_pu= 0.6;
13
14
15 %Potierreactance and armature resistance
16 Xp_pu= 0.18;
17 Ra=0.00232;
18
19
20 %Nominell induced voltage
21 Egn=1.3980;
22 delta_n=26.622; %26.622
23 %Rated armature current and terminal
    voltage:
24 Ian=1;
25 Uan=1;
26
27
28 % Saturation calculation
29 Sg1=0.601;%-c1
30 Sg12=0.4400;%-c2
31 %Calculation of Bsat and Asat:
32 Asat=(Sg1^2)/(1.2*Sg12);
33 Bsat=5*log((1.2*Sg12)/Sg1);

```



```

34
35
36 S_facn=Asat*exp(Bsat*(Egn-0.43));
37 Ifn=Egn
38
39 % Losses in rated operation(Given):
40 P_wf=(710.47*10^3)/Sn;% Constant windage
    and friction losses
41 P_cn=(539.87*10^3)/Sn; % constant
    armature core losses
42 P_an=(327.05*10^3)/Sn; % nominal armature
    winding losses
43 P_sn=(237.07*10^3)/Sn; % nominal stray
    load losses
44 P_fn=(477.81*10^3)/Sn; % nominal field
    winding current losses
45 P_brn=(5.93*10^3)/Sn; %nominal brush
    losses
46 P_exn=(33.96*10^3)/Sn; % nominal exictor
    losses
47 P_b=(156.17*10^3)/Sn %contstant bearing
    losses
48
49 %% plot Capabillitydiagram
50 Xd_pu=0.8;
51 Xq_pu=0.6;
52 V=1;
53 %Pmax =0.9
54 th = (71.1:0.905:180);
55 Sn1 = 1; %or whatever radius you want
56 x = Sn1*cosd(th) ;
57 y = Sn1*sind(th) ;
58
59
60 A_x=-1/Xq_pu;
61 B_x=-1/Xd_pu;
62
63 %small circle E=0
64 th1 = (0:0.1:180);
65 R=(abs(A_x)-abs(B_x))/2
66 c=abs(B_x)+R
67 x1= R*cosd(th1) - c;
68 y1= R*sind(th1) ;
69 %64.5
70 %third semi circle Emax
71 th2 = (64.5:0.0008:96);
72 R=2.20757
73 y2= R*cosd(th2);
74 x2= R*sind(th2) +A_x;
75
76
77 figure(1)
78 clf
79 plot(x,y,'k','linewidth',1.5), hold on
80 %plot([-0.326 0.326],[0.95 0.95],',
    Linewidth',1)%Pmax
81 %plot([0 0],[0 1],',Linewidth',1)%
    origoaxis
82 %plot([0 0.326],[0 0.95],',Linewidth',1)%
    Sn
83 plot(A_x,0,'o')
84 plot(B_x,0,'o')
85 %plot(x1,y1)%second semi circle
86 %plot([A_x 0.326],[0 0.95],',Linewidth',1)
    %second line
87 plot(x2,y2,'k','linewidth',1.5)%third
    semi circle Emax
88 xlabel('Q [pu]')
89 ylabel('P [pu]')
90 axis([-1.0 0.6 0 1])
91
92 %% Ploss calculations
93 P=0.0:0.001:1;
94 Q=-1:0.00146:0.6;
95 [Q,P]=meshgrid(Q,P);
96
97 %Weigth
98 A_w=100/(1100*100)
99
100 %armature current calculations
101 S=abs(sqrt((P.^2)+Q.^2));
102 Ia_pu=S./1;
103 PHI=atand(Q./P);
104
105
106 %field current calculations
107 A=Xq_pu.*Ia_pu.*cosd(PHI);
108 B=Ra.*Ia_pu.*sind(PHI);
109 C=Ra.*Ia_pu.*cosd(PHI);
110 D=Xq_pu.*Ia_pu.*sind(PHI);
111 delta=atand((A-B)./(Ua_pu+C+D));
112 %
113 E=Xp_pu.*Ia_pu.*cosd(PHI);
114 F=Ra.*Ia_pu.*sind(PHI);
115 G=Ra.*Ia_pu.*cosd(PHI);
116 H=Xp_pu.*Ia_pu.*sind(PHI);
117 phiportier=atand((E-F)./(Ua_pu+G+H));
118
119
120 %induced voltage and portier effective
    value
121 Eg=Ua_pu.*cosd(delta)+(Ra.*Ia_pu.*cosd(
    PHI+delta))+Xd_pu.*Ia_pu.*sind(PHI+
    delta);
122 Ep=Ua_pu.*cosd(PHI)-(Ra.*Ia_pu.*cosd(PHI+
    phiportier))+ Xp_pu.*Ia_pu.*sind(PHI+
    phiportier);
123 %Ep=abs(Ua_pu+((Ra+(j*Xp_pu)).*Ia_pu));
124
125
126 hj=1;
127 L_row=size(Eg,1);
128 L_col=size(Eg,2);
129 for i=drange(1,L_row);
130     for s=drange(1,L_col);
131         if 0.0<=Eg(i,s) & (Eg(i,s)<=1.7)

```

```

132         S_fac(i,s)=Asat*exp(hj.*Bsat*(Eg-172 %Expected Total losses(kW/h) and cost(
            (i,s)-0.43)); %kWhore/h) for each load op
133
134     else 173 Ploss_kW_per_h=Ploss_avg./8765;
135         S_fac(i,s)=1; 174
136
137 175 Cost=14.4.*Ploss_kW_per_h;
138     end 176 plot(Q,P,'bo')
139     end 177
140 end 178 %% Load operation calculation
141 179
142 %calculation of the armature reaction 180     L_row=size(P,1);
    reactance with saturation. 181     L_col=size(P,2);
143 Xad_sat=(Xd_pu-Xp_pu)./S_fac; 182     for i=drange(1,L_row);
144 Xd_pu_sat=Xad_sat+Xp_pu; 183         for s=drange(1,L_col);
145 184             M=((abs(Q(i,s))<abs(x)) | P(
146 % The induced voltage including 185                 i,s)<(y));
    saturation 186                 if M==true
147 Eg_sat=Ua_pu.*cosd(delta)+(Ra.*Ia_pu.* 187                     Q1(i,s)=Q(i,s);
    cosd(PHI+delta))+Xd_pu_sat.*Ia_pu.* 188                     P1(i,s)=P(i,s);
    sind(PHI+delta); 189
148 190             end
149 % The field current including saturation 191         end
150 If=Eg_sat./Xad_sat; 192     end
151 193 %plot(Q1,P1,'ro')
152 194     L_row1=size(P1,1);
153 % Active power Losses 195     L_col1=size(P1,2);
154 P_a=P_an.*((Ia_pu/Ian).^2); %armature 196     for n=drange(1,L_row1);
    winding losses depending on Ia for 197         for m=drange(1,L_col1);
    different load operations 198             M1=(Q(n,m)<x2) | P(n,m)<(y2);
155 P_f=P_fn.*((If/Ifn).^2); %field winding 199                 if M1==true
    current losses depending on If for 200                     Q11(n,m)=Q1(n,m);
    different load operations 201                     P11(n,m)=P1(n,m);
156 P_s=P_sn.*((Ia_pu/Ian).^2); % stray load 202
    losses depending on Ia for different 203
    load operations 204             end
157 P_br=P_brn.*((If/Ifn).^2); %brush losses 205         end
    depending on If for different load 206     end
    operations 207     plot(Q11,P11,'ro')
158 P_ex=P_exn.*(If/Ifn); % exictor losses 208
    depending on If for different load 209
    operations 210
159 P_c=P_cn.*((Ua_pu/Uan).^2); % Constant 211
    armature core losses 212
213
214
215
216
217
218
219
220
221
222
223
224
225
226
227
228
229
230
231
232
233
234
235
236
237
238
239
240
241
242
243
244
245
246
247
248
249
250
251
252
253
254
255
256
257
258
259
260
261
262
263
264
265
266
267
268
269
270
271

```

### I. Code for the distribution circles ,TEL and Cost

Listing 9. Code for the distribution circles.

```

1 %% Data input
2 div=299;
3 P=0.0:1/div:1;
4 Q=-1:1.6/div:0.6;
5 [Q,P]=meshgrid(Q,P);
6
7 %rated quantities for generator G1
8 Sn=160*10^6;
9 Ua_pu=1;
10 cosphi=0.95;
11 Pn=Sn*cosphi/Sn;
12 Qn=0.3259;
13 PHIn=atan(Qn/Pn);
14
15 Vn=15.8*10^3;

```

```

16 %fn= 60
17 Xd_pu=0.8 ;
18 Xq_pu= 0.6;
19
20
21 %Potierreactance and armature resistance
22 Xp_pu= 0.18;
23 Ra=0.00232;
24
25 %nominell induced voltage
26 Egn=1.3980;
27 delta_n=26.622; %26.622
28 %rated armature current and terminal
    voltage :
29 Ian=1;
30 Uan=1;
31 V=1;
32 E=Xp_pu.* Ian .* cosd(PHIn) ;
33 F=Ra.* Ian .* sind(PHIn) ;
34 G=Ra.* Ian .* cosd(PHIn) ;
35 H=Xp_pu.* Ian .* sind(PHIn) ;
36 phiportiern=atand((E-F)./(Ua_pu+G+H));
37
38 %polynomial koefisient
39 bv=1;
40 b_0=0.0105;
41 b_1=1.0172;
42 b_2=0.0328;
43 b_3=-0.218;
44 b_4=0.0514;
45
46 Egn=1.57;
47 Epn=Ua_pu.* cosd(PHIn)-(Ra.* Ian .* cosd(PHIn
    + phiportiern))+ Xp_pu.* Ian .* sind(PHIn+
    phiportiern)
48 Poly_Sn=b_0+(b_1.*Epn.^1)+(b_2.*Epn.^2)+(
    b_3.*Epn.^3)+(b_4.*Epn.^4)
49 Ifn=(Egn./bv)+(Poly_Sn)-(Epn./bv)
50
51
52 %losses in rated operation(Given):
53 P_wf=(710.47*10^3)/Sn;% Constant windage
    and friction losses
54 P_cn=(539.87*10^3)/Sn; % constant
    armature core losses
55 P_an=(327.05*10^3)/Sn; % nominal armature
    winding losses
56 P_sn=(237.07*10^3)/Sn; % nominal stray
    load losses
57 P_fn=(477.81*10^3)/Sn; % nominal field
    winding current losses
58 P_brn=(5.93*10^3)/Sn; %nominal brush
    losses
59 P_exn=(33.96*10^3)/Sn; % nominal exictor
    losses
60 P_b=(156.17*10^3)/Sn %contstant bearing
    losses
61
62
63 %% plot capabilitiy diagram
64 [x,y,x2,y2,x1_02,y1_02,x_p,y_p,c1]=
    New_capabilitydiagramG2_func(Xd_pu,
    Xq_pu)
65
66
67 %% data point limited by max. field
    current,armature current and PLS
68 [Qdata_ins,Pdata_ins]=data_point_lim_func
    (Xd_pu,Xq_pu,Ua_pu,V,P,Q,div,x_p,y_p)
69 %% Data points inside the cap.diag.
70 Qdata=Qdata_ins;
71 Pdata=Pdata_ins;
72
73 %% Radius and starting operation point
74 Q_point=0.33;
75 P_point=0.95;
76 [Radius,R1,R2,R3,R4,R5,R6,R7,R8,R9,R10,
    R11,R12,R13]=Circle_func_TEL(P);
77
78
79 %% Plot the cirle points
80 [P_one,P_two,P_three,P_four,P_five,P_six,
    P_seven,P_eight,P_nine,P_ten,P_eleven
    ,P_twelve,P_thirteen,Q_one,Q_two,
    Q_three,Q_four,Q_five,Q_six,Q_seven,
    Q_eight,Q_nine,Q_ten,Q_eleven,
    Q_twelve,Q_thirteen]=
    distrution_circle_func(Q_point,P_point
    ,Qdata,Pdata,R1,R2,R3,R4,R5,R6,R7,R8,
    R9,R10,R11,R12,R13);
81 %% clean the vector of zeros in order to
    not get NAN
82 [P_one,P_two,P_three,P_four,P_five,P_six,
    P_seven,P_eight,P_nine,P_ten,P_eleven
    ,P_twelve,P_thirteen,Q_one,Q_two,
    Q_three,Q_four,Q_five,Q_six,Q_seven,
    Q_eight,Q_nine,Q_ten,Q_eleven,
    Q_twelve,Q_thirteen]=
    Clean_vector_of_zero_func(P_one,P_two,
    P_three,P_four,P_five,P_six,P_seven,
    P_eight,P_nine,P_ten,P_eleven,
    P_twelve,P_thirteen,Q_one,Q_two,
    Q_three,Q_four,Q_five,Q_six,Q_seven,
    Q_eight,Q_nine,Q_ten,Q_eleven,
    Q_twelve,Q_thirteen);
83 %% Energy loss calculation
84 [TEL1,Cost1]=Total_Energy_Losses(P_one,
    Q_one);
85 [TEL2,Cost2]=Total_Energy_Losses(P_two,
    Q_two);
86 [TEL3,Cost3]=Total_Energy_Losses(P_three,
    Q_three);
87 [TEL4,Cost4]=Total_Energy_Losses(P_four,
    Q_four);
88 [TEL5,Cost5]=Total_Energy_Losses(P_five,
    Q_five);

```

```

89 [TEL6, Cost6]=Total_Energy_Losses(P_six , 19 y3_10= R11*cosd(th2)+ 0.5;
    Q_six); 20 x3_10= R11*sind(th2);
90 [TEL7, Cost7]=Total_Energy_Losses(P_seven , 21
    Q_seven); 22 % Circle 10
91 [TEL8, Cost8]=Total_Energy_Losses(P_eight , 23 th2 = (0:1:360);
    Q_eight); 24 R10=0.01*2^6.0;
92 [TEL9, Cost9]=Total_Energy_Losses(P_nine , 25 y3_10= R10*cosd(th2)+ 0.5;
    Q_nine); 26 x3_10= R10*sind(th2);
93 [TEL10, Cost10]=Total_Energy_Losses(P_ten , 27
    Q_ten); 28
94 [TEL11, Cost11]=Total_Energy_Losses( 29 % Circle 9
    P_eleven , Q_eleven); 30 th2 = (0:1:360);
95 [TEL12, Cost12]=Total_Energy_Losses( 31 R9=0.01*2^5.5;
    P_twelve , Q_twelve); 32 y3_9= R9*cosd(th2)+ 0.5;
96 [TEL13, Cost13]=Total_Energy_Losses( 33 x3_9= R9*sind(th2);
    P_thirteen , Q_thirteen); 34
97 TEL_vec=[TEL1, TEL2, TEL3, TEL4, TEL5, TEL6, 35
    TEL7, TEL8, TEL9, TEL10, TEL11, TEL12, 36 % Circle 8
    TEL13]; 37 th2 = (0:1:360);
98 Cost_vec=[Cost1 , Cost2 , Cost3 , Cost4 , Cost5 , 38 R8=0.01*2^5;
    Cost6 , Cost7 , Cost8 , Cost9 , Cost10 , Cost11 39 y3_8= R8*cosd(th2)+ 0.5;
    , Cost12 , Cost13 ] 40 x3_8= R8*sind(th2);
99 41
100 figure(2) 42
101 plot(Radius , TEL_vec , 'r') 43 % Circle 7
102 xlabel('Radius') 44 th2 = (122:1:360);
103 ylabel('Total Average Energy loss [GWh]') 45 R7=0.01*2^4.5;
104 46 y3_7= R7*cosd(th2)+ 0.5;
105 47 x3_7= R7*sind(th2);
106 figure(3) 48
107 plot(Radius , Cost_vec , 'b') 49
108 xlabel('Radius') 50 % Circle 6
109 ylabel('Cost[MWore/h]') 51 th2 = (0:1:360);
    52 R6=0.01*2^4;
    53 y3_6= R6*cosd(th2)+ 0.5;
    54 x3_6= R6*sind(th2);
    55
    56

```

*J. Code for additional functions used in dis. circle plot*

Listing 10. Additional function that plots circles

```

1 57 % Circle 5
2 function [Radius , R1, R2, R3, R4, R5, R6, R7, R8, 58 th2 = (0:0.020432:360);
    R9, R10, R11, R12, R13]= Circle_func_TEL(P 59 R5=0.01*2^3.5;
    ) 60 y3_5= R5*cosd(th2)+ 0.5;
3 a=P 61 x3_5= R5*sind(th2);
4 %% Circle function in TEL calculation 62
5 % Circle 12 63 % Circle 4
6 th2 = (0:1:360); 64 th2 = (0:1:360);
7 R13=0.01*2^7.5; 65 R4=0.01*2^3;
8 y3_10= R13*cosd(th2)+ 0.5; 66 y3_4= R4*cosd(th2)+ 0.5;
9 x3_10= R13*sind(th2); 67 x3_4= R4*sind(th2);
10 % Circle 12 68
11 th2 = (0:1:360); 69
12 R12=0.01*2^7.0; 70 % Circle 3
13 y3_10= R12*cosd(th2)+ 0.5; 71 th2 = (0:1:360);
14 x3_10= R12*sind(th2); 72 R3=0.01*2^2;
15 73 y3_3= R3*cosd(th2)+ 0.5;
16 % Circle 11 74 x3_3= R3*sind(th2);
17 th2 = (0:1:360); 75
18 R11=0.01*2^6.5; 76 % Circle 2

```

```

77 th2 = (0:1:360);
78 R2=0.01*2;
79 y3_2= R2*cosd(th2)+ 0.5;
80 x3_2= R2*sind(th2);
81
82 % Circle 1
83 th2 = (0:1:360);
84 R1=0.01;
85 y3_1= R1*cosd(th2)+ 0.5;
86 x3_1= R1*sind(th2);
87 Radius=[R1,R2,R3,R4,R5,R6,R7,R8,R9,R10,
          R11,R12,R13]
88 end

```

Listing 11. Additional function that clean vector of zero

```

1
2 function [P_one,P_two,P_three,P_four,
          P_five,P_six,P_seven,P_eight,P_nine,
          P_ten,P_eleven,P_twelve,P_thirteen,
          Q_one,Q_two,Q_three,Q_four,Q_five,
          Q_six,Q_seven,Q_eight,Q_nine,Q_ten,
          Q_eleven,Q_twelve,Q_thirteen]=
          Clean_vector_of_zero_func(P_one,P_two,
          P_three,P_four,P_five,P_six,P_seven,
          P_eight,P_nine,P_ten,P_eleven,
          P_twelve,P_thirteen,Q_one,Q_two,
          Q_three,Q_four,Q_five,Q_six,Q_seven,
          Q_eight,Q_nine,Q_ten,Q_eleven,
          Q_twelve,Q_thirteen)
3 %% clean the vector of zeros in order to
  not get NAN
4 m_one=(P_one & Q_one)~=0
5 P_one=P_one(m_one)
6 Q_one=Q_one(m_one)
7
8 m_two=(P_two & Q_two)~=0
9 P_two=P_two(m_two)
10 Q_two=Q_two(m_two)
11
12 m_three=(P_three & Q_three)~=0
13 P_three=P_three(m_three)
14 Q_three=Q_three(m_three)
15
16 m_four=(P_four & Q_four)~=0
17 P_four=P_four(m_four)
18 Q_four=Q_four(m_four)
19
20
21 m_five=(P_five & Q_five)~=0
22 P_five=P_five(m_five)
23 Q_five=Q_five(m_five)
24
25 m_six=(P_six & Q_six)~=0
26 P_six=P_six(m_six)
27 Q_six=Q_six(m_six)
28
29
30 m_seven=(P_seven & Q_seven)~=0

```

```

31 P_seven=P_seven(m_seven)
32 Q_seven=Q_seven(m_seven)
33
34 m_eight=(P_eight & Q_eight)~=0
35 P_eight=P_eight(m_eight)
36 Q_eight=Q_eight(m_eight)
37
38 m_nine=(P_nine & Q_nine)~=0
39 P_nine=P_nine(m_nine)
40 Q_nine=Q_nine(m_nine)
41
42 m_ten=(P_ten & Q_ten)~=0
43 P_ten=P_ten(m_ten)
44 Q_ten=Q_ten(m_ten)
45
46 m_eleven=(P_eleven & Q_eleven)~=0
47 P_eleven=P_eleven(m_eleven)
48 Q_eleven=Q_eleven(m_eleven)
49
50
51 m_twelve=(P_twelve & Q_twelve)~=0
52 P_twelve=P_twelve(m_twelve)
53 Q_twelve=Q_twelve(m_twelve)
54
55 m_thirteen=(P_thirteen & Q_thirteen)~=0
56 P_thirteen=P_thirteen(m_thirteen)
57 Q_thirteen=Q_thirteen(m_thirteen)
58 end

```

Listing 12. Additional function that plots datapoints inside cap.

```

1
2
3 function [Qdata_ins,Pdata_ins]=
          data_point_lim_func(Xd_pu,Xq_pu,Ua_pu,
          V,P,Q,div,x_p,y_p)
4 %% Data points limited by armature
  current and Emax
5 L_row=size(P,1);
6 L_col=size(P,2);
7 col=L_row*L_col;
8 Q=reshape(Q,1,col);
9 P=reshape(P,1,col);
10
11 for r =drange(1,col)
12     if (Q(r)-0).^2+(P(r)-0).^2-(1)<0;
13         Q1(r)=Q(r);
14         P1(r)=P(r);
15     end
16 end
17
18 A_x=-1/Xq_pu;
19 col1=length(P1);
20 Q11=[];
21 P11=[];
22 for i =drange(1,col1)
23     if (Q1(i)-A_x).^2+(P1(i)-0)
        .^2-(2.20757).^2<0;
24         Q11(i)=Q1(i);

```

```

25     P11(i)=P1(i);
26     end
27 end
28
29 %% Data points limited by min. field
    current
30 E2=0.2;
31 R=(0.5*(V^2)*(Xd_pu-Xq_pu))./(Xd_pu.*
    Xq_pu)+E2;
32 c=(0.5*(V^2)*(Xd_pu+Xq_pu))./(Xd_pu.*
    Xq_pu)-E2;
33 col2=P11;
34 Q_11=[];
35 P_11=[];
36 for i =drange(1,length(P11))
37     xdif=(Q11(i)+c).^2;
38     ydif=(P11(i)-0).^2;
39     d=sqrt(xdif+ydif);
40     if d>R;
41         Q_11(i)=Q11(i);
42         P_11(i)=P11(i);
43     end
44 end
45
46 %% Data points limited by PLS
47 p=polyfit(x_p,y_p,1);
48 s=-1:0.1:0;
49 a=p(1);
50 b=p(2);
51 y=a*s+b;
52
53 % Get the data point inside the function:
54 for i = drange(1,length(Q_11))
55     if Q_11(i)>(-P_11(i)+b)/-a;
56         Qdata_ins(i)= Q_11(i);
57         Pdata_ins(i)= P_11(i);
58     end
59 end
60 end
61
62 end

```

Listing 13. Additional function that plots datapoints inside the circle

```

1 function [P_one,P_two,P_three,P_four,
2     P_five,P_six,P_seven,P_eight,P_nine,
3     P_ten,P_eleven,P_twelve,P_thirteen,
4     Q_one,Q_two,Q_three,Q_four,Q_five,
5     Q_six,Q_seven,Q_eight,Q_nine,Q_ten,
6     Q_eleven,Q_twelve,Q_thirteen]=
7     distrution_circle_func(Q_point,P_point
8     ,Qdata,Pdata,R1,R2,R3,R4,R5,R6,R7,R8,
9     R9,R10,R11,R12,R13)
10
11 %% Plot distrubtion circle function
12
13 %plot circle 13
14 %perlocate the variables
15 Q_thirteen=[]
16
17 P_thirteen=[]
18 for rs =drange(1,length(Qdata))
19     if (Qdata(rs)-Q_point)^2+(Pdata(rs)-
20         P_point)^2-(R13)^2<0
21         Q_thirteen(rs)=Qdata(rs);
22         P_thirteen(rs)=Pdata(rs);
23     end
24 end
25
26 plot(Q_thirteen,P_thirteen,'ro')
27 %plot circle 12
28 %perlocate the variables
29 Q_twelve=[]
30 P_twelve=[]
31 for rs =drange(1,length(Q_thirteen))
32     if (Qdata(rs)-Q_point)^2+(Pdata(rs)-
33         P_point)^2-(R12)^2<0
34         Q_twelve(rs)=Qdata(rs);
35         P_twelve(rs)=Pdata(rs);
36     end
37 end
38
39 plot(Q_twelve,P_twelve,'go')
40
41 %plot circle 11
42 %perlocate the variables
43 Q_eleven=[]
44 P_eleven=[]
45 for rs =drange(1,length(Q_twelve))
46     if (Q_twelve(rs)-Q_point)^2+(P_twelve
47         (rs)-P_point)^2-(R11)^2<0
48         Q_eleven(rs)=Q_twelve(rs);
49         P_eleven(rs)=P_twelve(rs);
50     end
51 end
52
53 plot(Q_eleven,P_eleven,'ro')
54 %plot circle 10
55 %perlocate the variables
56 Q_ten=[]
57 P_ten=[]
58 for rs =drange(1,length(Q_eleven))
59     if (Q_eleven(rs)-Q_point)^2+(P_eleven
60         (rs)-P_point)^2-(R10)^2<0
61         Q_ten(rs)=Q_eleven(rs);
62         P_ten(rs)=P_eleven(rs);
63     end
64 end
65
66 plot(Q_ten,P_ten,'bo')
67
68 %plot circle 9
69 %perlocate the variables
70 Q_nine=[]
71 P_nine=[]
72 for rs =drange(1,length(Q_ten))
73     if (Q_ten(rs)-Q_point)^2+(P_ten(rs)-
74         P_point)^2-(R9)^2<0
75         Q_nine(rs)=Q_ten(rs);
76         P_nine(rs)=P_ten(rs);
77     end
78 end

```

```

61     end
62 end
63
64
65 plot(Q_nine , P_nine , 'co')
66
67 %plot circle 8
68 %perlocate the variables
69 Q_eight=[]
70 P_eight=[]
71 for rs =drange(1 , length(Q_nine))
72     if (Q_nine(rs)-Q_point)^2+(P_nine(rs)
73         -P_point)^2-(R8)^2<0
74         Q_eight(rs)=Q_nine(rs);
75         P_eight(rs)=P_nine(rs);
76     end
77 end
78
79 plot(Q_eight , P_eight , 'ro')
80
81
82 %plot circle 7
83 %perlocate the variables
84 Q_seven=[]
85 P_seven=[]
86 for rs =drange(1 , length(Q_eight))
87     if (Q_eight(rs)-Q_point)^2+(P_eight(
88         rs)-P_point)^2-(R7)^2<0
89         Q_seven(rs)=Q_eight(rs);
90         P_seven(rs)=P_eight(rs);
91     end
92 end
93
94 plot(Q_seven , P_seven , 'go')
95
96 %plot circle 6
97 %perlocate the variables
98 Q_six=[]
99 P_six=[]
100 for rs =drange(1 , length(Q_seven))
101     if (Q_seven(rs)-Q_point)^2+(P_seven(
102         rs)-P_point)^2-(R6)^2<0
103         Q_six(rs)=Q_seven(rs);
104         P_six(rs)=P_seven(rs);
105     end
106 end
107
108 plot(Q_six , P_six , 'yo')
109
110
111 %plot circle 5
112 %perlocate the variables
113 Q_five=[]
114 P_five=[]
115 for s =drange(1 , length(Q_six))
116     if (Q_six(s)-Q_point)^2+(P_six(s)-
117         P_point)^2-(R5)^2<0
118         Q_five(s)= Q_six(s);
119         P_five(s)= P_six(s);
120     end
121 end
122 %
123 plot(Q_five , P_five , 'bo')
124
125 %plot circle 4
126 %perlocate the variables
127 Q_four=[]
128 P_four=[]
129 for i =drange(1 , length(Q_five))
130     if (Q_five(i)-Q_point)^2+(P_five(i)
131         -P_point)^2-(R4)^2<0
132         Q_four(i)=Q_five(i);
133         P_four(i)=P_five(i);
134     end
135 end
136
137 plot(Q_four , P_four , 'co')
138
139 %plot circle 3
140 %perlocate the variables
141 Q_three=[]
142 P_three=[]
143 for ti=drange(1 , length(Q_four))
144     if (Q_four(ti)-Q_point)^2+(P_four(
145         ti)-P_point)^2-(R3)^2<0
146         Q_three(ti)=Q_four(ti);
147         P_three(ti)=P_four(ti);
148     end
149 end
150 %
151 plot(Q_three , P_three , 'ko')
152
153 %plot circle 2
154 % Perlocate the variables
155 Q_two=[]
156 P_two=[]
157 for it =drange(1 , length(Q_three))
158     if (Q_three(it)-Q_point)^2+(
159         P_three(it)-P_point)^2-(R2)^2<0
160         Q_two(it)=Q_three(it);
161         P_two(it)=P_three(it);
162     end
163 end
164 %
165 plot(Q_two , P_two , 'go')
166
167 % %plot circle 1
168 Q_one=[]
169 P_one=[]
170 for si =drange(1 , length(Q_two))
171     if (Q_two(si)-Q_point)^2+(P_two(si)
172         -P_point)^2-(R1)^2<0

```

```

169         Q_one( si)=Q_two( si);
170         P_one( si)=P_two( si);
171     end
172 end
173 %
174 plot( Q_one , P_one , 'bo' )
175 end

```

K. Code for the 2D density plot in figure 44

Listing 14. Code for the scatter plot in figure 44

```

1 %%rated quanteties for generator G1
2 Sn=160*10^6;
3 Ua_pu=1;
4 cosphi=0.95;
5 Pn=Sn*cosphi / Sn;
6 Qn=0.3259;
7 PHIn=atan( Qn/Pn );
8
9 V=1;
10 %fn= 60
11 Xd_pu=0.8 ;
12 Xq_pu= 0.6;
13
14
15 %%Potierreactance and armature resistance
16 Xp_pu= 0.18;
17 Ra=0.00232;
18
19
20 % full load dis.
21 div=10
22 P=0.0:1/div:1;
23 Q=-1:1.7/div:1;
24 [Q,P]=meshgrid(Q,P);
25
26 %% plot capabillity diagram
27 [x,y,x2,y2,x1_02,y1_02,x_p,y_p,c1]=
    New_capabilitydiagramG2_func(Xd_pu,
    Xq_pu)
28
29 %% data point limited by max. field
    current and armature current PLS
30 [Qdata_ins,Pdata_ins]=data_point_lim_func
    (Xd_pu,Xq_pu,Ua_pu,V,P,Q,div,x_p,y_p)
31 %% Data points inside the cap.diag.
32 Qdata=Qdata_ins;
33 Pdata=Pdata_ins;
34 Qdata=Qdata';
35 Pdata=Pdata';
36 m_one=(Pdata & Qdata)~=0
37 Pdata=Pdata(m_one)
38 Qdata=Qdata(m_one)
39
40 colormap( jet )
41 cb = colorbar( 'southoutside' );
42 ylabel( cb , ' probability of occurance (%)
    ' )

```

```

43 grid on
44 %21
45 densityscatter( Qdata , Pdata , 31 , 15)
46 %title( 'Uniform load distrubtion ' )
47 figure( 2)
48 subplot( 2 , 1 , 1)
49 histogram( Qdata )
50 xlabel( 'Reactive power' )
51 ylabel( 'Hours' )
52 subplot( 2 , 1 , 2)
53 histogram( Pdata )
54 xlabel( 'Active power' )
55 ylabel( 'Hours' )

```

L. Code for the Measured OCC of Åbjøra in figure 45

Listing 15. Code for the measured OCC in figure 45

```

1 %% Saturation curve
2 % If base 525.15 A
3 measured_points=DefaultDataset9
4 div=length( measured_points )
5 sat_data=measured_points % pu
6
7 % Saturation points
8 Eg_sat=sat_data( : , 2) %./100
9 ifd_sat=sat_data( : , 1) %./525.15
10 % Airgap line
11 Eg=0:1/div:1.9*100;
12 Ifd=5.10*Eg;
13
14 % Fitting curve
15 n=7;
16 C=0.160;
17 k=1.0308; % k=1.02275;
18 V=0.0:0.01:1.2*100;
19 If=(V+C.*V.^n).*k;
20
21 figure( 1)
22 clf
23
24 plot( ifd_sat , Eg_sat , 'r-' , 'linewidth' ,
    2.5) , hold on
25 plot( ifd_sat , Eg_sat , 'ko' )
26 plot( Ifd , Eg , 'b-' , 'linewidth' , 3.5)
27
28 plot( [525.15 525.15] , [ 0 102] , 'g' , '
    linewidth' , 2.5)
29 axis( [ 0 1000 0 130] )
30 title( 'Measured OCC' )
31 xlabel( 'If [A]' )
32 ylabel( 'U [%]' )
33
34 legend( 'airgapline' , 'data points' , 'non-
    linear saturation char.' )

```

M. Code for the replicated pu OCC of Åbjøra in figure 46



Listing 16. Code for the replicated OCC in figure 46

```

1 %% Saturation curve
2 % If base 525.15 A
3 Sat_data=DefaultDataset9
4 div=length(Sat_data)
5 sat_data=Sat_data % pu
6
7 % Saturation points
8 Eg_sat=sat_data(:,2)./100
9 ifd_sat=sat_data(:,1)./525.15
10 % Airgap line
11 Eg=0:1/div:1.3;
12 Ifd=Eg;
13
14 % Fitting curve
15 n=7;
16 C=0.160;
17 k=1.0308; % k=1.02275;
18 V=0.0:0.01:1.2;
19 If=(V+C.*V.^n).*k;
20
21 figure(1)
22 clf
23
24 plot(ifd_sat,Eg_sat,'go'), hold on
25
26 plot(Ifd,Eg,'b-', 'linewidth', 1.5)
27
28 plot(If,V,'r', 'linewidth', 1.5)
29 axis([0 1.8 0 1.6])
30 title('OPCC')
31 xlabel('If [pu]')
32 ylabel('Eg [pu]')
33
34 legend('data points','airgapline','non-
    linear saturation char.')
```

N. Code for the V-curve family shown in figure 47

```

Listing 17. Code for the V-curve family shown in figure 47
1 Sn = 103; %MVA
2 Vn = 11; %kV
3 Xq = 0.69; % (Pu)
4 Ra = 0.003155; % (ohm)
5 Xad = 8.7362; % (Pu) estimated from V-
    curve by knowing field current (Ifd)
6 Xd = 1.06;
7 In = Sn/(sqrt(3)*Vn);
8 ##### Plotting V-curves and
    field current relationship #####
9 figure(2)
10 V_t = linspace(11,11,100);
11 %% Plotting V-curves
12 P_m0 = 0:0.25:1;
13 for m = 1:length(P_m0)
14     P_m = Sn*P_m0(m);
15     P_t = linspace(P_m,P_m,100);
```

```

16 for k = 1:2
17     if k == 1
18         Q_t = linspace(0,-Sn,100);
19     else
20         Q_t = linspace(0,Sn,100);
21     end
22     I_t = (sqrt(P_t.^2+Q_t.^2)./(
        sqrt(3).*V_t));
23     [ifd]=Field_current2(P_t,Q_t); %
        The correct field current
24     Ifd_t = ifd
25     %Ifd_t = Field_current_two(P_t,
        Q_t, V_t, Sn, Vn, Ra, Xad, Xq,
        Xd);
26     %This field current could be used
        to plot the V-curves
27     plot(Ifd_t,I_t./In,'-')
28     leg1(m) = sprintf("P = %3.1f",
        P_m);
29     hold 'on'
30     grid on
31 end
32
33 end
34 %Plotting relationship between armature
    and field current at constant PF
35 PF = 0
36 PF0 = [1, 0.9, -0.9];
37 for f = 1:length(PF0)
38     PF = PF0(f);
39     if PF < 0
40         phi_t0 = -acos(PF);
41     else
42         phi_t0 = acos(PF);
43     end
44     S_t0 = linspace(0,Sn*1.2,100);
45     P_t0 = S_t0*cos(phi_t0);
46     Q_t0 = S_t0*sin(phi_t0);
47     [ifd]=Field_current2(P_t,Q_t);
48     Ifd_t_PF0=ifd
49     %Ifd_t_PF0 = Field_current_two(P_t0,
        Q_t0, V_t, Sn, Vn, Ra, Xad, Xq,
        %Xd); Adjust this field current so
        the PF fits
50
51     I_t0 = (sqrt(P_t0.^2+Q_t0.^2)./(sqrt
        (3).*V_t));
52     plot(Ifd_t_PF0,I_t0/In,'--')
53     leg2(f) = sprintf("PF = %3.1f", PF);
54     leg_tot = [leg1, leg2];
55     legend(leg_tot)
56     xlabel 'Field current [A]'
57     ylabel 'Armature current [Pu]'
58     axis([0 1400 0 1.5])
59 end
60 hold 'off'
```

O. Code for the iso-efficiency curve of Åbjøra in figure 49

Listing 18. Code for the efficiency map in figure 49

```

1  %% Data inputs
2  clear; clc;
3  Ra=0.00182; Xq=0.676; Xd=1.059 ; Xp
   =0.141;
4  b4=0.0817; b3=-0.2482; b2=-0.1645; b1
   =1.3647
5  ; b0=-0.2251; bv=1;
6  n1=7;
7  C=0.160;
8  k1=1.0308      %1.03;
9  sn=1; ua=1; pf=0.9; %fpn=0.95;
10
11 %losses along the loading
12 %s=103000; ua_o=1; ia_o=1; ifd_o=1.7665;
13 s=103*10^3; ua_o=1; ia_o=1; ifd_o
   =1065/525.15;
14
15
16 P_wf=172.92/s;      % windage and friction
   loss
17 P_cn=211.92/s;      % core loss
18 P_an=193.63/s;      % stator current loss
19 P_sn=82.99/s;       % additional loss
20 P_fn=173.65/s;      % rotor current loss
21 P_brn=2.13/s;       % brush loss
22 P_exn=15.88/s;      % excitation loss
23 P_b=240.9/s;      %356.23 % bearings loss
24 pcte=P_wf+P_b;      % constant power
25 k=0;
26 New_capabilitydiagram_AAbjora_func(Xd,Xq)
27 %% Efficiency calculation
28 % Chose the load op.:
29 P=0:0.01:1;
30 Q=-1:0.1:1;
31 for i=drange(1, length(P))      % active
   power from 0 to 1
32     for j=drange(1, length(Q))
33         P1=P(i);
34         Q1=Q(j);
35         ia=sqrt(P1^2+Q1^2);
36         phi=atan(Q1/P1);
37         %phi(isnan(Q))=0;
38         delta=atan(ia*(Xq*cos(phi)-(Ra*
           sin(phi)))/(ua+(Ra*ia*cos(phi)
           )+Xq*ia*sin(phi)));
39         egu=ua*cos(delta)+(Ra*ia*cos(
           delta+phi))+Xd*ia*sin(delta+
           phi);
40         ifu=egu/bv;
41         th=atan(ia*(Xp*cos(phi)-(Ra*sin(
           phi)))/(ua+(Ra*ia*cos(phi))+Xp
           *ia*sin(phi)));
42         ep=ua*cos(th)+(Ra*ia*cos(th+phi))
           +Xp*ia*sin(th+phi);
43         if ep>0.55
44             %ifs=b4*ep^4+b3*ep^3+b2*ep^2+
           b1*ep+b0-ep/bv;
           ifs=(ep+C*ep^n1).*k1-(ep/bv);
           else
           ifs=0;
           end
           ifd1=(ifu+ifs)*525.15;
           ifd=(ifu+ifs);
           P_a=P_an*(ia/ia_o)^2;
           P_f=P_fn*(ifd/ifd_o)^2;
           P_c=P_cn*(ua/ua_o);
           P_s=P_sn*(ia/ia_o)^2;
           P_ex=P_exn*(ifd/ifd_o);
           P_br=P_brn*(ifd/ifd_o)^2;
           ptot=pcte+P_s+P_a+P_br+P_f+P_c+
           P_ex;
           k=k+1;
           p(k)=P1;
           q(k)=Q1;
           n(k)=(P1/(P1+ptot)); %rend(k)=n(k)
           );
           Pf=P_f*s;
           Pex=P_ex*s;
           Pbr=P_br*s;
           sum=(P_f+P_ex+P_br)*s;
           ploss=ptot;
           %E=((1/n(k))-1)*P1;
           %E(k)=ptot; %; rend(k)=n(k);
           end
       end
   end
   %E=1460*s*10^3*E/10^9
   % EPoints=101;
   % E=8610*E;
   % E=E/10
   n=100*n
   nPoints=101;
   pMin=min(p); pMax=max(p);
   qMin=min(q); qMax=max(q);
   pVect=linspace(pMin,pMax,nPoints);
   qVect=linspace(qMin,qMax,nPoints);
   [pMat,qMat]=meshgrid(pVect,qVect);
   int=scatteredInterpolant(p',q',n');
   %int=scatteredInterpolant(p',q',E');
   nMat=int(pMat,qMat)
   %EMat=int(pMat,qMat);
   colormap jet;      % doc colormap
   % % % %v=[91.2 94.9 96.5 97.4 97.9 98.2
   98.5]
   v=[ 99.008 98.834 97.8927298325486 98.68
       98.285 96.944 98.868 98.509 97.294 ];
   %v=[98.83 98.68 98.285 96.944 ]
   % % % e=[9,9.5,10,10.5,11,11.5,12,12.5];
   % %
   % % % her ploter jeg operasjons punktene
   P
   =[0.9,0.675,0.450,0.225,1,0.75,0.5,0.25]

```

```

98 Q=[0.436,0.323,0.218,0.109,0,0,0,0]
99 % %P_one=[0.933]
100 % %Q_one=[0.335]
101 %
102 figure(1)
103 % clf
104 % %plot(Q_one,P_one,'ko')
105 [c,h]=contour(qMat,pMat,nMat,v)% , hold on
106 plot(Q,P,'bo')
107 grid on
108 clabel(c,h,'FontSize',16,'LabelSpacing',
109         ,200,'FontName','Times New Roman')
110 title('Efficiency')
111 ylabel('Active power (pu)','FontName','
112         Times New Roman')
113 xlabel('Reactive power (pu)','FontName',
114         'Times New Roman')
115 axis equal;
116 axis([-1 .7 0 1]);

```

P. Code for the total energy loss of Åbjøra in figure 50

Listing 19. Code for the energy loss map in figure 50

```

1 %% Data inputs
2 clear; clc;
3 Ra=0.00182; Xq=0.676; Xd=1.059 ; Xp
4   =0.141;
5 b4=0.0817; b3=-0.2482; b2=-0.1645; b1
6   =1.3647
7 ; b0=-0.2251; bv=1;
8 n1=7;
9 C=0.160;
10 k1=1.0308 %1.03;
11 sn=1; ua=1; pf=0.9; %fpn=0.95;
12 %losses along the loading
13 %s=103000; ua_o=1; ia_o=1; ifd_o=1.7665;
14 s=103*10^3; ua_o=1; ia_o=1; ifd_o
15   =1065/525.15;
16 P_wf=172.92/s; % windage and friction
17   loss
18 P_cn=211.92/s; % core loss
19 P_an=193.63/s; % stator current loss
20 P_sn=82.99/s; % additional loss
21 P_fn=173.65/s; % rotor current loss
22 P_brn=2.13/s; % brush loss
23 P_exn=15.88/s; % excitation loss
24 P_b=240.9/s; %356.23 % bearings loss
25 pcte=P_wf+P_b; % constant power
26 k=0;
27 New_capabilitydiagram_AAbjora_func(Xd,Xq)
28 %% Efficiency calculation
29 P=0:0.01:1;
30 Q=-1:0.01:1;
31 for i=drange(1,length(P)) % active
32   power from 0 to 1
33   for j=drange(1,length(Q))
34     P1=P(i);
35     Q1=Q(j);
36     ia=sqrt(P1^2+Q1^2);
37     phi=atan(Q1/P1);
38     delta=atan(ia*(Xq*cos(phi)-(Ra*
39       sin(phi)))/(ua+(Ra*ia*cos(phi)
40       )+Xq*ia*sin(phi)));
41     egu=ua*cos(delta)+(Ra*ia*cos(
42       delta+phi))+Xd*ia*sin(delta+
43       phi);
44     ifu=egu/bv;
45     th=atan(ia*(Xp*cos(phi)-(Ra*sin(
46       phi)))/(ua+(Ra*ia*cos(phi))+Xp
47       *ia*sin(phi)));
48     ep=ua*cos(th)+(Ra*ia*cos(th+phi))
49       +Xp*ia*sin(th+phi);
50     if ep>0.55
51       %ifs=b4*ep^4+b3*ep^3+b2*ep^2+
52       b1*ep+b0-ep/bv;
53       ifs=(ep+C*ep^n1).*k1-(ep/bv);
54     else
55       ifs=0;
56     end
57     ifd1=(ifu+ifs)*525.15;
58     ifd=(ifu+ifs);
59     P_a=P_an*(ia/ia_o)^2;
60     P_f=P_fn*(ifd/ifd_o)^2;
61     P_c=P_cn*(ua/ua_o);
62     P_s=P_sn*(ia/ia_o)^2;
63     P_ex=P_exn*(ifd/ifd_o);
64     P_br=P_brn*(ifd/ifd_o)^2;
65     ptot=pcte+P_s+P_a+P_br+P_f+P_c+
66       P_ex;
67     k=k+1;
68     p(k)=P1;
69     q(k)=Q1;
70     n(k)=P1/(P1+ptot); %rend(k)=n(k);
71     Pf=P_f*s;
72     Pex=P_ex*s;
73     Pbr=P_br*s;
74     sum=(P_f+P_ex+P_br)*s;
75     E(k)=((1/n(k))-1)*P1;
76     %E(k)=(ptot*s*10^3)/10^9; %; rend
77     (k)=n(k);
78   end
79 end
80 EPoints=101;
81 E=E;
82 %E=E/10

```

```

77 n=n*1;
78 %nPoints=101;
79 pMin=min(p); pMax=max(p);
80 qMin=min(q); qMax=max(q);
81 pVect=linspace(pMin,pMax,EPoints);
82 qVect=linspace(qMin,qMax,EPoints);
83 [pMat,qMat]=meshgrid(pVect,qVect);
84 %int=scatteredInterpolant(p',q',n');
85 int=scatteredInterpolant(p',q',E');
86 nMat=int(pMat,qMat)
87 EMat=int(pMat,qMat);
88 %EMat=(8610*EMat*s*10^3)/10^9
89 % colormap jet; % doc colormap
90 % %v=[91.2 94.9 96.5 97.4 97.9 98.2 98.5]
91 v=[ 99.008 98.834 98.68 98.285 96.944
     98.868 98.509 97.294 ];
92 %v=[98.83 98.68 98.285 98.200 96.944 ]
93 e=[0.00675 0.007 0.0075 0.008 0.0082724
     0.0085 0.009 0.0095 0.01 ];
94 %e=[]
95 % P
     =[0.9,0.675,0.450,0.225,1,0.75,0.5,0.25];
96 Q=[0.436,0.323,0.218,0.109,0,0,0,0]
97 P=[0]
98 Q=[0.5]
99 % P_one=[0.933]
100 % Q_one=[0.335]
101 plot(Q,P,'bo')
102 % plot(Q_one,P_one,'ko')
103 [c,h]=contour(qMat,pMat,EMat,e)
104 clabel(c,h,'FontSize',16,'LabelSpacing',
        ,200,'FontName','Times New Roman')
105 title(' P_{loss} (pu)')
106 ylabel('Active power (pu)', 'FontName','
        Times New Roman')
107 xlabel('Reactive power (pu)', 'FontName','
        'Times New Roman')
108 axis equal;
109 axis([-1 .7 0 1]);

```

Q. Code for the 2D density plot of Åbjøra in figure 51

Listing 20. Code for the 2D histogram in figure 51

```

1 Data=AAbjoradata
2 Sbase=103.0
3 Pdata=Data(:,2)
4 Qdata=Data(:,1)
5 Pdata=Pdata./Sbase
6 Qdata=Qdata./Sbase
7 Xd_pu=1.059 ;
8 Xq_pu= 0.69;
9 % plot(Qdata,Pdata,'ro')
10 % axis([-1 0.6 0 1])
11
12 New_capabilitydiagram_AAbjora_func(Xd_pu,
    Xq_pu)

```

```

13 %% Denstiy scatter
14 figure(1)
15 %Density=densityscatter(Qdata,Pdata
    ,8000,15)
16 densityscatter(Qdata,Pdata,50,3)
17 title('Concentrated laod distrution')
18 % S=Pdata+j*Qdata
19
20 % figure(5)
21 % clf
22 % plot(Qdata,Pdata,'k*','Markersize',0.5)
23
24 figure(2)
25 subplot(2,1,1)
26 histogram(Qdata)
27 xlabel('Reactive power')
28 ylabel('Hours')
29 subplot(2,1,2)
30 histogram(Pdata)
31 xlabel('Active power')
32 ylabel('Hours')
33 %figure(22)
34 %print -depsc -tiff -r300 -painters
    full_load_toptobottom.eps

```

R. Code for the synch. condenser plot in figure 52

Listing 21. Code for the synch. cond dis. in Fig. 52

```

1 %for i =drange(1,600)
2 t=375
3 P=0.0:1/t:1;
4 Q=-1:1.7/t:0.7;
5 [Q,P]=meshgrid(Q,P);
6 [Qdata_ins,Pdata_ins]=DatainscapAAbjora(
    P,Q);
7 Q=Qdata_ins;
8 P=Pdata_ins;
9
10 %% ZONE 1
11 % It is better to start at almost zero
12 k=0.01;
13 xv1 = [-0.95 0.7 0.7 -0.95 -0.95 ];
14 yv1 = [0 0 k k 0 ];
15
16 %vertical Displacment(VD)
17 %Horizontal Displacment(HF)
18 %If HD>Height, HD=Height
19 %xv = [VD width width VD VD ];
20 %yv = [HD HD heighth heighth HD ]
21
22 xq1 = Q;
23 yq1 = P;
24 [in,on] = inpolygon(xq1,yq1,xv1,yv1);
25 Q_zone1=xq1(in);
26 P_zone1=yq1(in);

```

```

29 %% Zone 2
30 %for i =drange(1,900)
31 P1=0.0:1/30:1;
32 Q1=-1:1.7/30:0.7;
33 [Q1,P1]=meshgrid(Q1,P1);
34 [Qdata_ins ,Pdata_ins ] =DatainscapAAbjora(
    P1,Q1);
35 Q1=Qdata_ins ;
36 P1=Pdata_ins ;
37
38 % It is better to start at almost zero
39 k2=k+0.02
40 k_one=1;
41 xv_two = [-0.95 0.7 0.7 -0.95 -0.95 ];
42 yv_two = [k2 k2 k_one k_one k2 ];
43
44 %vertical Displacment(VD)
45 %Horizontal Displacment(HF)
46 %If HD>Height, HD=Heigth
47 %xv = [VD width width VD VD ];
48 %yv = [HD HD heigth heigth HD ]
49
50 xq_two = Q1;
51 yq_two = P1;
52 [in ,on] = inpolygon(xq_two ,yq_two ,xv_two ,
    yv_two);
53 numel(xq_two(in));
54
55 Q_zone_two=xq_two(in);
56 P_zone_two=yq_two(in);
57 figure (1)
58 %plot(Q_zone1,P_zone1,'ro'), hold on
59 %plot(Q_zone_two,P_zone_two,'bo')
60
61 Q_vec=[Q_zone1 ,Q_zone_two]
62 P_vec=[P_zone1 ,P_zone_two]
63
64 Q_vec=Q_vec'
65 P_vec=P_vec'
66
67 figure (1)
68 densityscatter(Q_vec ,P_vec ,35 ,15)
69 title('synch. condenser distrubtion')
70 [n_wae ,n_aae]=WAE_func_jonas(Q1 ,P1)
71 AAE=n_aae
72 WAE=n_wae
73 [n_wae ,n_aae]=WAE_func_jonas(Q_vec ,P_vec)
74 AAE=n_aae
75 WAE=n_wae
76
77 %[WAE_sum,WAEI]=WAE_cal_func(Q_vec ,P_vec)
78 %[AAEI]=AAE_calc_func(Q_vec ,P_vec)

```

### S. Code for the uniform load dis. in figure 52

Listing 22. Code for the uniform load dis in figure 52

```

1 % full load dis.

```

```

2 P1=0.0:1/31:1;
3 Q1=-1:1.7/31:0.7;
4 [Q1,P1]=meshgrid(Q1,P1);
5 [Qdata_ins ,Pdata_ins ] =DatainscapAAbjora(
    P1,Q1);
6 Q1=Qdata_ins ;
7 P1=Pdata_ins ;
8 Q1=Q1'
9 P1=P1'
10 %plot(Q1,P1,'bo')
11 figure (1)
12 densityscatter(Q1,P1,50,15)
13 title('full load distrubtion')
14 [n_wae ,n_aae]=WAE_func_jonas(Q1 ,P1)
15 AAE=n_aae
16 WAE=n_wae
17
18 %[WAE_sum,WAEI]=WAE_cal_func(Q_vec ,P_vec)
19 %[AAEI]=AAE_calc_func(Q_vec ,P_vec)

```

### T. Code for the max active power threshold 53

Listing 23. Code for the max active power threshold in figure 53

```

1 %% Data inputs
2 clear; clc;
3 Ra=0.00182; Xq=0.676; Xd=1.059 ; Xp
    =0.141;
4 b4=0.0817; b3=-0.2482; b2=-0.1645; b1
    =1.3647
5 ; b0=-0.2251; bv=1;
6 n1=7;
7 C=0.160;
8 k1=1.0308; %1.03;
9 sn=1; ua=1; pf=0.9; %fpn=0.95;
10
11 %losses along the loading
12 %s=103000; ua_o=1; ia_o=1; ifd_o=1.7665;
13 s=103*10^3; ua_o=1; ia_o=1; ifd_o
    =1065/525.15;
14
15
16 P_wf=172.92/s; % windage and friction
    loss
17 P_cn=211.92/s; % core loss
18 P_an=193.63/s; % stator current loss
19 P_sn=82.99/s; % additional loss
20 P_fn=173.65/s; % rotor current loss
21 P_brn=2.13/s; % brush loss
22 P_exn=15.88/s; % excitation loss
23 P_b=240.9/s; %356.23 % bearings loss
24 pcte=P_wf+P_b; % constant power
25 k=0;
26 %New_capabilitydiagram_AAbjora_func(Xd,Xq
    )
27 %% Efficiency calculation
28
29 P=0.001:1/500:1;

```

```

30 Q=-1:1.7/500:0.7;
31 [Q,P]=meshgrid(Q,P);
32
33 [Qdata_ins ,Pdata_ins ] =DatainscapAAbjora (
    P,Q)
34 Q=Qdata_ins ;
35 P=Pdata_ins ;
36 x_vec=[];
37 WAE_vec=[];
38 AAE_vec=[];
39 j=0
40 %% Zone 1
41 for i =drange(1,1*10^0)
42     % It is better to start at almost
        zero
43     k=(i/10^3);
44     xv = [-0.95 0.7 0.6 -0.97 -0.95 ];
45     yv = [0.0001 0.0001 k k .0001 ];
46
47 %vertical Displacment(VD)
48 %Horizontal Displacment(HF)
49 %If HD>Height, HD=Heigth
50 %xv = [VD width width VD VD ];
51 %yv = [HD HD heigth heigth HD ]
52     v=1;
53
54     xq = Q;
55     yq = P;
56
57     [in ,on] = inpolygon(xq,yq,xv,yv);
58     numel(xq(in));
59
60     %plot(xv,yv,'g','LineWidth',2) %
        polygon
61
62     Q_zone1=xq(in);
63     P_zone1=yq(in);
64
65     [n_wae ,n_aae]=WAE_func_jonas(Q_zone1 ,
        P_zone1);
66     WAE_sum=n_wae;
67     AAEI=n_aae;
68     j=j+1
69     x_vec(j)=k;
70     WAE_vec(j)=WAE_sum;
71     AAE_vec(j)=AAEI;
72 end
73
74 figure(22)
75 clf
76 plot(x_vec,WAE_vec,'r'), hold on
77 plot(x_vec,AAE_vec,'b')
78 title('WAE vs AAE')
79 legend('WAE','AAE')
80 xlabel('Active power [pu]')
81 ylabel('Efficiency [%]')
82 figure(32)
83 clf

```

```

84 plot(Q_zone1 ,P_zone1 , 'ro', 'DisplayName', '
    Zone3')% points inside

```

U. Code for the min active power threshold [53](#)

Listing 24. Code for the min active power threshold in figure [54](#)

```

1 %% Data inputs
2 clear; clc;
3 Ra=0.00182; Xq=0.676; Xd=1.059 ; Xp
    =0.141;
4 b4=0.0817; b3=-0.2482; b2=-0.1645; b1
    =1.3647
5 ; b0=-0.2251; bv=1;
6 n1=7;
7 C=0.160;
8 k1=1.0308;
9 sn=1; ua=1; pf=0.9;
10
11 %losses along the loading
12 %s=103000; ua_o=1; ia_o=1; ifd_o=1.7665;
13 s=103*10^3; ua_o=1; ia_o=1; ifd_o
    =1065/525.15;
14
15
16 P_wf=172.92/s; % windage and friction
    loss
17 P_cn=211.92/s; % core loss
18 P_an=193.63/s; % stator current loss
19 P_sn=82.99/s; % additional loss
20 P_fn=173.65/s; % rotor current loss
21 P_brn=2.13/s; % brush loss
22 P_exn=15.88/s; % excitation loss
23 P_b=240.9/s; % bearings loss
24 pcte=P_wf+P_b; % constant power
25 k=0;
26 %New_capabilitydiagram_AAbjora_func(Xd,Xq
    )
27 %% Efficiency calculation
28
29 P=0.001:1/1000:1;
30 Q=-1:1.7/1000:0.7;
31 [Q,P]=meshgrid(Q,P);
32
33 [Qdata_ins ,Pdata_ins ] =DatainscapAAbjora (
    P,Q)
34 Q=Qdata_ins ;
35 P=Pdata_ins ;
36 x_vec=[];
37 WAE_vec=[];
38 AAE_vec=[];
39 j=0
40 %% Zone 1
41 for i =(10^3)-1:-1:1
42     % It is better to start at almost
        zero
43     k=(i/10^3);
44     xv = [-0.95 0.7 0.6 -0.97 -0.95 ];

```

```

45     yv = [1 1 k k 1 ];
46     %yv = [0.0001 0.0001 k k .0001 ];
47     %vertical Displacment(VD)
48     %Horizontal Displacment(HF)
49     %If HD>Height, HD=Height
50     %xv = [VD width width VD VD ];
51     %yv = [HD HD height height HD ]
52     v=1;
53
54     xq = Q;
55     yq = P;
56
57     [in,on] = inpolygon(xq,yq,xv,yv);
58     numel(xq(in));
59
60     %plot(xv,yv,'g','LineWidth',2) %
61     polygon
62
63     Q_zone1=xq(in);
64     P_zone1=yq(in);
65
66     [n_wae, n_aae]=WAE_func_jonas(Q_zone1,
67     P_zone1);
68     WAE_sum=n_wae;
69     AAE1=n_aae;
70     j=j+1
71     x_vec(j)=k;
72     WAE_vec(j)=WAE_sum;
73     AAE_vec(j)=AAE1;
74 end
75
76 figure(22)
77 clf
78 plot(x_vec,WAE_vec,'r'), hold on
79 plot(x_vec,AAE_vec,'b')
80 title('WAE vs AAE')
81 legend('WAE','AAE')
82 grid on
83 xlabel('Active power [pu]')
84 ylabel('Efficiency [%]')
85 axis([0 1 0 100])
86
87 figure(32)
88 clf
89 plot(Q_zone1,P_zone1,'ro','DisplayName','
90     Zone3')%

```

```

5 ; b0=-0.2251; bv=1;
6 n1=7;
7 C=0.160;
8 k1=1.0308; %1.03;
9 sn=1; ua=1; pf=0.9; %fpn=0.95;
10
11 %losses along the loading
12 %s=103000; ua_o=1; ia_o=1; ifd_o=1.7665;
13 s=103*10^3; ua_o=1; ia_o=1; ifd_o
14 =1065/525.15;
15
16 P_wf=172.92/s; % windage and friction
17 loss
18 P_cn=211.92/s; % core loss
19 P_an=193.63/s; % stator current loss
20 P_sn=82.99/s; % additional loss
21 P_fn=173.65/s; % rotor current loss
22 P_brn=2.13/s; % brush loss
23 P_exn=15.88/s; % excitation loss
24 P_b=240.9/s; %356.23 % bearings loss
25 pcte=P_wf+P_b; % constant power
26 k=0;
27 %New_capabilitydiagram_AAbjora_func(Xd,Xq
28 )
29 %% Efficiency calculation
30 Nel = [];
31 eta_wae = [];
32 eta_aae = [];
33 % adjust the number of elements
34 for j =1:200;
35 t=j+2;
36 P=0.0:1/t:1;
37 Q=-1:1.7/t:0.7;
38 [Q,P]=meshgrid(Q,P);
39 [Qdata_ins,Pdata_ins] =
40 DatainscapAAbjora(P,Q);
41 Q=Qdata_ins;
42 P=Pdata_ins;
43
44 %figure(20)
45 %clf
46 %plot(Q,P,'bo')
47
48 n=[];
49 ploss =[];
50 for i=1:length(P);
51
52 P1=P(i);
53 Q1=Q(i);
54 ia=sqrt(P1^2+Q1^2);
55 phi=atan(Q1/P1);
56 delta=atan(ia*(Xq*cos(phi)-(Ra*
57     sin(phi)))/(ua+(Ra*ia*cos(phi)
58     )+Xq*ia*sin(phi)));
59 egu=ua*cos(delta)+(Ra*ia*cos(
60     delta+phi))+Xd*ia*sin(delta+

```

#### V. Code for the uniform dis. with increasing $N$ [55](#)

Listing 25. Code for increasing number of elements shown in figure [55](#)

```

1 %% Data inputs
2 clear; clc;
3 Ra=0.00182; Xq=0.676; Xd=1.059 ; Xp
4     =0.141;
5 b4=0.0817; b3=-0.2482; b2=-0.1645; b1
6     =1.3647

```

```

50     P1=P(i);
51     Q1=Q(i);
52     ia=sqrt(P1^2+Q1^2);
53     phi=atan(Q1/P1);
54     delta=atan(ia*(Xq*cos(phi)-(Ra*
55         sin(phi)))/(ua+(Ra*ia*cos(phi)
56         )+Xq*ia*sin(phi)));
57     egu=ua*cos(delta)+(Ra*ia*cos(
58         delta+phi))+Xd*ia*sin(delta+

```

```

    phi);
56 ifu=egu/bv;
57 th=atan(ia*(Xp*cos(phi)-(Ra*sin(phi)))/(ua+(Ra*ia*cos(phi))+Xp
    *ia*sin(phi)));
58 ep=ua*cos(th)+(Ra*ia*cos(th+phi))+Xp*ia*sin(th+phi);
59 if ep>0.55;
60     %ifs=b4*ep^4+b3*ep^3+b2*ep^2+
        b1*ep+b0-ep/bv;
61     ifs=(ep+C*ep^n1).*k1-(ep/bv);
62 else;
63     ifs=0;
64 end
65 ifd1=(ifu+ifs)*525.15;
66 ifd=(ifu+ifs);
67
68 P_a=P_an*(ia/ia_o)^2;
69 P_f=P_fn*(ifd/ifd_o)^2;
70 P_c=P_cn*(ua/ua_o);
71 P_s=P_sn*(ia/ia_o)^2;
72 P_ex=P_exn*(ifd/ifd_o);
73 P_br=P_brn*(ifd/ifd_o)^2;
74
75 ptot=pcte+P_s+P_a+P_br+P_f+P_c+
    P_ex;
76
77 %k=k+1;
78 ploss(i)=ptot;
79 eta=(P1/(P1+ptot));
80 n(i)=eta*100;
81 end
82
83 n_wae = sum(n)/length(n);
84 eta_wae(j) = n_wae;
85 Eloss = (sum(ploss)*(s*10^3)*365*24/
    length(n))/10^9;
86 E = (sum(P)*(s*10^3)*365*24/length(n)
    )/10^9;
87 n_aae = 100*E/(E+Eloss);
88 eta_aae(j) = n_aae;
89 Nel(j) = length(n);
90 end
91
92 figure(33)
93 clf
94 plot(Nel, eta_wae, 'r-', 'Linewidth', 2.5),
    hold on
95 plot(Nel, eta_aae, 'b-', 'Linewidth', 2.5)
96 grid on
97 axis([0 180000 95.5 98.5])
98
99 figure(29)
100 clf
101 plot(Q,P, 'bo')

```

### W. Code for additional functions in Abjora plots

Listing 26. Function that calculates WAE and AAE for AAbjora

```

function [n_wae, n_aae]=WAE_func_jonas(
    Qdata_ins, Pdata_ins)
    %% Data inputs
    %clearvars -except Pdata Qdata; clc;
    Ra=0.00182; Xq=0.676; Xd=1.059; Xp
        =0.141;
    b4=0.0817; b3=-0.2482; b2=-0.1645; b1
        =1.3647;
    ; b0=-0.2251; bv=1;
    n1=7;
    C=0.160;
    k1=1.0308; %1.03;
    sn=1; ua=1; pf=0.9; %fpn=0.95;
11
12 %losses along the loading
13 %s=103000; ua_o=1; ia_o=1; ifd_o=1.7665;
14 s=103*10^3; ua_o=1; ia_o=1; ifd_o
    =1065/525.15;
15
16
17 P_wf=172.92/s; % windage and friction
    loss
18 P_cn=211.92/s; % core loss
19 P_an=193.63/s; % stator current loss
20 P_sn=82.99/s; % additional loss
21 P_fn=173.65/s; % rotor current loss
22 P_brn=2.13/s; % brush loss
23 P_exn=15.88/s; % excitation loss
24 P_b=240.9/s; %356.23 % bearings loss
25 pcte=P_wf+P_b; % constant power
26 k=0;
27
28 Q=Qdata_ins;
29 P=Pdata_ins;
30
31 %figure (20)
32 %clf
33 %plot(Q,P, 'bo')
34
35
36 n=[];
37 ploss = [];
38 for i=1:length(P); % active
    power from 0 to 1
39
40 P1=P(i);
41 Q1=Q(i);
42 ia=sqrt(P1^2+Q1^2);
43 phi=atan(Q1/P1);
44 delta=atan(ia*(Xq*cos(phi)-(Ra*
        sin(phi)))/(ua+(Ra*ia*cos(phi)
        )+Xq*ia*sin(phi)));
    egu=ua*cos(delta)+(Ra*ia*cos(
        delta+phi))+Xd*ia*sin(delta+
        phi);
45

```



```

46 ifu=egu/bv;
47 th=atan(ia*(Xp*cos(phi)-(Ra*sin(phi)))/(ua+(Ra*ia*cos(phi))+Xp
    *ia*sin(phi)));
48 ep=ua*cos(th)+(Ra*ia*cos(th+phi))+Xp*ia*sin(th+phi);
49 if ep>0.55;
50 %ifs=b4*ep^4+b3*ep^3+b2*ep^2+
    b1*ep+b0-ep/bv;
51 ifs=(ep+C*ep^n1).*k1-(ep/bv);
52 else;
53 ifs=0;
54 end
55 ifd1=(ifu+ifs)*525.15;
56 ifd=(ifu+ifs);
57
58 P_a=P_an*(ia/ia_o)^2;
59 P_f=P_fn*(ifd/ifd_o)^2;
60 P_c=P_cn*(ua/ua_o);
61 P_s=P_sn*(ia/ia_o)^2;
62 P_ex=P_exn*(ifd/ifd_o);
63 P_br=P_brn*(ifd/ifd_o)^2;
64
65 ptot=pcte+P_s+P_a+P_br+P_f+P_c+
    P_ex;
66
67 %k=k+1;
68 ploss(i)=ptot;
69 eta=(P1/(P1+ptot));
70 n(i)=eta*100;
71 end
72
73 n_wae = sum(n)/length(n);
74 %eta_wae(j) = n_wae;
75 Eloss = (sum(ploss)*(s*10^3)*365*24/
    length(n))/10^9;
76 E = (sum(P)*(s*10^3)*365*24/length(n)
    )/10^9;
77 n_aae = 100*E/(E+Eloss);
78 %eta_aae(j) = n_aae;
79 %Nel(j) = length(n);
80 end

```

Listing 27. Function that plots AAbjoras capability diagram

```

1 function [x_p,y_p] =
    New_capabilitydiagram_AAbjora_func(
    Xd_pu,Xq_pu)
2 %% Plot Capabilitydiagram
3 Pn=0.9
4 phin=acosd(Pn)
5 Qn=Pn*tand(phin)
6 Xd_pu=1.06;
7 Xq_pu=0.69;
8 V=1;
9 %Pmax =0.9
10 th = (63.7:1:126.152);
11 Sn1 = 1; %or whatever radius you want
12 x = Sn1*cosd(th);
13 y = Sn1*sind(th);
14
15 A_x=-1/Xq_pu;
16 B_x=-1/Xd_pu;
17
18 %small circle E=0
19 E0=0.0
20 th1 = (0:0.1:180);
21 R=(0.5*(V^2)*(Xd_pu-Xq_pu))/(Xd_pu.*
    Xq_pu)+E0
22 c=(0.5*(V^2)*(Xd_pu+Xq_pu))/(Xd_pu.*
    Xq_pu)-E0
23 x1= R*cosd(th1) - c;
24 y1= R*sind(th1);
25
26
27 %small circle E=0.1
28 E1=0.1
29 th1 = (0:0.1:22.5);
30 R=(0.5*(V^2)*(Xd_pu-Xq_pu))/(Xd_pu.*
    Xq_pu)+E1
31 c=(0.5*(V^2)*(Xd_pu+Xq_pu))/(Xd_pu.*
    Xq_pu)-E1
32 x1_01= R*cosd(th1) - c;
33 y1_01= R*sind(th1);
34
35
36 %small circle E=0.2
37 E2=0.2
38 th1 = (0:0.1:45.5);
39 R=(0.5*(V^2)*(Xd_pu-Xq_pu))/(Xd_pu.*
    Xq_pu)+E2
40 c=(0.5*(V^2)*(Xd_pu+Xq_pu))/(Xd_pu.*
    Xq_pu)-E2
41 x1_02= R*cosd(th1) - c;
42 y1_02= R*sind(th1);
43
44
45 %small circle E=0.3
46 E3=0.3
47 th1 = (0:0.1:180);
48 R=(0.5*(V^2)*(Xd_pu-Xq_pu))/(Xd_pu.*
    Xq_pu)+E3
49 c=(0.5*(V^2)*(Xd_pu+Xq_pu))/(Xd_pu.*
    Xq_pu)-E3
50 x1_03= R*cosd(th1) - c;
51 y1_03= R*sind(th1);
52
53 %small circle E=0.4
54 E3=0.4
55 th1 = (0:0.1:180);
56 R=(0.5*(V^2)*(Xd_pu-Xq_pu))/(Xd_pu.*
    Xq_pu)+E3
57 c=(0.5*(V^2)*(Xd_pu+Xq_pu))/(Xd_pu.*
    Xq_pu)-E3
58 x1_04= R*cosd(th1) - c;
59 y1_04= R*sind(th1);
60

```

```

61 %64.5
62 %third semi circle Emax
63 th2 = (64.5:0.8:95.5);
64 x2=Qn
65 x1=A_x
66 y2=Pn
67 y1=0
68 R=sqrt((x2-x1).^2+(y2-y1).^2);
69 y2= R*cosd(th2);
70 x2= R*sind(th2) +A_x;
71
72
73 %%
74
75 figure(1)
76 clf
77 plot(x,y,'k','linewidth',1.5), hold on
78 %plot([-0.4359 0.4359],[0.9 0.9],'
    Linewidth',1)%Pmax
79 %plot([0 0],[0 1],'Linewidth',1)%
    origoaxis
80 % %plot([0 0.326],[0 0.95],'Linewidth',1)
    %Sn
81 %plot(A_x,0,'o')
82 %plot(B_x,0,'o')
83 plot(x1,y1)%first semi-circle
84 plot(x1_01,y1_01,'k','linewidth',1.5)%
    second semi-circle
85 %plot(x1_02,y1_02)%third semi-circle
86 %plot(x1_03,y1_03)%fourth semi-circle
87 %plot(x1_04,y1_04)%fifth semi-circle
88 % %plot([A_x 0.326],[0 0.95],'Linewidth
    ',1)%second line
89 plot(x2,y2,'k','linewidth',1.5)%third
    semi circle Emax
90 xlabel('Q [pu]')
91 ylabel('P [pu]')
92
93
94
95 %% The practical stability limit:
96 % data inputs
97 Xd=1.06 ;
98 Xq= 0.69;
99 V=1
100 i=j
101 eq=0.08:0.01:1.151
102
103 % Calculation of delta
104 % derivate P in regard to delta to get
    the maximum delta
105 a=(eq.*Xq)/(V.*(Xd-Xq))
106 b=sqrt(a.^2+8)
107 cosdelta=(1/4).*(-a+b)
108 delta=acosd(cosdelta)
109
110 %Calculate the active power and reactive
    power

```

```

111 % with eq ranging from 0-1 and use max
    delta
112 c=(eq.*V)/(Xd).*sind(delta)
113 d=(0.5*V.^2).*((Xd-Xq)/Xd*Xq).*sind
    (2.*delta)
114 P=c+d
115 e=(V.^2).*((Xd-Xq)/Xd.*Xq).*(sind(
    delta)).^2
116 f=((V.^2)/Xd)
117 Q=((eq.*V)/Xd).*cosd(delta)-f-e
118
119 % In order to get the PLS multiply with
    a stability margin
120 %twentyfive percent stability margin
121 stabm=0.75;
122 S=(j*Q+P).*stabm
123 x_p=imag(S)
124 y_p=real(S)
125 plot(x_p,y_p,'k','linewidth',1.5)
126 axis([-1 0.7 0 1])
127 %end

```

Listing 28. Function that plots datapoints ins. cap. of AAbjora

```

1 function [x_p,y_p] = function [Qdata_ins ,
    Pdata_ins ] =DatainscapAAbjora(P,Q)
2 Xd_pu=1.06 ;
3 Xq_pu= 0.69;
4 V=1;
5 [x_p,y_p] =
    New_capabilitydiagram_AAbjora_func(
    Xd_pu,Xq_pu);
6 x_p=x_p;
7 y_p=y_p;
8 %[ Qdata_ins , Pdata_ins ]=
    data_point_lim_func(Xd_pu,Xq_pu,Ua_pu,
    V,P,Q,div ,x_p,y_p)
9
10 %% Data points limited by armature
    current and Emax
11 L_row=size(P,1);
12 L_col=size(Q,2);
13 col=L_row*L_col;
14 Q=reshape(Q,1,col);
15 P=reshape(P,1,col);
16 Q1=[];
17 P1=[];
18 for r =drange(1,col)
19     if (Q(r)-0).^2+(P(r)-0).^2-(1)<0;
20         Q1(r)=Q(r);
21         P1(r)=P(r);
22     end
23 end
24
25 A_x=-1/Xq_pu;
26 col1=length(P1);
27 % Nominal op. (0.9,0.44)
28 Q11=[];
29 P11=[];

```

```

30 R=sqrt((0.44+1.4493)^2+(0.9)^2);
31 for i =drange(1, col1);
32     if (Q1(i)-A_x).^2+(P1(i)-0).^2-(R)
33         .^2<0;
34         Q11(i)=Q1(i);
35         P11(i)=P1(i);
36     end
37 end
38 %% Data points limited by min. field
39     current
40 E2=0.1;
41 R=(0.5*(V^2)*(Xd_pu-Xq_pu))./(Xd_pu.*
42     Xq_pu)+E2;
43 c=(0.5*(V^2)*(Xd_pu+Xq_pu))./(Xd_pu.*
44     Xq_pu)-E2;
45 col2=P11;
46 Q_11=[];
47 P_11=[];
48 for i =drange(1, length(P11))
49     xdif=(Q11(i)+c).^2;
50     ydif=(P11(i)-0).^2;
51     d=sqrt(xdif+ydif);
52     if d>R
53         Q_11(i)=Q11(i);
54         P_11(i)=P11(i);
55     end
56 end
57 %% Data points limited by PLS
58 p=polyfit(x_p, y_p, 1);
59 s=-1:0.1:0;
60 a=p(1);
61 b=p(2);
62 y=a*s+b;
63 Qdata_ins=[];
64 Pdata_ins=[];
65 %% Get the data point inside the
66     function:
67 for i = drange(1, length(Q_11))
68     if Q_11(i)>(-P_11(i)+b)/-a
69         Qdata_ins(i)= Q_11(i);
70         Pdata_ins(i)= P_11(i);
71     end
72 end
73 m_data=(Pdata_ins & Qdata_ins)~=0;
74 Pdata_ins=Pdata_ins(m_data);
75 Qdata_ins=Qdata_ins(m_data);
76 %plot(Qdata_ins, Pdata_ins, 'ro')
77 end
78
79 Listing 29. Function that plots field current using the fitting function methods
80 function [ ifd ]= Field_current2 ( Pt , Qt)
81 %% Data inputs
82 Ra=0.00182; Xq=0.676; Xd=1.059 ; Xp
83     =0.141;
84     b4=0.0817; b3=-0.2482; b2=-0.1645; b1
85         =1.3647
86     ; b0=-0.2251; bv=1;
87     n1=7;
88     C=0.160;
89     k1=1.0308 %1.03;
90     sn=1; ua=1; pf=0.9; %fpn=0.95;
91
92 %%losses along the loading
93 %s=103000; ua_o=1; ia_o=1; ifd_o=1.7665;
94 s=103*10^3; ua_o=1; ia_o=1; ifd_o
95     =1065/525.15;
96
97 P_wf=172.92/s; % windage and friction
98     loss
99 P_cn=211.92/s; % core loss
100 P_an=193.63/s; % stator current loss
101 P_sn=82.99/s; % additional loss
102 P_fn=173.65/s; % rotor current loss
103 P_brn=2.13/s; % brush loss
104 P_exn=15.88/s; % excitation loss
105 P_b=240.9/s; %356.23 % bearings loss
106 pcte=P_wf+P_b; % constant power
107 k=0;
108 ifd=[]
109 Sn=103
110 %% Field current calculation
111 % her velger du hvilken last operasjon du
112     onkser
113 P=Pt./Sn
114 Q=Qt./Sn
115 % P=0.9
116 % Q=0.43
117 for i=1:length(P) % active
118     power from 0 to 1
119     P1=P(i);
120     Q1=Q(i);
121     ia=sqrt(P1^2+Q1^2);
122     phi=atan(Q1/P1);
123     if Q1>= 0
124         phi= acos(P1/Sn);
125     elseif Q1 < 0
126         phi = -1*acos(P1/Sn);
127     end
128     %phi(isnan(Q))=0;
129     delta=atan(ia*(Xq*cos(phi)-(Ra*
130         sin(phi)))/(ua+(Ra*ia*cos(phi)
131         )+Xq*ia*sin(phi)));
132     egu=ua*cos(delta)+(Ra*ia*cos(
133         delta+phi))+Xd*ia*sin(delta+
134         phi);
135     ifu=egu/bv;
136     th=atan(ia*(Xp*cos(phi)-(Ra*sin(
137         phi)))/(ua+(Ra*ia*cos(phi))+Xp
138         *ia*sin(phi)));
139     ep=ua*cos(th)+(Ra*ia*cos(th+phi))
140         +Xp*ia*sin(th+phi);

```

```

50     if ep>0.55
51         %ifs=b4*ep^4+b3*ep^3+b2*ep^2+
           b1*ep+b0-ep/bv;
52         ifs=(ep+C*ep^n1).*k1-(ep/bv);
53     else
54         ifs=0;
55     end
56     k=k+1
57     ifd(k)=(ifu+ifs)*525.15;
58
59     end

```

Listing 30. Function that plots the approximated field current

```

1
2 function [Ifd ,Eg,I,P,Q] =
   Field_current_two(P, Q, V, Sn, Vn, Ra,
   Xad, Xq, Xd)
3 P = P/Sn;
4 Q = Q/Sn;
5 V = V/Vn;
6 In = Sn/(sqrt(3)*Vn); %kA
7 Zb = Vn^2/Sn;
8 Ra = Ra/Zb;
9 I = sqrt(P.^2+Q.^2)./V;
10
11 for n = 1:length(I)
12     if Q(n) >= 0
13         phi(n) = acos(P(n)/(V(n)*I(n)));
14     elseif Q(n) < 0
15         phi(n) = -acos(P(n)/(V(n)*I(n)));
16     end
17 end
18
19 delta = atan((Xq*I.*cos(phi)-Ra*I.*sin(
   phi))./(V+Ra*I.*cos(phi)+Xq*I.*sin(phi)
   ));
20 ed = V.*sin(delta);
21 eq = V.*cos(delta);
22 id = I.*sin(delta+phi);
23 iq = I.*cos(delta+phi);
24 Eg=(eq+Ra*iq+Xd*id)
25 Ifd =Eg./(Xad); %Pu
26 Ifd = Ifd*In*1000; %A
27 % Xad_cal = (eq+Ra*iq+Xd*id)/(625/5406.1)
   %Calibrating line

```